



Delft University of Technology

Understanding Levee Failures from Historical and Satellite Observations

Ozer, Ece

DOI

[10.4233/uuid:98e1ef84-91d0-4ee0-b37b-d7ab794cb367](https://doi.org/10.4233/uuid:98e1ef84-91d0-4ee0-b37b-d7ab794cb367)

Publication date

2020

Document Version

Final published version

Citation (APA)

Ozer, E. (2020). *Understanding Levee Failures from Historical and Satellite Observations*. [Dissertation (TU Delft), Delft University of Technology]. <https://doi.org/10.4233/uuid:98e1ef84-91d0-4ee0-b37b-d7ab794cb367>

Important note

To cite this publication, please use the final published version (if applicable). Please check the document version above.

Copyright

Other than for strictly personal use, it is not permitted to download, forward or distribute the text or part of it, without the consent of the author(s) and/or copyright holder(s), unless the work is under an open content license such as Creative Commons.

Takedown policy

Please contact us and provide details if you believe this document breaches copyrights. We will remove access to the work immediately and investigate your claim.

**UNDERSTANDING LEVEE FAILURES
FROM HISTORICAL AND SATELLITE OBSERVATIONS**

UNDERSTANDING LEVEE FAILURES FROM HISTORICAL AND SATELLITE OBSERVATIONS

Dissertation

for the purpose of obtaining the degree of doctor
at Delft University of Technology,
by the authority of the Rector Magnificus prof. dr. ir. T.H.J.J. van der Hagen,
chair of the Board for Doctorates,
to be defended publicly on 25 May 2020 at 15:00 o'clock

by

Işıl Ece ÖZER

Master of Science in Water Resources Engineering and in Safety Engineering,
KU Leuven, Belgium,
born in Istanbul, Turkey.

This dissertation has been approved by the promotor.

Composition of the doctoral committee:

Rector Magnificus,	chairperson
Prof. dr. ir. S.N. Jonkman,	Delft University of Technology, <i>promotor</i>
Prof. dr. ir. R.F. Hanssen,	Delft University of Technology, <i>promotor</i>

Independent members:

Prof. dr. ir. P.J.G. Teunissen,	Delft University of Technology
Prof. dr. ir. M. Kok,	Delft University of Technology
Prof. dr. ir. P.H.A.J.M. van Gelder,	Delft University of Technology
Dr. H.R.G.K. Hack,	University of Twente
Ir. P.C. Janssen,	Hoogheemraadschap van Delfland



Keywords: InSAR monitoring, levee failures, levee deformation, flood defenses, satellite radar interferometry, flood risk management

Printed by: Ipskamp Printing

Front & Back: G. Vairetti & G. Bernardi

Copyright © 2020 by I.E. Özer

ISBN 978-94-6384-135-1

An electronic version of this dissertation is available at
<http://repository.tudelft.nl/>.

*We must build dikes of courage
to hold back the flood of fear.*

Martin Luther King, Jr.

PREFACE

Although there is only one name on its cover, this thesis would not have been possible without the people who walked with me, supported and helped me through my PhD.

My biggest thank certainly goes to my promotors. Bas Jonkman for all the scientific discussions we had, his excellent supervision throughout the years, and the trust and freedom he provided me. Bas, I am happy to be one of those lucky PhDs that had a chance to be in your team. Ramon Hanssen for enlightening me with his broad scientific knowledge during these past years. His ability of showing me things from a different angle was always extremely valuable: not only professionally but also personally. Ramon, thanks for making my PhD more complicated, but undoubtedly more valuable.

A separate mention goes to my daily supervisors. Freek van Leijen for teaching me everything I know about InSAR, literally from scratch. His expertise, help, suggestions, and availability whenever I knocked on his door have all been necessary elements for the completion of this PhD. Myron van Damme for his guidance and helpful feedback throughout the different periods.

Besides, I would like to thank the independent members of my doctoral committee: Peter Teunissen, Matthijs Kok, Pieter van Gelder, Robert Hack, and Pieter Janssen for their time and interest in my research.

My colleagues from the Hydraulic Engineering department and the Radar group: it was a pleasure to work with each one of you. Wim Kanning, Oswaldo Morales Napoles, Kristina Reinders, Mark Voorendt, Matthijs Kok, and Timo Schweckendiek for the fruitful discussions we had and the feedback they gave me on numerous occasions. Ling Chang, Prabu Dheenathayalan, Sami Samiei Esfahany, Gert Mulder, Floris Heuff, and Mengshi Yang for willingly spending their time to guide me through the different aspects of InSAR. Judith Schooneveld-Oosterling and Diana Keijzer for their continuous assistance.

Special thanks to the Kamer-3.81 folks for being not colleagues but good friends. Erik, Job, Orson and Stephan, especially for all sort of things you did for my Dutch integration: eating boterham, sending a Tikkie, patiently speaking in Dutch with me, correcting my Dutch texts (incl. the summary of this thesis), en nog veel meer. Ermano for offering me his shoulder to lean on when I needed. Niklas for bringing his nice German humor to the office and hosting us in Dresden. I will definitely miss our office.

I will also miss the 17:01 borrels on Thursdays. Robert, Jessica, Chris, Keisha, Irene, Gina, Matthijs, Alex and Danny: you made the weeks seem shorter and this PhD experience a lot better! It started as just a couple of beers at PSOR, but through the noise and the crowd I found some true friends.

One of the things you learn while living abroad is how to create a big household with your friends. *Leuven crew*, thanks not only for your support during this PhD but also for making my last 8 years unforgettable. Alice, Pablo, Ed, Justin, Ana, Dan, Carlo, Oreste, Dr. Skorpio, Francesco, Marta, Amin, Baharak, Thomas, Ivana among many many other amazing people I met from all around the world. I know we will always be together,

wherever our lives will bring us. Special thanks to my *Benelux family*: Deniz, Giuliano, Leo and Lysette for the good times, the amazing trips we had together, all the eating and drinking (more than necessary sometimes), and the deep scientific discussions on all sort of things nobody cares about. And yes, climate is changing!

I am grateful to have my Turkish team, Merve, Tülay, Simge, Göksu, Yonca, Selen, and Ahmet, because every time I come back, it feels like I never left.

I would not be where I am now without the constant support, the unconditional trust and encouragement of my parents, Nezih and Necla, and my sister, Sevi. I know you will be always proud of me, whatever I am going to do in the future. *Teşekkürler, herşey için!*

Save the best for last, they say. Giacomo; my best friend, my travel buddy, my partner in all kinds of awkward moments, my husband, and my tatlım. Thanks for the endless love and support you gave me in every single day of this PhD journey. I cannot wait for the new chapter of our life, full of new adventures yet to come.

Işıl Ece Özer
Den Haag, April 2020

SUMMARY

Flood defense systems are critical in protecting against catastrophic events which often lead to significant damage, fatalities or substantial socio-economic and environmental impact. Even though levees form a significant part of the existing flood defense systems, there is a limited knowledge of the different levee behavior processes and the critical factors contributing to their failures. This research demonstrates the importance of collecting and analyzing historical failure events to gain new insights into levee failure mechanisms, and shows how satellite technology can both provide useful information on the deformation behavior of levees and be applicable for early warning systems.

The availability of sufficient data regarding levees and their failures is essential to reduce uncertainties, and thus to enhance the reliability analyses of flood defenses. A main contribution of this research is the development of an efficiently structured, open-access, global database, called International Levee Performance Database (ILPD), which comprises information on levee characteristics, failure mechanisms, geotechnical investigations, experiments and breach processes, currently for more than 1500 cases. The main purpose of the ILPD is to provide a global platform for systematically collecting and sharing data on levee performances in order to facilitate research in the field of flood risk and to stimulate the development of more accurate failure and breaching models.

Based on the available data, we perform a macro-scale analysis of levee failures and breaches, demonstrating the potential of the database to provide insights on levee behavior and to support flood risk assessments. From this analysis, we identify common failure mechanisms, breach characteristics, and the density of breach occurrence at the event-level. External erosion is recognized as the most frequent failure mechanism for levees. Our investigation of the breach characteristics of over a hundred failures during the flood events occurred in Germany (2002, 2013) reveals that initial failure mechanisms have an influence on breach characteristics and that failures due to instability and internal erosion are less frequent but lead to larger breaches. Moreover, we introduce two new breach density parameters which could be used to consider multiple failures in flood risk assessments. Our study shows that flood events with higher return periods tend to yield more severe consequences with respect to degree of damage, number, and density of levee breaches.

Another important aspect to consider regarding levee safety is the ability to identify if, where, and when a failure would suddenly occur. Current conventional levee inspection methods mostly rely on expert observers, which result in infrequent, qualitative and labor-intensive assessments. As climate projections commonly agree that the future will bring more extreme conditions, innovative and cost-effective complementary techniques for assessing levee safety become crucial. In this regard, satellite radar interferometry (InSAR), which provides frequent deformation data with high resolution, is ready to be used for monitoring the condition of levees with mm-level precision anywhere on the planet. Here, we provide a comprehensive overview of the state of the art

in using time-series InSAR for systematic levee monitoring in order to explore its use for assessing levee deformations and potential problematic locations in a fast, systematic, and cost-effective way. Moreover, we address frequently recurring technical questions related to the practical applicability of levee monitoring using InSAR technology. Even though its applicability is case-specific, the InSAR products holds an enormous information value: the deformation data can be derived quantitatively on a daily basis, which can complement levee management efficiently. Besides, the interpretation of the InSAR data for the overall assessment of levee safety requires a strong collaboration between satellite experts, geotechnical engineers and policy makers.

In this research, we demonstrate that apart from monitoring the conditions of levees, InSAR technology also provides insight into their dynamic structural behavior and enables the identification of critical situations. More specifically, we show that the sub-seasonal behavior of levees can be observed in greater detail, thus allowing to predict expected swelling and shrinkage due to variations of the meteorological conditions and to increase the ability of detecting anomalies. In order to identify and analyze this behavior from levee deformation observations obtained using Persistent Scatterer (PS)-InSAR, we develop a predictive deformation model, called vPT-model. By assessing whether the observed deformation is in line with this expected behavior, it becomes possible to identify anomalies in the levee deformation time-series. For this purpose, we propose a prototype early warning methodology to detect and analyze these anomalies on levees which can be indicative of potential problematic locations. Considering the ability of monitoring and modeling the levee behavior processes, such as extreme shrinkage or swelling behavior under severe conditions, it also becomes possible to detect subtle degrees of levee deformations which could indicate a failure being imminent. This would allow authorities to apply timely countermeasures, and thus, to prevent potential levee failures. Our study suggests that InSAR has surpassed the stage of being a mere scientific tool and has moved towards becoming an operational levee deformation monitoring system, which allows for the detection, tracking, and analysis of irregularities on levee sections with increased efficiency and quality.

Consequently, findings of this research will eventually contribute to complementing flood risk management, developing operational levee monitoring systems, and thus enhancing flood protection.

SAMENVATTING

Waterkeringen zijn van essentieel belang in de bescherming tegen overstromingen, die kunnen leiden tot schade, slachtoffers of substantieel sociaal-economische en milieu-impact. Hoewel dijken een belangrijk deel vormen van de bestaande waterkeringssystemen, is er slechts beperkte kennis van de verschillende gedragingsprocessen van dijken en de kritieke factoren die leiden tot het falen daarvan. Dit onderzoek toont het belang van het inventariseren en analyseren van historische gevallen van dijkfalen om nieuwe inzichten te verkrijgen in de faalmechanismen van dijken en laat zien hoe satelliettechnologie zowel nuttige informatie oplevert over het vervormingsgedrag van dijken als toepassingen heeft in waarschuwingssystemen.

De beschikbaarheid van voldoende gegevens over dijken en de faalmechanismen daarvan is essentieel om onzekerheid te reduceren en daarmee de betrouwbaarheidsanalyses van waterkeringen te verbeteren. Een belangrijke bijdrage van dit onderzoek is de ontwikkeling van een efficiënt opgezette, openbaar toegankelijke en wereldwijde database, genaamd de International Levee Performance Database (ILPD), met informatie over dikeigenschappen, faalmechanismen, resultaten van geotechnische onderzoeken, experimenten en doorbraakprocessen voor op dit moment al meer dan 1500 gevallen. Het belangrijkste doel van de ILPD is het bieden van een wereldwijd platform om systematisch data over de prestaties van dijken te verzamelen en te delen en daarmee verder onderzoek op het gebied van overstromingsrisico te faciliteren en de ontwikkeling van betrouwbaardere faalkans- en dijkdoorbraakmodellen te stimuleren.

Op basis van de beschikbare data hebben we een analyse op macroschaal uitgevoerd voor opgetreden gevallen van dijkfalen en -doorbraken, en daarmee de potentie van de database aangetoond in het verkrijgen van meer inzicht in het gedrag van dijken en het verfijnen van waterveiligheidsanalyses. In deze analyse identificeren we vaak voorkomende faalmechanismen, kenmerken die leiden tot dijkdoorbraken, en de ruimtelijke spreiding van doorbraken op het niveau van individuele hoogwatergevalen. Hieruit blijkt externe erosie als meest frequent faalmechanisme van dijken. Ons onderzoek van de kenmerken van meer dan honderd dijkdoorbraken bij overstromingen in Duitsland (2002, 2013) brengt aan het licht dat de initiële faalmechanismen van invloed zijn op de kenmerken van een verdere dijkdoorbraak en dat de faalmechanismen instabiliteit en interne erosie minder frequent voorkomen maar wel leiden tot grotere doorbraken. Daarnaast introduceren we twee nieuwe dichtheidsparameters die gebruikt kunnen worden om de kans op meerdere faalgevallen in een waterveiligheidsanalyse te voorspellen. Onze studie toont aan dat hoogwatercondities met een hogere terugkeertijd grotere gevolgen hebben wat betreft de mate van schade, en het aantal en de ruimtelijke dichtheid van dijkdoorbraken.

Een ander belangrijk aspect in relatie tot het vaststellen van de veiligheid van dijken is het vermogen om te bepalen of, waar en wanneer een dijk plotseling faalt. Gangbare dijkinspectiemethoden vertrouwen hoofdzakelijk op waarnemingen van experts, wat

resulteert in infrequente, kwalitatieve en arbeidsintensieve beoordelingen. Gezien klimaatprojecties in de toekomst extremere weerscondities voorspellen, zijn complementaire innovatieve en kosteneffectieve technieken voor het bepalen van dijkveiligheid van cruciaal belang. Interferometrische synthetische aperture radar (InSAR), die frequent vervormingsgegevens met hoge resolutie meet, is in staat om wereldwijd de staat van dijken met mm-precisie te monitoren. We geven een uitgebreid overzicht van de nieuwste ontwikkelingen ten aanzien van de toepassing van InSAR in het systematisch monitoren van dijken en verkennen het gebruik daarvan om vervormingen en potentiële probleemlocaties snel, systematisch en kosteneffectief te beoordelen. Verder adresseren we veelvoorkomende technische vragen ten aanzien van de praktische toepasbaarheid van dijkmonitoring aan de hand van InSAR technologie. Hoewel de toepasbaarheid situatieafhankelijk is, hebben InSAR producten een enorme informatiewaarde: vervormingsgegevens kunnen kwantitatief op dagelijkse basis worden bepaald en daarmee bijdragen aan efficiënt dijkmanagement. Daarbij vraagt de interpretatie van InSAR-gegevens voor de beoordeling van dijkveiligheid om een nauwe samenwerking tussen satellietexperts, geotechnische ingenieurs en beleidsmakers.

In dit onderzoek demonstreren we dat InSAR-technologie, naast het monitoren van dijkcondities, inzicht biedt in het dynamisch gedrag van dijken en het identificeren van kritieke situaties. Specifieker laten we zien dat het seizoensgebonden deformatiegedrag van dijken in meer detail kan worden waargenomen, wat het mogelijk maakt om het krimpen en zwellen door variërende weersomstandigheden te voorspellen en afwijkingen te detecteren. Om dit gedrag te identificeren en te analyseren op basis van waarnemingen van het vervormingsgedrag van dijken verkregen door het gebruik van Persistent Scatterer (PS)-InSAR, ontwikkelen we een voorspellend vervormingsmodel, genaamd het vPT-model. Door te bepalen of de waargenomen vervorming in lijn is met het verwachte gedrag, wordt het mogelijk om onregelmatigheden in de tijdreeks van het vervormingsgedrag te identificeren. We stellen een prototype methodologie voor een waarschuwingssysteem voor om deze onregelmatigheden te detecteren en te analyseren voor dijken die indicatief kunnen zijn voor mogelijk risicovolle locaties. Met de mogelijkheid om de gedragingsprocessen van de dijk te monitoren en te modelleren, zoals extreem krimp- en zwelgedrag onder zware omstandigheden, wordt het ook mogelijk om subtiele vervormingen te detecteren als indicatie voor dreigend falen. Onze studie geeft aan dat InSAR de fase als louter wetenschappelijk hulpmiddel heeft gepasseerd en is opgeschoven richting een operationeel monitoringssysteem voor dijkvervormingen, dat de detectie, het volgen en de analyse van onregelmatigheden op dijksecties mogelijk maakt met een verbeterde efficiëntie en prestatie.

Concluderend dragen de bevindingen uit dit onderzoek bij aan de beheersing van de waterveiligheid door het ontwikkelen van operationele dijkmonitoringsystemen.

CONTENTS

Preface	vii
Summary	ix
Samenvatting	xi
1 Introduction	1
1.1 Motivation	1
1.2 Research Rationale	1
1.2.1 Learning from the Past	3
1.2.2 Learning from the Present	4
1.2.3 Towards the Future.	5
1.3 Research Objectives.	7
1.4 Thesis Outline	8
1.5 the SAFElevee project	9
2 Towards an International Levee Performance Database (ILPD) and Macro-scale Analysis of Levee Failures	11
2.1 An Overview of the Existing Databases	12
2.2 Towards an International Levee Performance Database (ILPD)	15
2.2.1 Purpose of ILPD	15
2.2.2 The design and the structure.	15
2.2.3 Categorization of levee failure mechanisms	16
2.3 Macro-scale Analysis of Levee Failures	19
2.3.1 General database statistics.	19
2.3.2 Investigation of the 2002 and 2013 failures in Elbe region, Germany .	22
2.3.3 Levee breach analysis	25
2.4 Discussion	30
2.4.1 On the International Levee Performance Database (ILPD)	30
2.4.2 On using event-level analysis for risk assessments	32
2.5 Key Conclusions	32
3 Applicability of Satellite Radar Imaging to Monitor Levee Conditions	35
3.1 A Review of Existing Levee Monitoring Techniques	36
3.2 Methodology	37
3.2.1 Basic concepts of Interferometric Synthetic Aperture Radar (InSAR) .	37
3.2.2 Time-series processing.	38
3.3 Characteristics, Quality and Applicability	40
3.3.1 Satellite characteristics.	40
3.3.2 Observation characteristics	44
3.3.3 Applicability on case studies	46

3.4	Performance Assessment	47
3.4.1	Sensitivity of deformation vectors	49
3.4.2	Decomposition of deformation vectors	50
3.5	Discussion on the Potential of Using Satellites for Levee Monitoring	52
3.6	Key Conclusions	56
4	Sub-seasonal Levee Deformation to Enhance Flood Protection	59
4.1	Soil Behavior under Wetting and Drying Conditions	60
4.2	Methodology	60
4.2.1	Study area: Delft, the Netherlands	61
4.2.2	Soil data	61
4.2.3	Meteorological data	61
4.2.4	Deformation data from PS-InSAR processing	61
4.2.5	Deformation modeling: vPT-model	62
4.2.6	Model parameter estimation.	63
4.2.7	Hypothesis testing: Overall Model Test (OMT)	64
4.3	Modeling the Swelling and Shrinkage Behavior of Levees	64
4.3.1	Application of the vPT deformation model.	65
4.3.2	Relation with soil types of the levee	67
4.4	Enhancing Flood Protection	70
4.4.1	Deformation estimation for the levee failure at Wilnis, the Netherlands.	70
4.5	Key Conclusions	71
5	Anomaly Detection along Levees	73
5.1	Detecting Anomalies in Levee Behavior	74
5.1.1	Modeling the normal behavior and anomalies	74
5.1.2	Multiple Hypothesis Testing (MHT)	76
5.1.3	Procedure for detecting anomalies using MHT.	78
5.2	Application on Case Studies.	80
5.2.1	Study area: Delft, the Netherlands	80
5.2.2	Study area: Grave, the Netherlands.	82
5.3	Discussion and Key Conclusions	85
6	Conclusions and Recommendations	89
6.1	Conclusions.	89
6.2	Main Contributions.	93
6.3	Future Research.	94
	Appendix	97
A	Test Set-up: Eemdijk Experiment	99
A.1	The use of corner reflectors	99
A.2	The design of the experiment	100
A.2.1	Installation of the corner reflectors	100

A.3	Data processing	101
A.4	Initial results	104
A.4.1	Identifying the signals	104
A.4.2	Measured reflection strength and deformation	105
A.5	Conclusions and Recommendations	107
	References	111
	Curriculum Vitæ	125
	List of Publications	127

1

INTRODUCTION

1.1. MOTIVATION

The design and maintenance of reliable flood defense systems is hindered by an insufficient understanding of their dynamic behavior and the mechanisms of their failures. In this research, we demonstrate the importance of collecting and analyzing historical failure events to gain new insights, and show how satellite technology can both provide useful information on the behavior of flood defenses and be applicable for early warning systems.

1.2. RESEARCH RATIONALE

FLOODS are one of the most common and catastrophic natural hazards, leading to destructive socio-economic consequences for populations across the world [1–3]. The impact is devastating: floods have resulted in more than 550,000 deaths between 1980 and 2017 [3–5], and the estimated worldwide damage has reached more than \$40 billion annually [6]. On average, 250 million people per year are directly affected by this ubiquitous natural phenomenon [6, 7]. Since the last decades of the 20th century, the damage costs attributed to floods have seen more than a tenfold increase, with the latter bound to grow throughout the 21st century [8]. Likewise, population growth and economic development in flood-prone areas have also increased substantially over the last decades and are foreseen to increase further in the forthcoming periods [1, 9]. As the natural causes of floods are directly linked to a changing climate, an increase in excessive rainfall coupled with melting of glaciers and sea level rise will lead to more intense and frequent floods in the near future [10–12]. Recent projections commonly agree that, by 2050, the mean sea level is expected to rise 20–30 cm [13–17]. As a result, approximately 300 million people are likely to be exposed to flooding at least once a year [12]. This will greatly challenge the state and robustness of the current flood risk management systems across the world, mostly where populations are more at risk, such as in coastal and low-

lying areas. Flood defenses are one of the fundamental measures to manage flood risk. These hydraulic structures have the primary objective to protect land against flooding along the coasts, rivers, lakes and other waterways [18]. The protection capacity of these structures against future conditions highly relies on their continuous maintenance and improvements.

In these circumstances, levees form a significant part of the existing flood defense systems to provide flood protection [19]. A levee (also referred to as dike or embankment) is defined as a water retaining structure consisting of soil (fully or partly) with sufficient elevation and strength to retain the water under extreme circumstances [18]. Levees can fail when their ultimate limit state is exceeded causing them no longer to fulfill their water retaining function [20]. The most commonly encountered levee failure mechanisms are given in Figure 1.1. Depending on the natural or man-induced driving

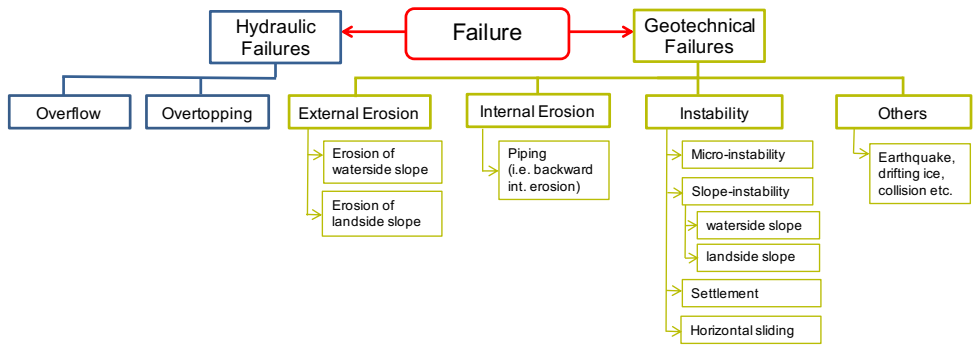


Figure 1.1: Overview of the most common levee failure mechanisms (e.g., see [19]).

mechanisms, levees can fail due to (a) hydraulic failures (e.g., overtopping) as a result of insufficient height, and/or (b) geotechnical failures (e.g., instability, erosion) as a consequence of insufficient strength [19, 21]. A specific failure mechanism can also lead to an initiation of a breach on the levee at a later stage. Failures of levees may cause significant damage, fatalities or substantial economic, social and environmental losses with the risk being highest in densely populated areas [22, 23]. Moreover, rapid economic and demographic growth, in combination with changes such as sea level rise, extreme weather conditions, and land subsidence increase the potential impact of a levee failure. Well-known examples from the history, such as the 1953 floods in the Netherlands, the failure of the levee system around New Orleans, USA (2005) and the recent floods in Thailand and Japan (2011) and Germany (2013), have shown how such failures can have catastrophic consequences.

Despite the critical function of levees in flood safety, little is known of what determines their structural behavior in time and what are the underlying causes of their failures. Although extensive research on individual mechanisms and processes of failures has been performed over decades, still large uncertainties exist regarding different aspects, such as the composition of levees, their behavior during critical conditions and the modeling of their failures [24]. The majority of these studies is performed with lim-

ited data from failed levees, since most of the evidence is washed away during real failures. In addition to these uncertainties, there is a limited knowledge on spatial patterns of levee failures and breaches, such as the expected density of breach occurrence per individual flood events. The availability of sufficient data is essential to achieve better insights into these uncertainties and thus to develop more accurate methods for managing flood risk. In addition to that, in most cases, periodical inspections meant to assess the overall conditions of the levee systems have not been able to foresee failure processes. For instance, a survey of levee failures during the 2002 flood in Elbe region, Germany [25] and an analysis for the last 10 years of levee failures in England [26] showed that the levees failed at sections that were considered to be safe according to conventional levee assessments [27]. Hence, many problems cannot be detected by conventional methods in advance, making additional and innovative techniques desirable. These techniques are most beneficial if they are applicable on a wide geographical scale with good precision and require less resources.

1.2.1. LEARNING FROM THE PAST

In order to reduce the uncertainty involved in levee failures, there is a need to better understand the different levee behavior processes and if possible, to identify the critical factors contributing to a failure mechanism. A better insight regarding levee parameters, such as deformation, geometry, and soil properties, will improve the estimated response and capacity of the structure in case of an extreme event¹ [28]. However, the causes and mechanisms of levee failures may be multiple, complex and interrelated. Analyzing these conditions requires a global consideration of failures by putting into perspective all parameters and their relations.

One of the possible ways to significantly improve our understanding of levee failures is to analyze historical failure events, large-scale experiments and other performance observations. Since large-scale experiments are challenging and costly and the spatial variability in subsoil typically plays an important role, historical levee failures can be used to provide insights into the real failure processes and conditions. This highlights the need for an international, open access knowledge platform to systematically collect and share data on levee failures. An efficiently structured database, that stores a wide range of data type, e.g., from general information on flood events to detailed information on failure processes, can provide valuable material to the scientific community as well as to the public and private sectors in the field of flood safety. The insights that can be achieved by analyzing such data could contribute not only to advance understanding of levee failures and their mechanisms, but also to improve failure and breaching models.

Individual efforts have been undertaken to document flood defense failures after disasters, but no systematically gathered large-scale, open access dataset is currently available for thorough scientific research. The databases identified for levees, e.g., [29–31], include little detailed geotechnical or hydraulic information that would allow more in-depth analysis of historical failures. This limits the use of these databases for detailed analysis of the failure processes, such as the development of empirical levee breach parameters, or the validation and calibration of process-based models.

¹Despite the randomness of the nature, e.g., water levels or wave heights.

1.2.2. LEARNING FROM THE PRESENT

Apart from learning from past failures, being able to identify if, where, and when a failure would suddenly occur is an important aspect to consider with respect to safety. External parameters, such as meteorological conditions (especially drought), tidal changes, waves, groundwater and surface water level, and traffic, may affect the levee deformation behavior and strength significantly. Prior to a levee failure, before any sign of a geotechnical failure (see Figure 1.1) becomes visible, the levee may have shown subtle degrees of deformations which could indicate a failure being imminent [23, 32, 33]. The ability of detecting these behaviors, which may happen within a longer time span than the process of a failure itself (i.e., from days to months), can be interpreted as indicators of potential weak spots. Therefore, improved methods to detect small deformations of levees at an early stage are likely to give a significant contribution to levee safety assessment.

Although early detection of these deformation indicators could facilitate on-time levee assessment and maintenance before a failure occurs [34], frequent monitoring of the condition of levees is challenging. Current conventional levee inspection methods mostly rely on expert observers, which result in infrequent, qualitative and labor-intensive assessments [33, 35–37]. Common remote sensing (e.g. LiDAR, thermal infrared) and in-situ monitoring methods (e.g. leveling, GNSS, creep/strain meters) are also costly and time-consuming, and are, therefore, usually only applied to locations considered to be at high risk after a visual inspection. Hence, especially in countries with extended flood defense infrastructure, such as the Netherlands, China, UK, and US, there is a need for innovative and cost-effective techniques to monitor levee conditions for larger areas. These techniques could be most beneficial if they contribute to detecting which locations are most prone to sudden failures and estimating far in advance whether a levee would fail. This can be done by analyzing the response of a levee under normal loading conditions in order to identify locations at risk of failing during extreme loading conditions, such as storm, high river discharge or drought.

However, understanding and monitoring levee behavior over an extended area, requires the availability of frequent deformation data with high resolution, which are not provided by current inspection methods. In recent years, satellite radar imaging, in particular using interferometry (InSAR) [38, 39], has become an efficient tool to monitor the surface displacements. The technique holds a large potential to monitor the condition of levees with millimeter-level precision, anywhere on the planet. It instantaneously provides millions of observations with meter-level spatial resolution, supported by revisit times in the order of days, at very low costs compared to conventional surveying methods. It has been successfully applied on urban areas [40], railways [41], dams [42], highways [43], landslides [44], tectonic movements [45], and land subsidence [46].

This study focuses on observing and analyzing the three main phenomena of levee deformation on different time scales using InSAR technology (1.2). First, long-term (i.e., inter-annual) levee deformation, such as the subsidence of the levee occurring over a period of years, mainly depends on the type and composition of the soil and can be considered irreversible. Second, levees show short-term (i.e., sub-seasonal) deformation, due to varying loading conditions, such as changing water levels, precipitation, and temperature, occurring over periods of days to weeks depending on the soil and loading con-

ditions. Lastly, levees can be subject to instantaneous deformations, such as irregularities or sudden changes in the deformation behavior. This also includes a sudden failure when the load on the levee exceeds its strength, usually in a time scale of hours to days. A crucial safety question is if and when such a failure may happen. Inter-annual levee deformation has been monitored by several studies [33, 47, 48] which demonstrated the potential of using satellite radar imaging to assess levee safety. However, the technique has not yet been explored by considering these three different deformation behaviors for the purpose of overall levee safety. Thus, the technique can be used to understand the behavior of levees under normal loading conditions, and also to detect anomalous deformations at an early stage, which is likely to give a significant contribution to levee safety assessments.

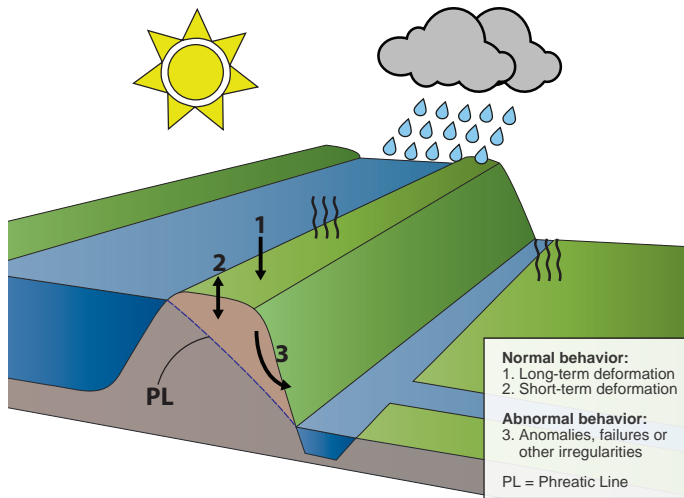


Figure 1.2: Three main phenomena on the levee behavior. Phreatic line (PL) is defined as the top flow line of the saturated soil mass where it is separated from the unsaturated soil mass.

1.2.3. TOWARDS THE FUTURE

Both learning from past failures and present levee behaviors, as explained in the previous sections, can be integrated into the management of flood risk in order to improve the efficacy of its different phases. Flood risk management is defined as an integral approach aiming to reduce the likelihood and/or the impact of floods by systematically incorporating measures, such as prevention, protection and preparedness [49]. An illustration of a general approach to flood risk management including its most important steps is given in Figure 1.3.

As a sub-category of flood risk management, the assessment of flood risk is commonly performed by following sequential steps that are identified as (a) definition of the system and the scope; (b) qualitative and quantitative analysis of the given situation, such as assessing the boundary conditions, probability of failures, and estimation

of damage and risk involved; and (c) evaluation of the calculated risk based on cost-benefit analysis [18, 19]. In addition to these steps, flood risk management incorporates a decision-making phase (i.e., risk reduction and control) aiming to reduce the risk by applying necessary measures, such as reducing load, consequences and probability of failure. This step also includes assessing the measures for risk control, for example, monitoring, inspection or maintenance [18]. Since applying measures for risk reduction and control could lead to changes in the definition of system, these steps are usually carried out multiple times until the system reaches an optimal design, i.e., acceptable risk at a low cost [18].

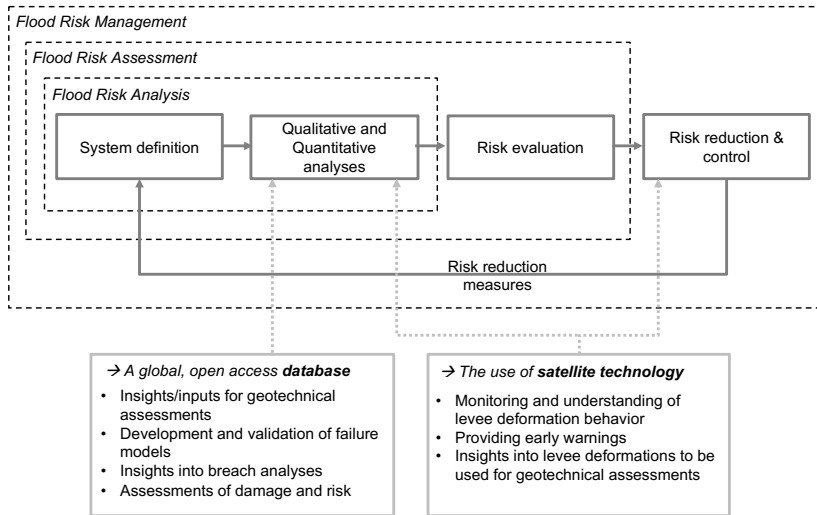


Figure 1.3: An illustration of a general approach to flood risk management with the possible contributions to its different phases by learning from past and present data (adapted from [18, 19]).

Understanding levee deformation behavior and levee failures will possibly contribute to the different phases of flood risk management. The insights obtained by analyzing a large amount of historical data from a database are expected to provide valuable inputs for qualitative and quantitative analyses of the risk, such as improvement of failure models, geotechnical safety assessment of levees, damage estimates and risk calculations. Besides, the use of satellite technology for levee safety can support not only qualitative and quantitative analyses, but also the risk reduction and control steps of flood risk management. On one hand, the understanding of how levees deform in time will offer valuable information to geotechnical assessments by reducing the uncertainties in their structural behavior. On the other hand, the application of satellites for levee deformation monitoring is expected to give a contribution to activities concerning risk reduction and control, such as in the development of early warning systems for detecting anomalies along the levees.

1.3. RESEARCH OBJECTIVES

In this research, a global approach is adopted for mitigating the potential impacts of floods by combining the lessons learned from the past and the expertise acquired from the present information on levee conditions. The overarching aim of this study is to demonstrate how the analysis of historical failure events and the use of satellite radar technology can contribute to the safety of flood defense systems. To enable this, the **research objective** is to improve understanding of levee deformation behavior as well as levee failure patterns by investigating both historical failures and satellite observations. Particularly, the contribution of this research is to provide insights into levee failure mechanisms and breach characteristics, and also to explore the use of satellite technology for understanding levee behavior and for providing early warnings over the entire levee structure. These aspects are formulated by three research questions given below.

Research question – 1: How can we improve understanding of levee failure mechanisms by analyzing historical failures in order to support flood risk management?

In order to collect and share valuable data on the historical failures, a large-scale, open access levee performance database, hereafter called International Levee Performance Database (ILPD), will be developed as a searchable inventory of information about levee failures. Based on the latest version of the database, a macro-scale analysis of levee failures will be performed, in order to improve understanding of their patterns and to outline the most common failure mechanisms at the global- and event-level. Particular focus will be given on expected breach characteristics of failures for different flood events. Hence, this part of the thesis aims to introduce a global information-sharing platform for facilitating research on levee failures, and to provide insights on levee behavior and breach characteristics for improving flood risk assessments.

Research question – 2: To what extent can satellite radar interferometry provide a continuous monitoring for levees and give indications of potential failures?

Considering the historical situation that is investigated in the previous part, the use of satellite technology will be explored to complement existing approaches for assessing long-term (e.g., inter-annual) levee deformation behavior in a fast, systematic and cost-effective way. This part of the thesis aims to provide a comprehensive overview of the state of the art in using time-series InSAR for systematic levee deformation monitoring, and to discuss the applicability of the technique, supported by case studies on levee monitoring in the Netherlands. Technical aspects with respect to levee monitoring using SAR technology will also be elaborated such as estimating deformation in different directions, satellite characteristics, and precision.

Research question – 3: How can the observed deformations of levees be interpreted in order to characterize levee patterns and detect anomalous behaviors under dynamic loading conditions?

To further understand levee behavior in normal conditions (Figure 1.2), the short-term (e.g., sub-seasonal) patterns of levees will be analyzed in greater detail. Their swelling and shrinkage due to variation of the loading conditions will be predicted using continuous levee deformation measurements obtained with Persistent Scatterer InSAR (PS-InSAR). Later, the results will be used to assess how deformations can be related to the geohydrological properties and the safety of the levee. After analyzing long-

and short-term deformation behavior, hence understanding the levee behavior in normal conditions, a prototype early warning method using a probabilistic approach will be presented for post-processing of PS-InSAR results in order to find deviations from these expected behaviors. This part of the thesis aims to improve the detection of anomalous levee responses which contributes to the development of reliable early warning methods using continuous deformation monitoring over the entire levee infrastructure.

1.4. THESIS OUTLINE

The structure of the thesis is outlined in Figure 1.3. The first research question is treated in Chapter 2, the second one is addressed in Chapter 3, while Chapter 4 and Chapter 5 cover the research question 3. The introduction (Chapter 1) provides background information to the research aim and the content. Chapter 2 focuses on the historical levee failures and is based on a journal article published in *Water* [50]. Chapters 3-5 explore the use of time-series InSAR for systematic levee deformation monitoring. Chapters 3 and 4 focus on understanding long- and short-term levee deformation behavior in normal conditions and they are built around two journal articles published in *Journal of Flood Risk Management* [51] and in *Scientific Reports* [52]. Whereas, Chapter 5 addresses the detection of deviations from this normal behavior, i.e. anomalies, which may be early indicators of a potential hazard. Chapter 6 concludes the thesis by summarizing the main contributions, suggesting possible directions for future research and providing recommendations.

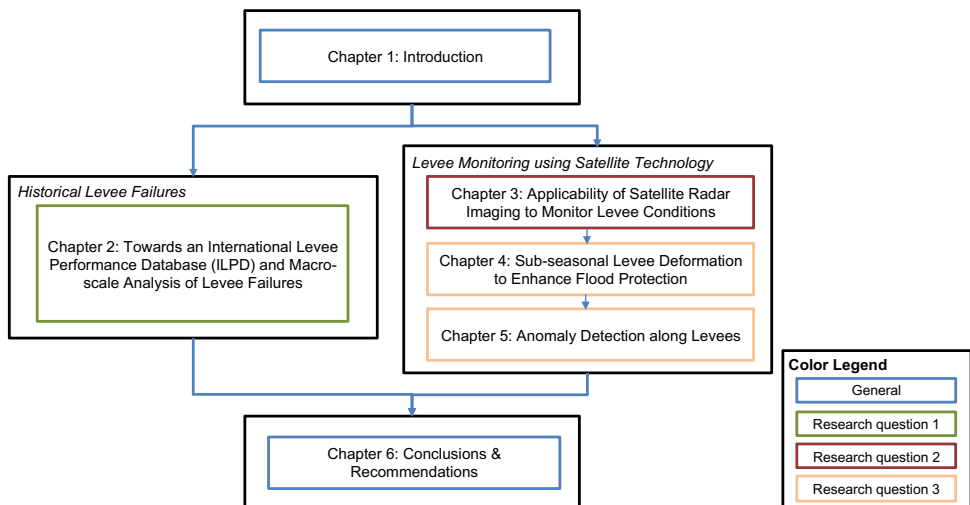


Figure 1.4: Visual outline of the thesis.

1.5. THE SAFELEVEE PROJECT

This research is performed as a part of the SAFElevee project which aims to improve the reliability of flood defense systems by a better understanding of their failure mechanisms. The research objectives of the project are (a) to improve the understanding of failure mechanisms and breaching of flood defense systems, (b) to enhance reliability analysis and design of safe levee systems, and (c) to provide systematically collected datasets for future scientific research. The SAFElevee project is structured within three research projects which are described below.

1. Understanding levee failure patterns: This research, which is covered in this thesis, focuses on (a) monitoring and understanding levee deformation behavior in time by using satellite technology, (b) developing an international levee performance database, (c) investigating historical levee failures and breach characteristics.
2. Hindcasting of individual levee failures: The second research project focuses on a more detailed analysis and hindcasting of individual levee failures for which sufficient data is available. Geotechnical and probabilistic analysis is used to improve our capability to model these events, also taking into account heterogeneity and uncertainty in soil conditions, e.g. see [53].
3. Breach growth modeling: The third research project addresses the breaching of levees and aims to develop more accurate models and theories of breach initiation and formation. It utilizes information from historical breaches and large-scale field experiments, e.g. see [54].

2

TOWARDS AN INTERNATIONAL LEVEE PERFORMANCE DATABASE (ILPD) AND MACRO-SCALE ANALYSIS OF LEVEE FAILURES

The introduction highlighted that our understanding of levee failures can be significantly improved by analyzing historical failures. Despite extensive research on individual mechanisms and processes of failures, still large uncertainties exist regarding different aspects, such as the composition of levees, their behavior during critical conditions and the modeling of their failures. A recognized challenge is that most of the analyses are performed with limited data from failed levees, since systematically gathered, open access, large-scale datasets are currently limited for thorough scientific research.

In this chapter, we introduce the International Levee Performance Database (ILPD) to assist sharing of data on levee characteristics, failure mechanisms, geotechnical investigations, and breach processes. This ranges from large-scale experiments including time-dependent data on hydrodynamic loading conditions to more general level data on post-flood failure investigations including video and photo footage. Moreover, we present a comprehensive overview of the first version of the ILPD (containing more than 1500 cases) and perform a macro-scale analysis of the available data on levee failures and breache characteristics.

The objectives of this study are (a) to facilitate research on levee failures by developing a global, well-structured, open access database and (b) to demonstrate the potential of the database in providing insights on levee behavior and supporting flood risk assessments based on historical records. Section 2.1 gives an overview of the example databases in the field of flood risk, dam and levee safety. In Section 2.2, we elaborate

Parts of this chapter have been published within [50].

on the purpose and structure of the ILPD and establish a terminology which is used for describing levee failures. In Section 2.3, we provide basic statistics on the currently (October, 2019) available ILPD data to illustrate the overall characteristics of the database. Furthermore, as an example for the use of a sub-dataset from the ILPD, we investigate the flood events in Germany, occurred in 2002 and 2013, and examine breach characteristics of over a hundred failures in order to outline the most common influence factors at an event-level. We also introduce two breach density parameters, which are related to expected amount of levee breaches and their width, intended to be used for the risk assessment of levees. Finally, in Section 2.4, we highlight the operational obstacles and strategies to further improve the ILPD and discuss the use of event-level analysis for risk assessments.

2.1. AN OVERVIEW OF THE EXISTING DATABASES

Flood defense failures can lead to major catastrophes in terms of loss of life and economic damage. Improved flood defense measures are required to safeguard flood-prone areas from floods in order to save many lives and avoid considerable damage costs. Aiming to prevent this, flood-prone countries make substantial investments in activities related to monitoring, maintenance and reinforcement of flood defenses. However, our understanding of levee failure mechanisms is still limited. Despite extensive research on individual mechanisms and processes of failures, the composition of levees, their behavior during critical conditions, and the modeling of their failures still remain uncertain [24]. There is a need for better validation and calibration of models or, in other words, better insight in their uncertainty.

Since the full-scale experiments are challenging and costly and the spatial variability in subsoil typically plays an important role, historical levee failures can be used to provide insights into the real failure processes and conditions. However, most of the analyses are performed with limited data from failed levees, since most of the evidence is washed away during real failures. This highlights the need for systematically and globally collected data and a sharing platform not only to advance understanding of levee failures and their mechanisms, but also to improve failure and breaching models. These insights could eventually contribute to the development of accurate techniques for innovative designs of flood defense systems, and support decisions and actions affecting levee safety [23].

Several databases and data collections already exist in the field of dam safety (Table 2.1). Apart from general information on the available dams around the world [55, 56], these databases may have a particular focus on dam breaches [57, 58], landslide dam failures [59], large dam failures [60], internal erosion of dams [61], dam incidents [62], and loss of life for risk assessments [63, 64]. Most of these databases include general information about the dams, such as geometry, type, reservoir capacity, and in some cases information on their failures, e.g., time to failure, breach information, peak discharge. Databases are also used for the analysis of accident statistics in other fields of Civil Engineering. Typical examples include global reports on natural disaster impacts and frequencies [8], remote sensing-based flood information [65], or data on flood protection standards [66].

In the field of levee safety, there is a small number of open access databases with

Table 2.1: An overview of the example databases in the field of flood risk, dam and levee safety.

Database / Reference	Field of application	Number of cases	Failures included	Data type ^a	Accessibility	Active (Y/N)
Peng and Zhang [59]	Landslide dams	1044 cases	Yes	General information	Open access	No
Utah State University database [63]	Dam failures	174 cases	Yes	General information with a particular focus on loss of life data for dam safety risk assessments	Open access	No
Flood Protection Standards (FLOPROS) database [66]	Flood protection standards	179 cases for design layer 68 cases for policy layer	No	Detailed information on design and policy standards (not on the actual flood defenses or their failures)	Open access	No
Association of State Dam Safety Officials (ASDSO) database [62]	Dam incidents	14 detailed case studies	Yes	Detailed information such as photos, videos, general information and lesson learned, reports, failure mechanisms	Open access	No
United States Bureau of Reclamation (USBR) database [64]	Dam failures focused on loss of life	60 cases	Yes	General information with a particular focus on loss of life	Open access	Yes
National Performance of Dams Program (NPDP) database [55]	Dam	>10,000 cases but few failure cases	Yes	General information including emergency plan, population at risk, storage capacity, failure mech., consequences, lessons learned	Open access	Yes
Dam Accident Database [56]	Dam failures	900 cases	Yes	General information, including some detailed data (hydrographs, reports, photos, etc.)	Not publicly available	No
Dartmouth Flood Observatory of Large Floods [65]	Remote sensing-based flood information	4700 flooding events	Yes	General information including duration of the event, loss of life, damage, severity, effected area, magnitude of the flood, etc.	Open access	Yes
The International Disaster Database (EM-DAT) [8]	Disaster, including flooding	>10,000 cases	No	Detailed information on the disaster related data	Open access	Yes

(Continues on the next page)

Table 2.1 (cont.): An overview of the example databases in the field of flood risk, dam and levee safety.

Database / Reference	Field of application	Number of cases	Failures included	Data type ^a	Accessibility	Active (Y/N)
Froehlich [58]	Dam failures	43 cases	Yes	General information on the breach formation	Not publicly available	No
Foster et al. [60]	Large dam failures	136 cases	Yes	General information	Not publicly available	No
Xu [57]	Dam failures	1443 cases	Yes	Detailed information	Not publicly available	No
ERINOH database [61]	Internal erosion of dams and levees	120 failure cases	Yes	General information, also including some detailed data (hydrographs, breach info, reports, photos, maps, etc.)	Not publicly available	No
van Baars and van Kempen [29]	Levee failures	337 cases	Yes	General information	Not publicly available	No
Italian Levee Database (INLED) [67]	Levee information	Currently, a few cases	Yes	General information	Not publicly available	No
Danka [30]	Levee failures	1004 cases	Yes	General information	Open access	No
Department of Water Resources (DWR) levee breach database [31]	Urban and non-urban levee failures in California	215 cases	Yes	General information	Open access	No
U.S. Army Corps of Engineers database [68]	National levee information of USA	> 10,000 cases (no separation for failures)	Yes	Detailed information on levee system evaluation and inspection, flood risk communication, flood plain management and risk assessment	Open access	Yes

^a General information includes geometry, construction time, type, failure mechanisms, capacity, material, peak outflow rate, breach information and also qualitative information.

some information available, see Table 2.1. Some online databases provide general information on levees at a regional [31], or at a national level without a particular focus on their failures [67, 68]. Individual efforts have been undertaken to document levee failures after disasters, e.g., New Orleans in 2005 [69, 70], Germany in 2002 [71], but no systematically gathered large-scale, open access datasets are available for thorough scientific research. In this dearth of information, some researchers have constructed data collections specifically on levee failures [29, 30]. Characteristic of these mostly table-formatted databases is that only generic information on failures is provided, e.g., general information on the levee geometry, material, breach information, failure mechanism. The databases identified for levees do not include any detailed geotechnical or hydraulic information that would allow more in-depth analysis of historical failures. This limits the use of these databases for detailed analysis of the failure processes, development of empirical levee breach models, or validation of process-based models.

2.2. TOWARDS AN INTERNATIONAL LEVEE PERFORMANCE DATABASE (ILPD)

2.2.1. PURPOSE OF ILPD

The main purpose of the ILPD is to provide a global platform for systematically collecting and sharing data on levee performances to facilitate research. Particularly, ILPD promotes (a) learning from what went wrong during past flood events to prevent floods from occurring in the future and (b) learning about how to model failure processes, and how failure mechanisms might be correlated. By facilitating this, the database can also enable the systematic validation of models and the evaluation of model accuracy. More specifically, the ILPD has been developed to provide collected datasets on:

- Actual failures during extreme catastrophic events, such as levee failures in New Orleans, USA [69], and failures during the levee construction phase;
- Failures in small- and full-scale experiments, such as levee breach experiments in the Netherlands [72];
- General investigations on the performance of flood defense systems, e.g., the case of New Orleans [73] or of the coastal floods in France [74];
- Detailed information on some earthen dam failures, as these show similarities with levee failures;
- Information on the consequences (e.g., damage, loss of life, flooded area, etc.) per extreme event.

2.2.2. THE DESIGN AND THE STRUCTURE

To allow for a wide range of data type and easy dissemination, the database is linked to a website from which data can be downloaded freely (leveefailures.tudelft.nl). All information stored in the ILPD is open access and sources are automatically provided along with the data upon downloading from the database.

Some extreme events, like Hurricane Katrina in 2005 or the 1953 floods in the Netherlands, caused multiple levee failures at different locations. To capture this, data is structured by events and failures, each associated to a unique ID's in the ILPD. One event can consist of several individual failures, each containing specific data. The failure cases which are clustered in the same event are either caused by the same hazard event or are part of the same experimental program. This way, data on each specific levee failure adds to the understanding of the real failure processes, whereas information on the overall consequences, such as total damage or loss of life, can be linked to events.

The ILPD has a three-level structure with increasing degree of detail. The first level (Level.1: Metadata) provides general information on individual failure cases as well as on flood events in a table-based format (exportable to .csv files), for example historical levee failures in Hungary provided by [30]. This generic qualitative and numeric data may also include information on the consequences, such as total damage, loss of life and flooded area. Level.1 data mainly consists of information on the levee (geometry, location, material, type, etc.), flow boundary conditions (return periods, max. water level, peak flow discharge, etc.), breach (width, invert level, peak discharge, etc.), soil properties, management organization, documentation (video, photo, etc.) and references. The second level (Level.2: Intermediate) includes well-documented information on historical failures, such as loading conditions and soil profiles, and modelling results; or hindcasted information based on field investigations of actual failures (e.g., New Orleans in 2005 [70]). The detailed information aims to provide more insight into the physical processes and to facilitate rapid analysis of failures. Since every dataset contains unique information, providing detailed data in a table-based format severely limits the ease of analysis of different datasets simultaneously. Thus, a more structured format is preferred in order to support rapid analysis of data from several detailed datasets (exportable to .JSON files). Lastly, the third category (Level.3: In-depth) contains detailed information on failure processes including time-dependent data on the hydrodynamic loading conditions and geotechnical information. These dataset (exportable to .pdf/.csv files) mostly consist of experimental data, such as those provided by [75].

A screenshot of the opening page of the website is provided in Figure 2.1. The interactive map allows for navigation to all available failure cases. Each marker on the map represents the location of a failure case. Underneath, the cases pictured on the map are listed. When the case of interest is selected, basic information of the failure is presented and the media (if available) can be viewed. After selecting one or more cases, a click on the button 'Export selection' gives a pop-up window in which the type of data to be downloaded can be chosen. On the left side of the map, several filter criteria can be set. The database can be filtered based on time span, country, case study type, defense type or failure mechanism. Moreover, more filter criteria are available using the 'Add filter criterion' feature and a combination of different filter criteria can be made as well.

2.2.3. CATEGORIZATION OF LEVEE FAILURE MECHANISMS

Given that various terminologies exist for levee failure mechanisms and other related parameters, a challenge in setting up an international database is to establish a list of uniform definitions. Flood defenses are hydraulic structures whose primary objective is to provide flood protection along the coasts, rivers, lakes and other waterways [18]. A

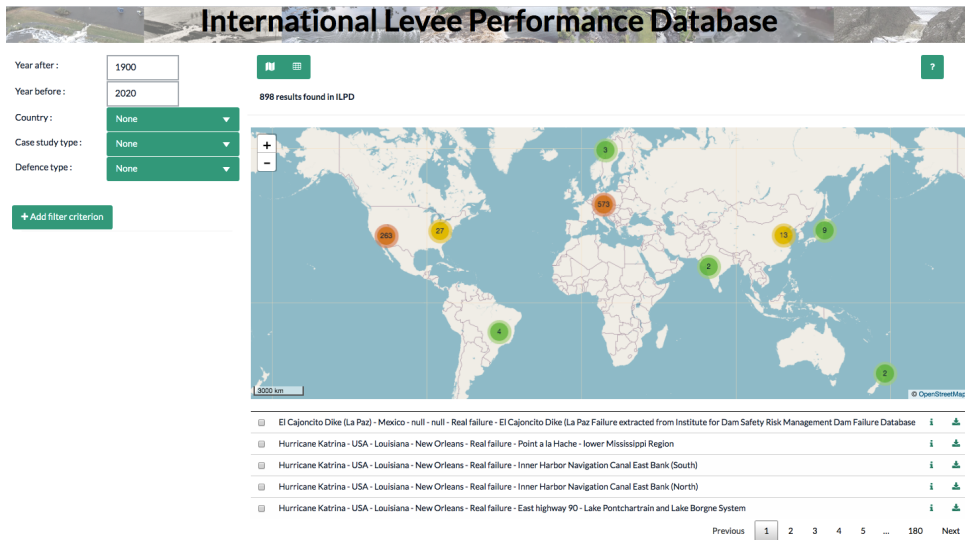


Figure 2.1: A screenshot of the opening page of the ILPD (leveefailures.tudelft.nl).

levee (also referred to as dike or embankment) is a water retaining structure consisting of soil (fully or partly) with a sufficient elevation and strength to be able to retain the water under extreme circumstances [19]. A typical levee cross section is given in Figure 2.2. Earthen levees, which form a large part of the existing flood defense systems, can be constructed with (a) homogeneous soil (*homogeneous earthfill*), (b) several soil types (*layered structure*), or (c) a hard structure (*levee-structure combination*), such as a levee with a floodwall. Examples of other types of flood defense systems are dams, dunes, storm surge barriers or temporary flood defenses.

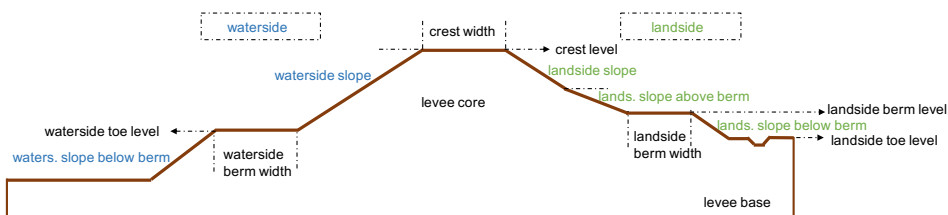


Figure 2.2: General levee cross section, showing the main elements of a levee included in the ILPD.

Levees can fail when their ultimate limit state is exceeded causing them no longer to fulfill their water retaining function [20]. The most commonly encountered levee failure mechanisms and their most common contributing factors are given in Figure 2.3 [19]. Hydraulic failures occur due to insufficient height, whereas insufficient strength leads to geotechnical failures [21]. Breaching of a levee refers to the loss of integrity or a major

geometric change [20, 76]. However, occurrence of a failure mechanism does not necessarily lead to a breach. For example, significant amount of overflow may cause severe floods without leading to a breach in the structure. Moreover, since the occurrence of the initial failure mechanism might trigger other mechanisms [21], a sequence of multiple failure mechanisms can be observed on the levee. For example, failures may be initiated with overtopping, followed by external erosion that causes a breach at the latter stage (Figure 2.3). All identified failure mechanisms are entered in the database in a chronological order.

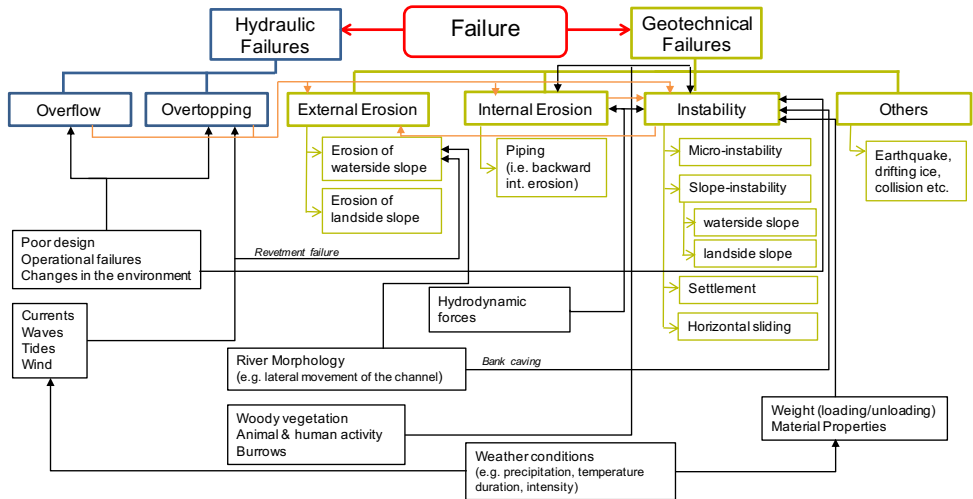


Figure 2.3: An overview of most relevant levee failure mechanisms (see Figure 1.1) and their most common contributing factors (e.g., see [19]).

The most relevant levee failure mechanisms observed in the database are defined briefly here [77].

- **Overtopping and Overflow:** Overflow occurs when still water level is higher than the crest level of the levee. Whereas, overtopping is observed when still water level remains below the crest level but waves run-up and pass the crest level.
- **External erosion:** External erosion occurs when the slope of the levee is not sufficiently resistant to the hydraulic loads, that is, when the shear stress induced by flows exceeds the critical value associated with the nature of the materials of the levee [19]. Currents and waves are the main aggravating factors of external erosion which can occur on the landside or waterside slope of the levee. Overtopping/overflow of a levee can induce major damages linked to external erosion, especially on the landside slope.
- **Internal erosion:** Internal erosion, which refers to a generic event, is initiated by hydrodynamic forces acting on soil particles within a levee foundation which are

carried downstream by seepage flow [19]. In this process, migration of material particles induced by pore pressure and flow forms channels within the foundation soils. These pipes undermine the structure of the levee and lead to failure. Internal erosion related failure mechanisms consist of: concentrated leaks, backward erosion, contact erosion, and suffusion [78]. Backward erosion, known as piping, is typically most relevant for levees. It occurs if uplift, seepage, heave and piping occur respectively. Seepage also increase the likelihood of instability because of changes to pore pressure distribution within the levee. Uplift pressure in foundation soils can generate major instability.

- **Slope-instability (i.e., instability):** Instability occurs when the forces (i.e., excess pore pressure) on a levee are higher than the shear resistance which is determined by the soil's shear strength. *Landside slope instability* occurs due to the infiltration of water into the levee body and its foundation, leading to forcing of the levee body, and decreasing shear strength of the soil. Whereas, *waterside slope instability* occurs due to sudden drawdown of the outside water level after heavy saturation of the levee body. In this situation, the pore pressures at the base of the potential slide plane stay high, while the horizontal pressure or support from the river water is reduced.
- **Micro-instability:** Micro-instability occurs when the seepage water causes the phreatic surface to rise and reach the waterside slope of a levee. The term “micro” is used to distinguish the stability problems related to this phenomenon from the slope-instability which essentially concern the whole levee body directly.
- **Settlement:** Settlement is a deformation mechanism in the vertical direction, mainly resulting in an insufficient crest height which may lead to failure mechanisms like overtopping/overflow.
- **Horizontal sliding:** Similar to instability of the landside slope, sliding occurs along the base of the levee body. In this case, the main driving force is the horizontal force of the water exerted on the waterside slope. This mechanism is typically an issue for levees which are made of relatively light material such as peat, where the effective stresses at the base are very low.

2.3. MACRO-SCALE ANALYSIS OF LEVEE FAILURES

2.3.1. GENERAL DATABASE STATISTICS

A large number of failure cases are collected all around the world and their basic statistics are reported in this section to provide an overview of the characteristics of the database. Currently (October, 2019), the ILPD includes 1572 failure cases of which 1538 are the failures of flood defenses occurred in different time periods, and 34 of them are full- and small-scale experiments collected from different countries (Figure 2.4a). The available information mainly concerns the failures of levees (1418 cases) and levee-structure combinations (14 cases) occurred along rivers (89%), coasts (10%) and canals (1%), but also of some earthen dams (106 cases) due to their similar composition to levees. The majority of the levee failures before 1900s mostly occurred in the Carpathian Basin in

Hungary, as reported by [30, 79], but these only contain generic information. The other cases reported in the ILPD, occurred in the last 100 years, are mostly from Germany, the Netherlands, USA, UK and Czech Republic (2.4b). It is noted (and further discussed in Section 2.4) that the geographical and temporal distributions shown in Figure 2.4 only represent the data currently included in the database.

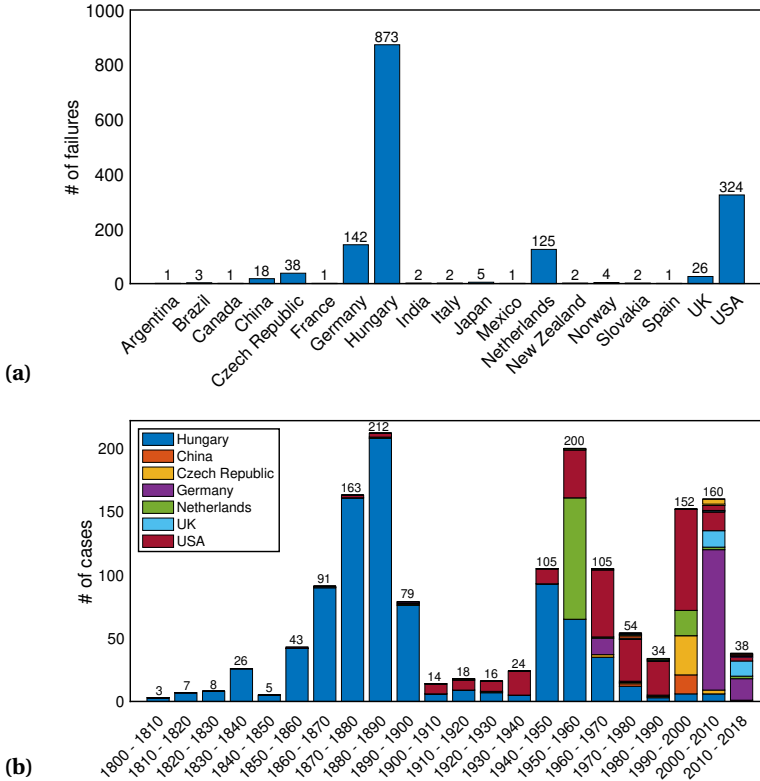


Figure 2.4: Statistics on the failures (a) per country, (b) per time period entered in ILPD.

Most failure entries in the database contain general information (Level.1: 1498 cases), such as levee and breach characteristics. As an example, Figure 2.5 shows that the crest height of the failed levees, which is defined as the differences between the toe level and the crest level, varies mostly between 1-5 m, whereas the crest width is in the range of 2-5 m. The database also includes more detailed information on the Level.2 (59 cases) and the Level.3 (14 cases) data.

Most of the events in the database are associated with single failures. However, 38% of the failures occurred during events (65 in total) with more than one failure. Examples for the documented events with the large number of breaches are in Germany (2002) with 111 failures, Netherlands (1953) with 97 failures, and Czech Republic (1997) with 33 failures.

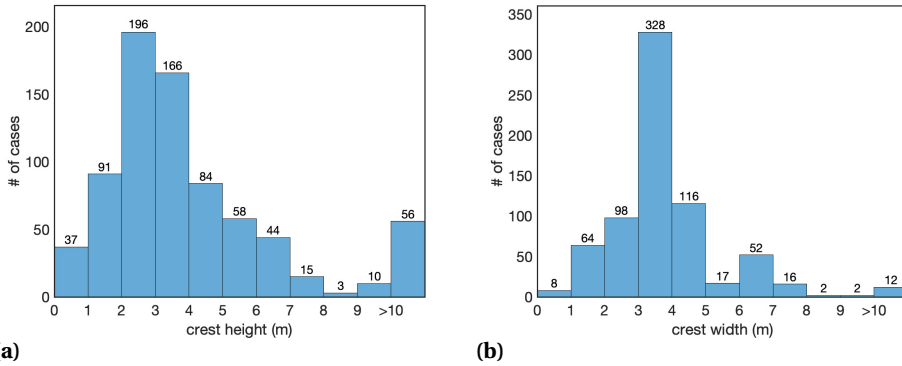


Figure 2.5: Statistics on the failures (a) per country, (b) per time period entered in ILPD.

FAILURE MECHANISMS

Analysis of the identified failure mechanisms within the collected cases in the database (Figure 2.6a) shows that more than half of the failures, of which their causes are known, occurred due to external erosion (61.5%), internal erosion (16.8%), instability (14.2%), overflow/overtopping (2.5%). Besides, the rest of the failures were due to other causes (4.7%). It is noted that excluding the Hungary dataset [30], which forms the majority of the database, does not significantly affect this distribution (Figure 2.6a).

A comparison between observed failure mechanisms for levees and earthen dams (Figure 2.6b) reveals that external erosion of the slope is more likely to occur in levees. This can be explained by the fact that water level and discharge in rivers, as well as currents and waves in seas, are mostly affected by meteorological and hydrological conditions which are more uncertain than for dams. Whereas, water levels in the reservoirs behind dams are generally more controlled. Moreover, the reason for a more frequent occurrence of internal erosion in earthen dams is associated with the higher hydraulic head differences due to the larger size of dams.

Levee breaching was observed for most of the failure cases that are entered in ILPD. Failures that did not lead to a breach at the later stage were mostly due to overflow/ overtopping (23 cases). Information on the breach characteristics, given in Figure 2.7, shows that there is a considerable variation in breach depth and width values. Previous studies on breach models reveal that, under certain conditions, breach depth and width are correlated during some of the breach development stages [72, 80]. However, breaching is a complex process that depends on many different factors (e.g., structure type, loading conditions, soil characteristics, etc.), thus the relation between breach depth and width may not always be explained by a simple relation model (Figure 2.7c).

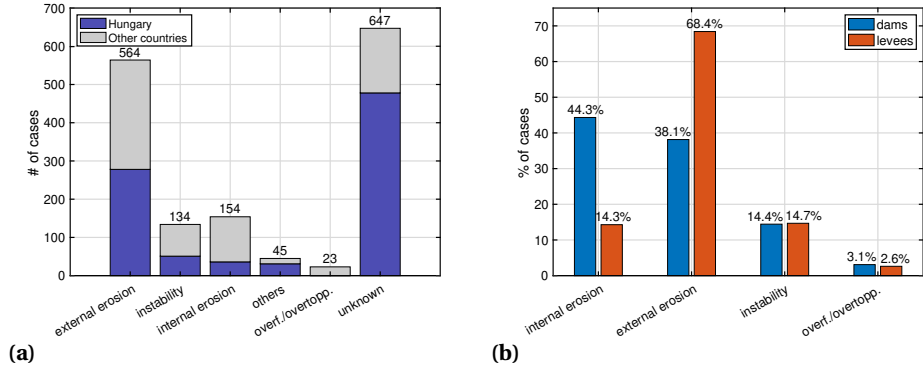


Figure 2.6: Statistics on (a) the observed failure mechanisms in ILPD (b) a comparison between earthen dams and levees for the most common failure mechanisms.

2.3.2. INVESTIGATION OF THE 2002 AND 2013 FAILURES IN ELBE REGION, GERMANY

Further analysis of data from the ILPD at the event-level can provide insights in identifying (a) typical vulnerabilities and common failure mechanisms, (b) breach characteristics, and (c) the density of breach occurrence. Although events and levee systems are diverse, this information can be used to inform and improve (local) flood risk assessments. As an example sub-dataset from the ILPD, information has been analyzed on the performance of river levees along the Elbe tributaries in Germany, which flooded in 2002 and 2013 (Figure 2.8). A general overview of the flood events is provided first, followed by a macro-scale analysis of the failures and the associated breaches.

OVERVIEW OF THE 2002 AND 2013 FLOOD EVENTS

The database reports on 111 levee failures along the Mulde and the Elbe rivers observed during the flooding event of August 2002, in Saxony and Saxony-Anhalt regions, Germany, as a result of extreme meteorological conditions, followed by extreme discharges and water levels [25]. Floods occurred mainly due to overflow/overtopping and breaching of levees at many locations. Return periods of river discharges exceeded 500 years at some tributaries of the Elbe and the return period along the Elbe and Mulde varied between 100-300 years [71, 81]. Considering that the design return periods for the flood defenses in Germany is usually 100 years, the levees along the rivers were significantly overloaded. Incomplete flood warnings, bad maintenance of flood defense structures and a lack of awareness were recognized as the weaknesses of the flood risk management [82]. The total damage was estimated around 11.6 billion euros which is the highest amount for a damage caused by a natural hazard in Germany.

Eleven years later, in June 2013, another big flood hit large parts of the same regions in Germany where multiple levee failures occurred. ILPD includes data from 17 cases of levee failures occurred in Saxony-Anhalt during this event (Figure 2.8). Return periods of discharges were estimated between 50-500 years depending on the location. In

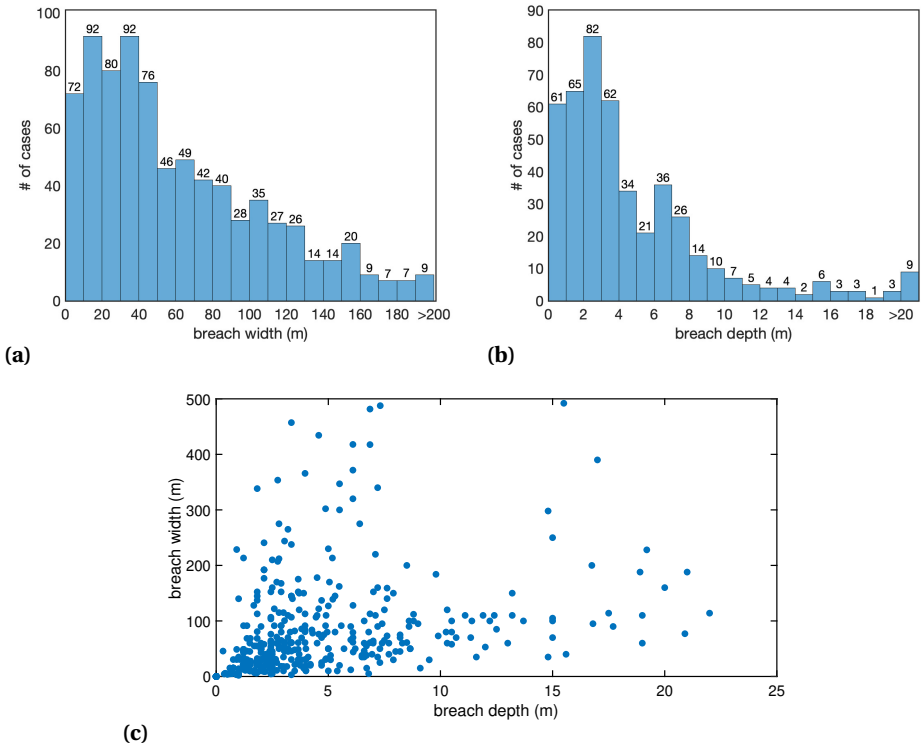


Figure 2.7: Statistics on (a) breach depth (450 cases), (b) breach width (785 cases) and (c) breach depth vs. width for (402 cases, Pearson coefficient, $r = 0.164$).

this flooding event, the most seen failure mechanism was instability. Contrary to 2002, water levels in 2013 were mostly close to the crests of the levees, hence only few overflow/overtopping cases have been observed. Due to the high peak discharge, two catastrophic levee failures occurred in the central part of the Elbe River, namely Breitenhagen and Fischbeck (right side of Figure 2.8). The first failure near Breitenhagen occurred due to instability of the landside slope which later resulted in a 150 m wide breach, and inundated an area of 80 km² [53]. Simultaneously, the second failure near Fischbeck initiated with large cracks followed by settlement of the landside slope, resulting in a 100 m wide breach within hours. The main failure type is recorded as instability induced by internal erosion.

Although both the 2002 and 2013 events were large scale floods with severe consequences in history, the main differences between the two were as follows. In June 2013, heavy precipitation (total 170.5 mm within 24 hours) in combination with high soil moisture levels, which in nearly 40% of Germany were at the highest levels since 1962 [85, 86], resulted in levee breaches and flooding mainly in the central Elbe, Mulde, and Saale catchments. Instead in 2002, extraordinary precipitation (record breaking rainfall of to-

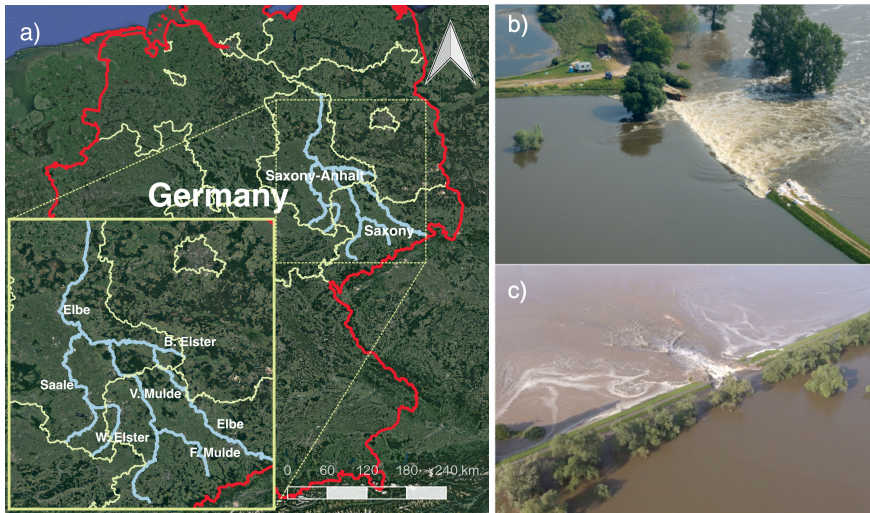


Figure 2.8: (a) Investigated rivers along the Elbe tributaries in Germany, which flooded in 2002 and 2013, (b) Fischbeck, 2013 (source: [83]), (c) Breitenhagen, 2013 (source: [84]).

tal 312 mm within 24 hours) was the main driven mechanism [82]. Although hydrological conditions and flood levels were more severe compared to the 2002 event, the cost of damage in 2013 was much lower (6-8 billion euros) and fewer levee failures occurred. This was most likely the result of more effective flood management after the 2002 event, in particular more effective disaster management and improvements in maintenance of flood defenses [82].

ANALYSIS OF THE FAILURES

After these events, data was collected on levee failure cases, including location, geometry, levee structure, subsoil structure, vegetation, breach geometry, and failure time. According to post-investigations [71, 87], different degrees of damage (i.e., damage type) have been observed on the levees. Based on the change in levee cross section, the breaches occurred in 2002 and 2013 are classified into three groups (Figure 2.9) as (a) partial failure (10%), where the breach depth was less than the crest height; (b) total failure (26%), when the crest was completely washed away; and (c) total failure with scour (41%), when, in addition to the crest, the soil beneath the toe level was also eroded. In most of the cases, the causes of levee failures were attributed to a combination of loads and local conditions (e.g., old breaches, tree roots, poor maintenance) [71].

An overview of the main failure mechanisms is given in Table 2.2. In 2002, there were more external erosion due to the overtopping/overflow cases, whereas in 2013, instability of the landside slope was the most common failure mechanism.

During the progress of these failures, multiple failure mechanisms were observed. In Figure 2.10 the occurrences of the different main failure mechanisms are associated with the initial mechanisms that have triggered them. Failure initiation mechanisms were

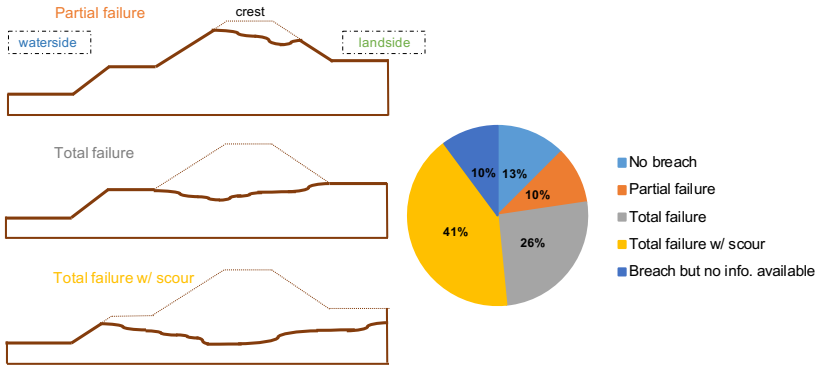


Figure 2.9: Damage degrees of the failed levees in Elbe region, Germany, 2002 and 2013 [71].

Table 2.2: Overview of the main failure mechanisms for the 2002 and 2013 events.

Main failure mechanisms	Number of cases		
	2002 event	2013 event	Total
External Erosion	59 (53.2%)	5 (29.4%)	64 (50%)
Instability	26 (23.4%)	6 (35.3%)	32 (25%)
Internal Erosion	14 (12.6%)	5 (29.4%)	19 (14.8%)
Overflow/Overtopping	9 (8.1%)	1 (5.9%)	10 (7.8%)
Unknown	3 (2.7%)	0 (0%)	3 (2.4%)
Total	111	17	128

mostly overtopping which was later followed by external erosion (58 cases), instability (21 cases), and internal erosion (7 cases). At some locations, overflow/overtopping (10 cases) occurred, but did not lead to a levee breach. For example, four different levee breaches during the 2002 event have initiated with an instability of the landside slope which slipped away partially and the remaining part continued to be eroded gradually by overflowing water (external erosion).

2.3.3. LEVEE BREACH ANALYSIS

Although various breach prediction models have been developed empirically [88–90] and physically [91–93], there is still limited insight in the characteristics of breaches during real events. In this section, it is demonstrated for the Elbe case how information from the ILPD can be used to analyze breach dimensions, including the relationship with the failure mechanisms. Another important knowledge gap concerns the number

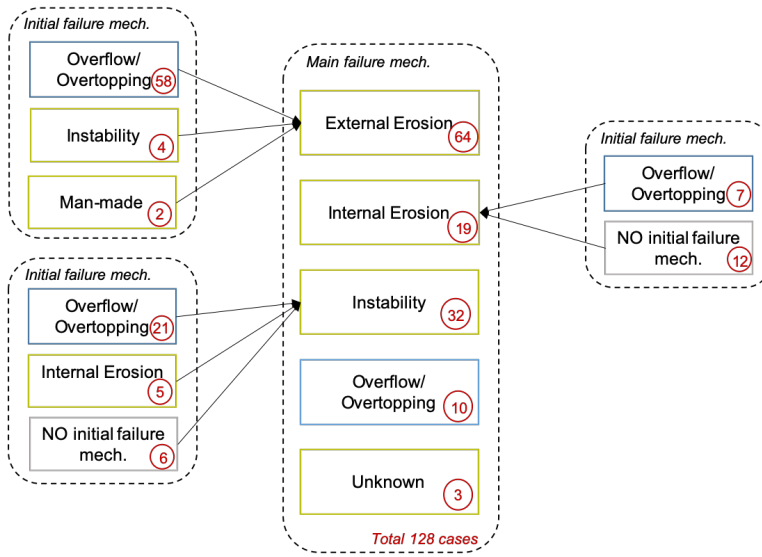


Figure 2.10: Initial and main failure mechanisms of the failed levees in the Elbe region, Germany, occurred in 2002 and 2013.

of breaches and their width (i.e., breach density) which can be expected during flood events.

ANALYSIS OF THE FAILURES

Data collected on the levee failures that occurred during these two flooding events have been used to analyze the breach parameters. Table 2.3 shows the total breach width and the average breach width per failure for each damage type, classified according to Figure 2.9. If the damage to the crest increases (from partial failure to total failure with scour), the average breach width per failure becomes also larger. Although width and depth of levee breaches are not necessarily linearly correlated (Figure 2.7c), this analysis shows that when the breach is deep, then it is more likely to be wide as well. This is also in line with some breach growth models (e.g., [72]) which predict a lateral and vertical erosion in the later stages of the breaching process.

Table 2.3: Breach width analysis per damage type, Germany 2002 and 2013.

Damage type	# of cases	Total breach width	Avg. breach width per failure
Partial failure	14	466 m	33 m
Total failure	33	1740 m	53 m
Total failure w/ scour	52	3901 m	75 m

In order to further analyze the breach characteristics of the failures, the relation between breach parameters and failure mechanisms is assessed. First, the ratios between breach depth and crest level (i.e., relative breach depth) are compared with the breach width per main failure mechanisms (Figure 2.11a). It can be observed that, by normalizing the breach depth (as *breach depth / crest level*), the breach width is also larger for the failures with total scour. Moreover, the main failure mechanisms of most of the large breaches are observed as instability or internal erosion. Second, a comparison between breach surface (as *breach depth × breach width*), and geometry of the levees (i.e., cross section area) is given in Figure 2.11b per failure mechanisms. The levee surface could affect the breaching in different ways. A larger levee is associated with a larger hydraulic head (more forcing) but would also require more erosion during breaching (more resistance). Figure 2.11b shows that levees with large cross sections tend to have larger breach surfaces. Furthermore, the failures with large breaches ($> 500 \text{ m}^2$) are due to instability, with only a few failures caused by internal erosion. Variations in breach surface for similar levee geometry might be explained by the differences in hydraulic head conditions. Moreover, recent studies show that even if the hydraulic load is the same, the duration of the load is also an important parameter in development of breach surfaces [94].

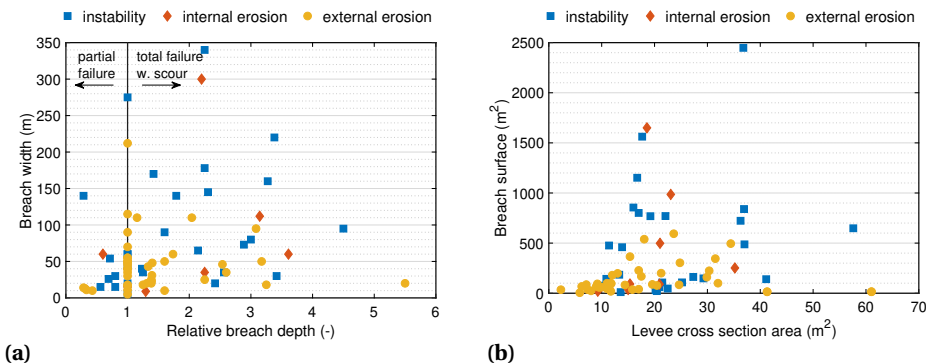


Figure 2.11: Relation between (a) relative breach depth and breach width per failure mechanism; (b) breach surface and geometry of the levees per failure mechanism.

The understanding of failure patterns could be further deepened by checking how the failure initiated. Thus, the following analysis of the levee failures considers both their initial and main mechanisms. In Figure 2.12, the total and average breach width per failure mechanisms are compared. For instance, it can be seen that, if an external erosion case is initiated by instability, it is more likely to have a wider breach per failure than for an external erosion case that is triggered by overflow/overtopping. This can be explained as follows. When an instability occurs, most of the times a relatively large part of the crest is pushed away by internal forces with the following sequence of external erosion making the damage larger. Whereas, if the failure starts with overflow/overtopping which by time erodes the crest externally (external erosion), the levee is most likely to have smaller damages compared to the previous case. Another inter-

esting observation is that some types of failure occur more often (e.g., external erosion triggered by overflow/overtopping) but with a relatively smaller average breach width per failure (i.e., smaller damage).

2

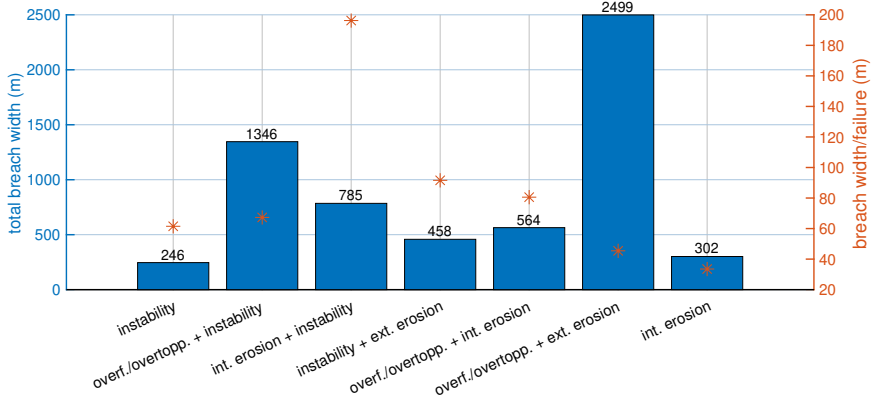


Figure 2.12: Breach width analysis per failure mechanism occurred during the flooding event in Germany, 2002 and 2013.

It is also noticed in Figure 2.12 that when an instability failure mechanism is initiated by internal erosion (e.g., piping), it is more likely to have wider breaches, whereas if it is initiated by overflow/overtopping, the size of the breach is smaller than the previous case, but still larger than an instability failure without any initial mechanism. Figure 2.13 gives a schematization of these three cases. This trend can be explained by the fact that internal erosion, occurring directly in the subsoil, creates an extra hydraulic pressure below the crest. By time, the piping disconnects the upper part of the levee from its foundation, undermining the stability of a large section of the levee. In general, this analysis shows that the underlying failure mechanisms are of importance in the breach development.

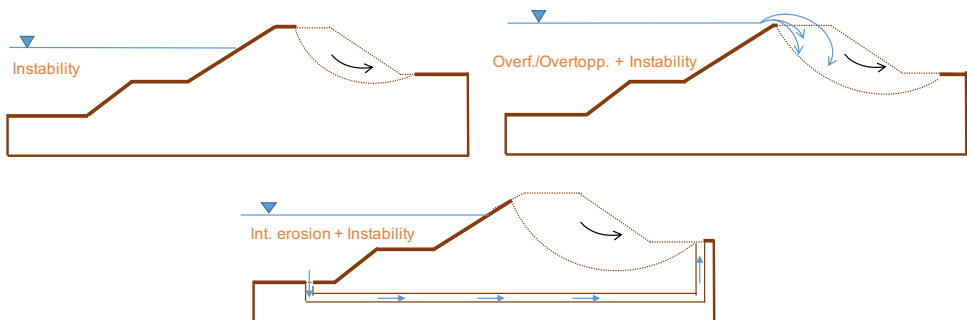


Figure 2.13: A schematization of an instability failure with three possible initiation mechanisms.

BREACH DENSITY ANALYSIS

One of the important aspects to consider in flood risk assessments is the levee breach density, which is related to the expected amount of levee breaches and their width. Risk assessments often assume that a breach can occur at random locations and often focus on a single breach and/or consider multiple breaches less likely [95]. However, actual flood events often comprise of multiple failures and breaches. Thus, it would be beneficial to estimate the expected breach density in order to complement the risk assessment of levees. Previously, a study [96] had addressed the distance between breaches as a function of overtopping rate for the two coastal levees failed during the events of New Orleans 2005 and Denmark 1976. However, related analyses have not been performed for river flood events yet.

In order to analyze the breach density, we first define two parameters, namely *Failure intensity* (km^{-1}) and *Breach width ratio* (-), as

$$\text{Failure intensity} = \# \text{ of failures} / \text{river length} \quad (2.1)$$

$$\text{Breach width ratio} = (\text{total breach width} / \text{river length}) \times 100 \quad (2.2)$$

where *total breach width* and *river length* are expressed in km. The failure intensity represents the occurrence of failure cases along the investigated river normalized by its length, whereas the breach width ratio corresponds to the ratio (in percentage) between the sum of all registered breach widths and the river length.

We analyze these parameters and compare with the return periods of discharge per each river for three flood events with multiple failures occurred in Germany in 2002 and 2013 (discussed previously), and also in Czech Republic in 1997, which are all stored in ILPD. The Czech event, also known in history as “The Great Flood of 1997”, mainly affected the Oder and Morava basins with multiple levee failures, of which 27 have been recorded in the ILPD. For both countries the river levees were supposed to be designed for events with return periods of 100 years [97].

The calculated parameters for the 1997 and 2002 events range between 0.02 and 0.68 km^{-1} for the failure intensity, and between 0.08% and 4.5% for the breach width ratio, as shown in Figure 2.14. For the 2013 event, the values of the calculated breach width ratio (between 0.1%- 0.4%) and failure intensity (between 0.03 - 0.1 km^{-1}) are smaller than for the 2002 event, which can be explained by the strengthening of the levees after 2002, as pointed out in Section 2.3.2. However, although the conditions during the 2013 event was more severe, return periods found in the literature were either assessed with smaller values than for the 2002 event [98], or defined too general, i.e., “>100 years” [99, 100]. Thus, the values for the 2013 event were not included in the rest of the analysis.

Considering the events of Germany 2002 and Czech Republic 1997, it is noticed that when the return period (Y) increases, the failure intensity and the breach width ratio also increase. For the seven rivers considered, a non-linear regression analysis using an exponential fitting function has been performed on the available data for both breach density parameters (trust-region optimization algorithm available in the MATLAB *fit* function). The resulting functional relations and the corresponding R^2 -values are given in Table 2.4. For instance, considering a river stretch of 50 km with a 125-year event, one would expect approximately 3 failures with a total width of 140 m according to these relations.

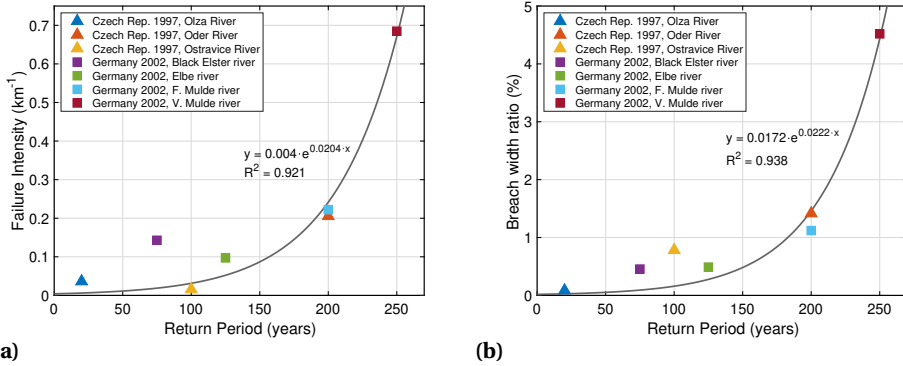


Figure 2.14: (a) Failure intensity (km^{-1}) and (b) Breach width ratio (-) along the rivers investigated during Germany, 2002 and Czech Republic, 1997 events.

Whereas, a 200-year event would lead to 12 failures with a total width of 730 m for the same stretch. The functional relations given below are obtained from a limited amount of data. If more information regarding cases from different events will become available in the future, it can be used to validate the relations found and to refine the analysis.

Table 2.4: Regression functions and R^2 -values for the breach density parameters and return periods.

Breach density parameter	Regression function	R^2 -values
Failure intensity (km^{-1})	$Failure\ intensity = 0.004 \times e^{(0.0204 \times Y)}$	0.921
Breach width ratio (-)	$Breach\ width\ ratio = 0.0172 \times e^{(0.0222 \times Y)}$	0.938

For the same events investigated above, we also explore the occurrences of different failure mechanisms and the degree of damage for different return periods (Figure 2.15a). In general, the total number of failures increases with the change in the return period. However, as it is given in the figure, external erosion is more likely to occur for high return periods. This can be explained by the fact that a high return period is related to high water levels and river discharges, which in turn leads to overtopping/overflow followed by an external erosion. Moreover, it is shown in Figure 2.15b that higher return periods lead to larger degrees of damage on the levees.

2.4. DISCUSSION

2.4.1. ON THE INTERNATIONAL LEVEE PERFORMANCE DATABASE (ILPD)

The ILPD is expected to become a global platform and scientific tool for various purposes, such as to advance the understanding of failure mechanisms and breaching of

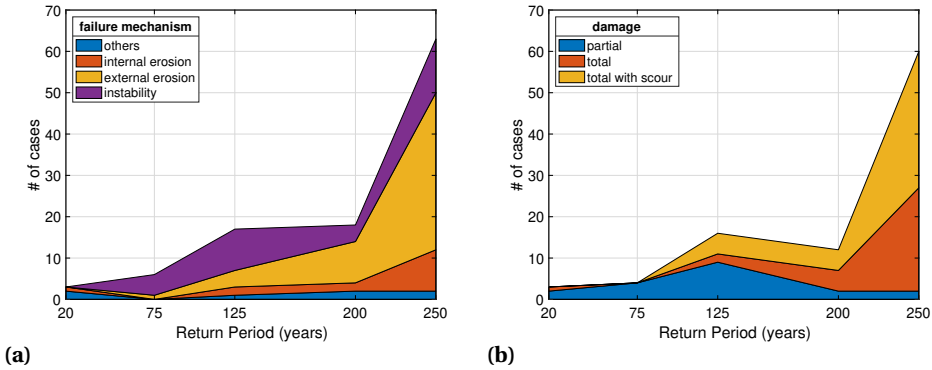


Figure 2.15: Distribution of (a) failure mechanisms and (b) degree of damage for different return periods (Y) along the rivers investigated during Germany, 2002 and Czech Republic, 1997 events.

flood defenses, and to improve model development and validation. The first available version of the ILPD presented in this paper provides good coverage of some regions, e.g., the Netherlands for the 20th century, and it is already being used to support detailed studies, such as (a) geotechnical analysis of individual failures [53] and (b) detailed breach analysis [54]. In all other cases with only generic data, entries could still serve as a starting point for researchers to collect more detailed information. It is foreseen that the future expansion of the database will further offer valuable information to the scientific community as well as to the public and private sectors. More extensive datasets will give new insights into the field of flood risk and will stimulate the development and validation of more accurate techniques and modeling tools. This could eventually contribute to improving design methods of flood defenses, and to supporting risk assessments related to levee safety.

However, some operational obstacles must be overcome in order for the ILPD to become broadly applicable and representative. One of the main obstacles that we encountered is the issue of data sharing. It is believed that most of the detailed information is kept as an internal source since making the data public is a sensitive matter in many cases. A possible reason is that levee authorities and governments in many countries prefer not to advertise events whereby their levees failed. For instance, countries with few reported failure cases (e.g., China, Italy) in Figure 2.4 are not necessarily safer than the others (e.g., the Netherlands or Hungary) since many failures are known through media or registered information (e.g., EU documentation). This in fact highlights the importance of being transparent about data sharing and collaborations.

Another difficulty that arises while obtaining data is the language barrier. Across the world, detailed reports of flood events are obviously written in the official language of the country (e.g., Japanese). Especially when it concerns large quantities of data, extracting information from these reports for the ILPD becomes challenging. A way to potentially counteract this issue would be, for example, to request experts of international committees (e.g., ICOLD) to enter data related to their country into the database. However, this

poses a new challenge, namely a higher demand on maintaining the database and providing support. Although there are some standard and ILPD-specific definitions for failure mechanisms and other parameters, people tend to use their own terminology, thus generating inconsistencies between cases. This is the reason why only the project members are currently allowed to enter data in the website. Thus, improving the ILPD towards a global, uniform database would require very systematic and intense data collection, also with the involvement and commitment of local stakeholders and levee managers.

2.4.2. ON USING EVENT-LEVEL ANALYSIS FOR RISK ASSESSMENTS

Even though flood events and defense systems have specific characteristics and conditions, insights from the macro-scale analysis of the historical failures can be used to complement the (local) flood risk assessments. Firstly, the analysis of actual events could serve as calibration or reference for risk evaluations by highlighting dominant failure mechanisms and breach characteristics. For instance, as concluded in this study for the Elbe region, although some mechanisms occur more often, the damage that they cause on the levee can be less compared to the ones that has less occurrence. Likewise, it has been shown that it is important to consider not only the final failure mechanism that cause a breach, but also the underlying processes that initiate the failure. These observations can be used by the local authorities as a starting point in assessing specific situations.

Another point is that current risk assessments generally tend to pay limited attention to failure scenarios with multiple breaches [95]. It is normally assumed in river levees that the occurrence of one breach reduces the expected likelihood of other breaches, as the inflow through the breach limits water levels downstream (i.e., retention effect). However, observations from the river floods studied here show that multiple breaches do occur during actual river floods, particularly when the system is overloaded by “design floods”. Thus, the observed breach densities and their identified relation with the return periods could be used, for instance in combination with fragility curves, to make more informed (simplified) risk assessments. Although in this study a general overview on the breach density parameters has been given, further research on this topic is recommended. A probabilistic analysis could be included by updating the failure probabilities at the failure locations based on the local information affecting the strength of the levee, such as vegetation type, old breaches, changes in soil profile.

2.5. KEY CONCLUSIONS

In this paper, we introduced the International Levee Performance Database (ILPD), aiming to create a global information-sharing platform to assist research on levee performances. Besides, we conducted a macro-scale analysis of the currently available data. We outline common failure mechanisms of which external erosion of the slope is identified as the most frequent for levees and internal erosion for earthen dams. As an illustrative use of an ILPD sub-set, we examined breach characteristics of over a hundred failures during the flood events occurred in Germany (2002, 2013). Based on this analysis, we identified potential linkages between initial failure mechanisms, main failure mechanisms and the eventual breach characteristics. For instance, it is concluded that

initial failure mechanisms play an important role in defining breach characteristics and that failures due to instability and internal erosion are less frequent but lead to a larger breach size. Based on events with multiple failures included in the database, we also identified a relation between the return period and the expected breach density during a flood event. Such relation can be improved and validated on cases from different events that will become available in the future.

The ILPD currently contains over 1500 entries covering historical failures, experiments and other performance observations. Even though we focused on the analysis of data at an event-level, ILPD sub-datasets can be used for more detailed analyses of individual failure processes, for instance, to investigate how occurrence of failure mechanisms is related to levee and loading characteristics or to analyze breach properties in more detail. Thus, the aim of the database for the future is to provide extensive and high-quality datasets to support the development and validation of accurate methods and models for failure mechanisms and breaching of flood defenses. This is currently only restricted by the limited amount of data shared in the database, which is why a joint effort of the international scientific community, private companies and governments is required to make the ILPD complete and representative. The insights provided by the analysis of the historical flood events contained in the ILPD, in combination with hydraulic/geotechnical models, could eventually be used to complement risk assessments and to design more robust and resilient flood defenses, with a smaller likelihood of catastrophic breaching.

3

APPLICABILITY OF SATELLITE RADAR IMAGING TO MONITOR LEVEE CONDITIONS

The previous chapter discussed historical levee failures and highlighted that understanding levee behavior can be significantly improved by analyzing historical performance observations. Apart from learning from the past failures, to ensure safety we need to be able to identify if, where, and when a levee failure would suddenly occur. Thus, levees require continuous monitoring to detect which sections are most vulnerable. As stated in the Introduction of this thesis, current levee inspection methods mostly rely on limited information obtained by visual inspection. This hampers the timely detection of problematic locations and the assessment of levee conditions. In this context, satellite radar imaging, in particular Interferometric Synthetic Aperture Radar (InSAR), holds a large potential to complement current inspection methods. However, for levee management, the usability of the technique requires significant radar expert knowledge.

To account for this, we provide a comprehensive overview of the state of the art in using time-series InSAR for systematic long-term (e.g., inter-annual) levee deformation monitoring. The current chapter aims to assess the usability and applicability of time-series InSAR as a way of complementing existing monitoring approaches and levee investigation methods. Section 3.2 introduces a general review of the basic principles of InSAR and PS-InSAR. Section 3.3 discusses the applicability of radar satellite imaging on levee management, which is influenced by different factors, with the support of different case studies in the Netherlands. In Section 3.4, we clarify the most important technical aspects with respect to levee monitoring using InSAR technology, such as deformation estimation in different directions, satellite characteristics, precision and reliability. Moreover, we discuss the potential of using satellite radar imaging for levee monitoring,

Parts of this chapter have been published within [51].

and analyze the links between levee deformations and various failure mechanisms in Section 3.5.

3.1. A REVIEW OF EXISTING LEVEE MONITORING TECHNIQUES

Frequent monitoring of the condition of levees is crucial as well as challenging. This is also the case for the Netherlands, where almost 12 million people (70% of the total population) live in flood prone areas, and 70% of the economic value produced would be endangered in case of a catastrophic event [101]. Currently, the country is protected by a network of 22,500 km of flood defense structures, of which nearly 17% are primary levees protecting populated areas from flooding by major rivers, big lakes and the sea. Hence, levee monitoring requires a considerable effort and significant financial means. The Netherlands invest over one billion Euro per year in activities related to monitoring, maintenance, and reinforcement of the flood defenses, with the intention to maintain or increase their safety levels. However, according to a national safety report in 2014 [102], about 30% of these primary levees did not comply with the required safety level, which is bound to reach 50% due to the new and generally stricter safety standards introduced in 2017 [101].

Conventional levee monitoring methods mainly consist of visual inspections [19, 103, 104], restricted to a typical frequency of twice a year in the Netherlands [105]. During these inspections, the integrity of the structures is assessed using qualitative inspection parameters [106], for example, by checking the presence of any damage, crack, animal burrows, or irregular vegetation on the levees. Although some of these features may be clearly visible, many failure modes of levees are usually preceded by small and slow changes in geometry and structure, which may not be detectable by visual inspections [34]. Remote sensing techniques, such as LIDAR (laser altimetry) [107, 108], aerial photography, passive microwave radiometry (PMR), thermal and near infrared photogrammetry, are usually applied only for the locations at which a problematic situation has been detected by visual inspections [37, 109]. Methods using advanced in-situ sensors instrumentation, e.g., sensor installations in a levee body, are also available [103], but are difficult to deploy at the extended spatial scales involved with levee systems due to the costs and work load requirements. Consequently, current detection and monitoring methods are still strongly reliant on time-consuming evaluation of expert judgments, which may result in subjective, infrequent, and qualitative assessments [33, 35–37]. Hence, especially in countries with extended flood defense infrastructure, such as the Netherlands, there is a need for innovative and cost-effective techniques to monitor levee conditions, that should be applicable on a wide scale with good precision and requiring less resources.

Over the last decades, satellite remote sensing techniques have evolved rapidly. Satellite radar interferometry, or Interferometric Synthetic Aperture Radar (InSAR), has become an efficient tool to monitor the stability or deformation of the earth's surface [38, 110]. It instantaneously provides millions of observations with meter-level spatial resolution and millimeter-level precision, supported by revisit times in the order of days, at very low costs compared to conventional surveying methods. In particular, the Persis-

tent Scatterer InSAR (PS-InSAR) methodology is routinely applied because of its ability to detect high-quality and consistent scattering points on the surface. The wide range of InSAR applications includes urban areas [40, 111], railways [41], dams [42], highways [42], and tectonic movements [45]. Especially in the Netherlands, InSAR has been successfully applied to monitor land deformation, for example, due to ground water extraction [112], peat soil decomposition [113], sinkhole detection [114], gas extraction [115, 116] and mining [117].

Monitoring levee systems using InSAR provides high precision in long-term deformation estimates compared to the conventional methods. A project [32] explores the technical feasibility of InSAR for levee deformation monitoring and suggest a collaboration of radar and levee experts to improve the application of the technique. Another study [33] demonstrates that with such method, levee deformations can be effectively monitored. An application of InSAR for monitoring the subsidence of New Orleans, USA [47] concludes that the highest subsidence rates observed between 2002 and 2005 match with the levees of the Mississippi River–Gulf Outlet canal that breached catastrophically during Hurricane Katrina in 2005.

3.2. METHODOLOGY

3.2.1. BASIC CONCEPTS OF INTERFEROMETRIC SYNTHETIC APERTURE RADAR (INSAR)

Synthetic aperture radar (SAR) technology uses active radar sensors that transmit pulses of electromagnetic waves from space to Earth and record the back-scattered signals from the earth's surface. These signals are then used to construct an image, in which each resolution cell, or pixel, comprises the coherent sum of all reflections within that cell. This coherent sum has an amplitude, A , expressed in dB (i.e., the back-scatterer magnitude), and a phase, ψ , expressed in radians, which is stored as a complex number, named phasor, P , per pixel [38];

$$P = Ae^{i\psi} \quad (3.1)$$

where i is the imaginary number. The amplitude, A , is a function of the slope, distribution, roughness, and electrical properties of the objects in the resolution cell, as well as sensor characteristics, such as wavelength, λ , bandwidth, and incidence angle, θ_{inc} . The phase, ψ , is a function of the time delay between signal transmission and reception, but also influenced by the random distribution of all scatterers within the resolution cell.

The main principle of InSAR for deformation estimation is to interfere at least two SAR images acquired at different times over the same location [38, 118], creating a so-called interferogram. This is represented by the complex interferogram of two co-registered (pixel-to-pixel aligned) radar images (called master and slave images), i.e. P_{MS} , which is defined for every pixel as

$$P_{MS} = P_M - P_S^* = A_M A_S e^{i(\psi_M - \psi_S)} \quad (3.2)$$

where $*$ indicates the complex conjugate and M , S denotes the master and slave images, respectively. Applied to levees, differences in amplitude between two images show the

changes in reflection behaviour of the levee cover, whereas phase differences can be exploited to extract information about the displacements between two acquisition times, with millimeter-level precision (Figure 3.1). Therefore, the interferometric phase of a pixel, φ_{MS} , is defined as

$$\varphi_{MS} = W\{\psi_M - \psi_S\} \quad (3.3)$$

where $W\{\cdot\}$ is the modulo- 2π wrapping operator.

The interferometric phase of a pixel, φ_{MS} , that is, the difference between the phase values acquired at different times, includes several (a) “coherent” components, such as earth curvature, topography, atmospheric delay, and surface displacement, and (b) “incoherent” components, due to changes in the scattering mechanisms at the earth’s surface, for example, due to vegetation and measurement noise [38, 119]. The aim of any InSAR technique is to isolate the coherent signal of interest, for example, the displacement phase, φ_{defo} , from the other phase contributions. A displacement of the surface area during the time between two acquisitions results a phase difference (see Figure 3.1), given as

$$\varphi_{defo} = \frac{-4\pi}{\lambda} D_{LOS} \quad (3.4)$$

where D_{LOS} is the deformation (mm) in Line-of-Sight (LOS) direction, i.e., in the line connecting the satellite and the scatterer. In general, this isolation of the different coherent components is achieved by using time-series of tens to hundreds of acquisitions, which is possible for all pixels for which the incoherent components of the signal are not too dominant [39, 120, 121].

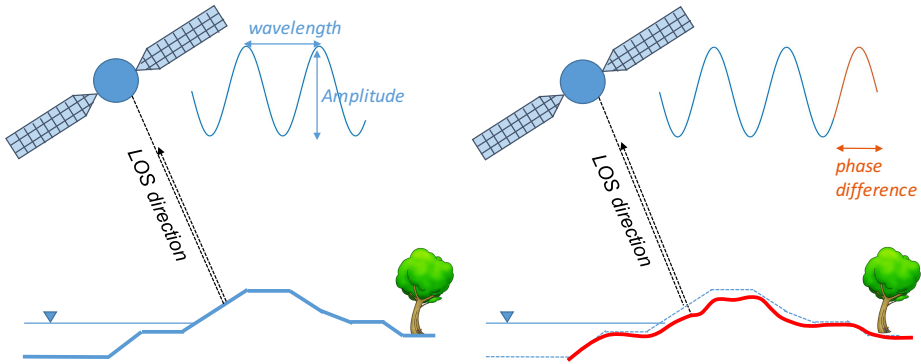


Figure 3.1: Two sequential Interferometric Synthetic Aperture Radar (InSAR) measurements before and after deformation occurs on a levee body. Displacement (mm) is measured in the line-of-sight (LOS) direction, that is, in the line between the satellite and the scatterer, as a fraction of the radar wavelength.

3.2.2. TIME-SERIES PROCESSING

The value of SAR imaging for levee monitoring is highest when time-series approaches are used. Current satellite constellations allow for near-daily acquisitions from varying

viewing geometries, with different resolutions, and irrespective of cloud cover and solar illumination [122]. There is a wealth of information to be gained from the SAR pixel time-series (Figure 3.2). Amplitude variability holds information on surface roughness and soil moisture changes, while the full complex per-pixel information can be exploited in an interferometric sense for measuring displacements, referred to as deformations in the rest of the study. Various time-series processing techniques may be applied to estimate the deformations from the data. PS-InSAR uses dominant point-like scatterers with a persistent scattering (PS) behaviour over time. This type of scatterers typically shows a coherent phase behaviour over long periods of time. Distributed scatterers (DS) exploits groups of pixels which have no dominant scatterers but have a similar phase behaviour over the group (Figure 3.2) [123, 124]. For both techniques, different data processing methods have been developed aiming to obtain a similar outcome: estimation of deformation time-series.

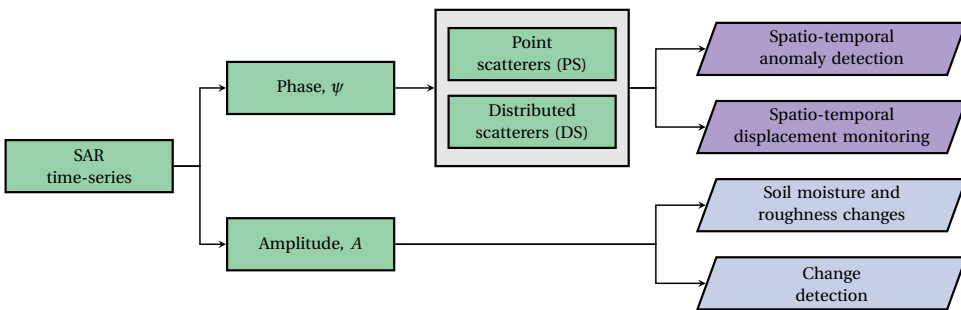


Figure 3.2: Overview of the Synthetic Aperture Radar (SAR) methods, observables, and physical parameters. The time-series of amplitude and phase can be used to derive several products for levee monitoring.

Among all possible methods, the most suitable approach depends on the surface cover, the number of available radar images, the orientation of the structures and the expected deformation signal. In this research, we focus on the PS-InSAR technique, which is typically composed of three main steps; (a) creating multiple interferometric combinations from complex data (“stack processing”), (b) detecting PS and estimating their deformation phase (“PSI analysis”), and (c) assessing the quality of the results (“post-processing”).

The interferometric stack processing of the radar data is performed using the Delft Object-oriented Radar Interferometric Software (DORIS) [125]. The processing consists of the following steps; (a) selecting a proper master image, (b) cropping the images based on the area of interest, (c) oversampling the slave images to avoid aliasing, and (d) co-registering slave and master images to cover the same area on Earth. In the last step, all slave images are interfered with a unique master image in order to create interferograms over the analyzed area. The flow chart for the complete process of PS-InSAR technique that is used in this research is given in Figure 3.3.

These radar interferometric data stacks contain dozens of image acquisitions, each with billions of image pixels. The PSI analysis aims to detect those pixels with a coher-

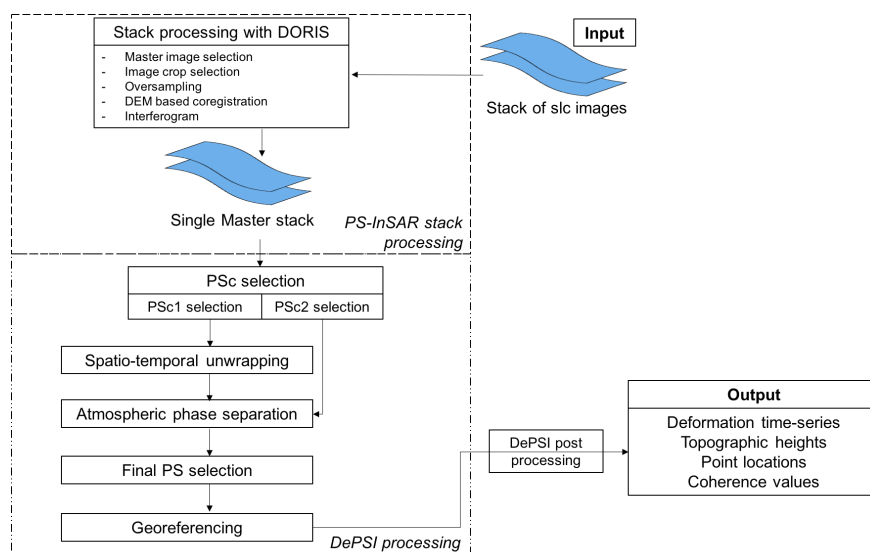


Figure 3.3: A flow chart demonstrating the different steps of the PS-InSAR technique used in this research (chart adapted from [126] and [127]).

ent phase behaviour. The Delft implementation of Persistent Scatterer Interferometry (DePSI) [126] algorithm is applied to transform the radar data stack into a set of detected PS on the levee surface and their deformation time-series are estimated. This is done by the following steps. First, the most coherent PS candidates (PSc1) are selected to create the reference spatial network based on the analysis of their amplitude dispersion per pixel. Then, the phases of those pixels are unwrapped in time and followed by space in order to estimate the different phase components and separate the atmospheric delay. Second-order PS candidates (PSc2) which show relatively lower coherence in phase stability are selected to densify the PS distribution. Eventually, all the 3D unwrapped PS candidates are subjected to a final selection based on a pre-assumed model. Lastly, a quality assessment is performed using additional quality metrics to remove the incorrectly detected PS and to describe the quality of the final results. For a detailed description of the processing approach and a comparison of several PS-InSAR techniques, see [123, 126, 127].

3.3. CHARACTERISTICS, QUALITY AND APPLICABILITY

3.3.1. SATELLITE CHARACTERISTICS

All available SAR satellites are in a so-called sun-synchronous polar orbit, moving both from south to north (ascending) and from north to south (descending) (Figure 3.4). This allows satellites to monitor a particular area from at least two viewing directions. For higher altitudes, there are generally more orbits that cover the same area on the ground, leading to a higher revisit rate. SAR satellites provide radar images from 1992 to the present to monitor surface motion. Thus, historical deformation, for which no other

survey data may be available, can be investigated since satellite data are archived for further exploitation. An overview of the most important past and current radar satellite missions suitable for levee deformation monitoring is given in Table 3.1.

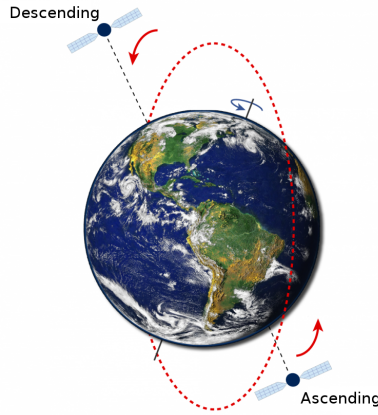


Figure 3.4: Satellite orbit, consisting of an ascending and a descending part (source: SkyGeo).

One of the attractive characteristics of the radar instruments in these orbits is the day and night monitoring of the earth's surface in all weather conditions, which provides frequent data acquisitions at low cost. Moreover, the wide areal coverage enables a global perspective on deformation behaviour using huge amounts of data from various satellites with high spatial and temporal resolution. Its high measurement accuracy allows us to monitor small deformations at mm-level, depending on the characteristics of the radar and the conditions of the monitored levee.

Technological developments and new generations of satellites and sensors led to significant improvements in SAR data with reduced repeat cycle or increased spatial resolution [111], see Table 3.1. To demonstrate the differences between sensors, Figure 3.5 shows the levees on the island of Marken, the Netherlands, using medium resolution satellites, ERS (1992–2000), Envisat (2003–2010), and a high-resolution satellite, TerraSAR-X (2009–2016). Figures 3.5a and 3.5b show that the levees present deformation velocities for the two different time periods obtained from ERS and Envisat satellites, respectively. Figure 3.5c reveals that the higher spatial resolution results in a strong increase of the number of PS points compared to the results of ERS and Envisat. This can be explained by the fact that PS-InSAR detects one PS point per cell, and consequently a smaller resolution cell leads to more PS per km^2 . Moreover, the measured deformation values and the absolute positions of the measurement points are estimated more precisely. Additionally, the reduced repeat cycle of a X-band satellite (11 days) allows for monitoring the levees more frequently. Note that all results show significant deformation rates on the north and south levees of the island.

All deformation estimates obtained by PS-InSAR are projections of the three-dimensional (3D) deformation vector onto the line-of-sight (LOS) direction of the satellite. This direction from satellite to object is determined by the heading angle of the satellite with respect to the north, α_h and the incidence angle of the radar, θ_{inc} . In the

Table 3.1: Most important past and current radar satellite missions suitable for levee deformation monitoring and their characteristics.

Mission	Time period	ΔT_{rep} (days)	ΔT_{rev} (days)	Band	Spatial resolution (m)	Precision ^b (mm)	λ (mm)	θ_{inc} (deg)	Availability
ERS-1/2	1991-2000 ^a	35	8	C	4x20	1.4	56	23	Free
Envisat	2002-2010	35	8	C	4x20	1.4	56	23	Free
RadarSAT-2	2007-	24	6	C	10x9 ^c	1.4	55	20-49	Commercial
TerraSAR-X/ Tandem-X/ Paz	2007-	11	3	X	3x3 ^c	0.8	31	20-45	Commercial
Cosmo-Skymed 1/2/3/4	2007-	4	1	X	3x3 ^c	0.8	31	20-60	Commercial
Sentinel-1 a/b	2014-	6	2	C	20x5 ^c	1.4	55	29-46	Free

Notes: ΔT_{rep} , repeat cycle; ΔT_{rev} , potential revisit time for mid-latitudes; λ , radar wavelength; θ_{inc} , incidence angle (ascending - descending).

^a After 2000, ERS-1/2 was not suitable anymore for deformation applications.

^b Equivalent precision of the phase measurement, assuming a signal-to-noise ratio of 10 dB (5% of the semi-wavelength).

^c Higher spatial resolutions are possible for specific instrument modes.

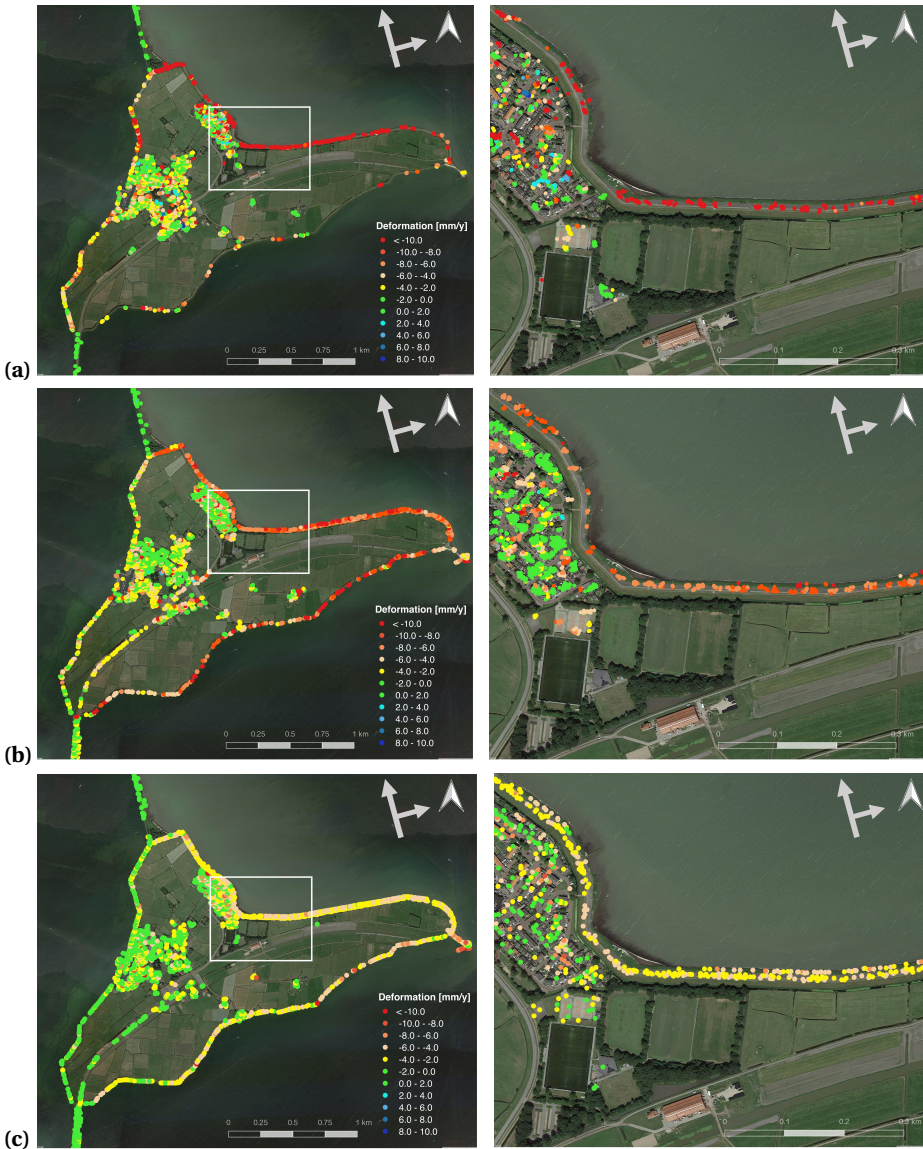


Figure 3.5: Relative deformation velocity maps of Marken monitored by (a) ERS (1992–2000), (b) Envisat (2003–2010), (c) TerraSAR-X (2009–2016).

figures of this study, which have North on top, the heading of the satellite is expressed by a vector accompanied by an orthogonal viewing direction of the satellite (top view). The incidence angle, θ_{inc} , is here defined as the vertical angle relative to the plumb line (Figure 3.6).

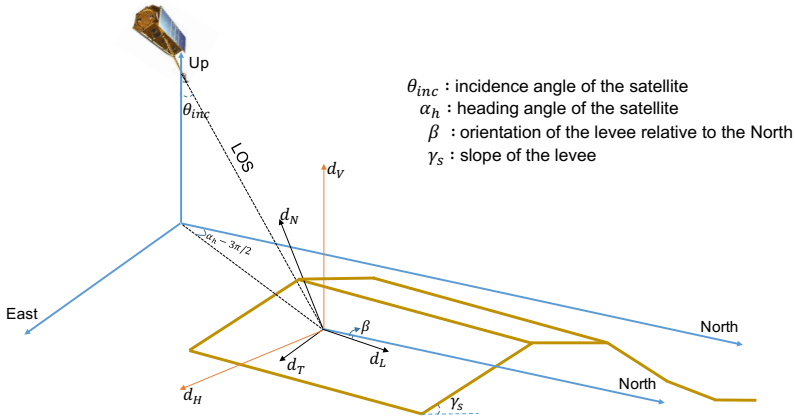


Figure 3.6: Three-dimensional coordinate transformations for levee section from the line-of-sight (LOS) vector to a local Cartesian reference system.

3.3.2. OBSERVATION CHARACTERISTICS

The usability and applicability of InSAR depends largely on the type of observations and their quality. In this section, we describe the characteristics of observations, their quality assessment, and precision.

OBSERVABLES

The SAR phase values per scatterer (observation point or PS point) and per acquisition are called *input observables*. From these we can obtain *derived observables*, such as (a) the difference in phase between two acquisitions for one scatterer (i.e., change in time per location), (b) the difference in phase between two scatterers for one acquisition (i.e., change in space at a given time), and (c) the difference between (a) and (b). The latter is termed the double-difference phase observable, and it forms the basic element in interferometric analysis [128]. In other words, the double-difference between two PS points on a levee is used to quantify the deformation occurring between two time instants at one location relative to the deformation at the same time instants at the other location.

RELATIVITY

Deformation time-series of PS in every data set are relative to each other: the double-difference observations. Integrating the differences to a common reference point and a reference time may be convenient in the visualization, but is not strictly necessary. Thus, the radar measurements are inherently relative in time and space. When absolute motion estimates are desired, PS-InSAR measurements can be transformed into a common geodetic datum [129].

MEASUREMENT PRECISION

The measurement precision expresses the quality of the *input observables*, that is, the SAR phase values per scatterer. This precision is dependent on the thermal noise floor of the SAR instrument and on the amount of backscatter received from Earth. While the

latter part is location-dependent, we typically work with scatterers with a signal-to-noise ratio (SNR) level of 10–24 dB, which translates to a precision of 5–1% of the semiwavelength of the radar (see Table 3.1). Expressed in millimeters, this yields a precision (i.e., standard deviations) between 0.2 and 1.4 mm, which is why the technique is said to have mm-level precision.

The precision of the *derived observables* (the double-differences) follows from error propagation. If the input observables are considered to be independent (uncorrelated), the precision of the double-differences would be doubled, that is, between 0.4 and 2.8 mm. However, these precision are feasible only under the assumption that the observations for a single scatterer in two acquisitions are completely correlated or “coherent”. In practice, however, this assumption may not be valid for a large number of pixels in an image. As a consequence, the measurement precision of the double-difference observations may be much lower, a process termed temporal decorrelation. Since the degree of temporal decorrelation is not related to the original measurement precision anymore, but rather to the conditions on the earth’s surface, the precision of the double-difference observations turns out to be very variable spatially. In fact, the vast majority of scatterers is often “incoherent”, and therefore not useful for retrieving geometry changes. Fortunately, there are billions of observations in a SAR image, and therefore the survival of a limited percentage does still yield very high point densities, as proved by the examples in the figures.

PARAMETERS

The double-difference phase measurements are the input for the parameter estimation. These phase measurements are sensitive to a number of unknown parameters, such as to their topographic position, to the variable delay of the radio signal through the atmosphere, to the deformations, and are ambiguous, or “wrapped”, to values between 0° and 360°. All these parameters need to be estimated from the phase measurements, which is the main challenge of the interferometric data processing. For levee monitoring, the deformations are the main parameters of interest, which can be further parameterized as a time-series of LOS deformations, or as parametric or non-parametric functions fitting the deformations. Expressed as a single relative velocity per point, these parameters can be easily visualized on a plane map projection.

QUALITY ASSESSMENT

The double-difference nature of the measurements yields double-difference deformation parameters. The quality of these parameters can be expressed by a variance–covariance matrix, which is generally a full matrix. Note that the non-zero covariance in the matrix causes the quality of the results to be independent of the choice of the location or time of the reference point. When a specific parametric model is chosen to describe the deformations over time, the residues between the observations and the model can be used as a posteriori quality metric, equivalent to a goodness-of-fit metric [126]. Obviously, this metric does not only express noise or errors in the measurements, but the degree of applicability of the chosen temporal model as well.

GEO-LOCALIZATION

In PS-InSAR processing, a precise geo-localization of PS points is necessary to interpret the results correctly. Positioning of the PS points is less precise than their deformation estimates. The positioning precision is 1–2 m for C-band data and less than 1 m for X-band data [130]. Using the exact PS locations, reflections from the ground can be separated from those originating from higher level objects, which may show a different deformation behaviour [131]. Georeferencing is thus of high importance in the analysis of the results, in particular when the deformation is localized [114].

3.3.3. APPLICABILITY ON CASE STUDIES

While the radar satellite images cover the entire earth, not every pixel contains a valuable deformation measurement. As discussed above, the main condition for this applicability is the degree of coherence. The coherence, c , is a number in the range [0,1] that expresses the degree to which radar pixels can be compared over time. A value of 1 relates to perfect comparability, while a value of 0 implies that the radar signal is not comparable. The coherence of the PS depends on the consistency and electrical properties of the surface. Vegetation and its temporal dynamics and soil types have a direct influence on the coherence, and thus the availability of PS [132]. Most of the coherent scatterers stem from non-vegetated areas, such as the waterside slope of the levee with rock revetments. To illustrate this, the mean coherence estimates per pixel were calculated for a levee segment at Marken that was examined in Figure 3.5. For this specific levee segment, the difference between water (low coherence) and the levee as a line structure can be clearly identified in Figure 3.7. Considering the radar look direction and the surface cover, the points with high coherence are mostly from the non-vegetated waterside slope of the levee, that is, the rubble at the toe, paths, and revetments near the crest.

The condition of coherence limits the spatial coverage over the levee profile, and therefore the applicability of the technique. However, for wider deformation signals, measured deformations from one area can be an indication of another part of the levee. Moreover, recent approaches on estimating deformation in areas with low coherence, and in the absence of sufficient PS appear to be promising [132, 133]. A low PS density can also be overcome by installing in-situ devices, that is, corner reflectors or active transponders, which provide a strong signal in the SAR images resulting in adequate deformation estimates [129, 131, 134]. The applicability of corner reflectors for levee deformation monitoring is explored by an external project which is described in Appendix A.

The applicability of levee deformation monitoring using the PS-InSAR approach is demonstrated via case studies located in different parts of the Netherlands. The long-term deformation behaviour of these levees is estimated from both ascending and descending orbits, using available satellite acquisitions in order to estimate the deformation time-series of each PS point for different time periods. Although the processing results may generally be visualized by a constant (linear) deformation rate, every PS point has a complete time-series of deformation estimates in the LOS direction. Figure 3.8 shows the results of levee deformation monitoring in Zeeland, in the South-west of the Netherlands, using satellite images acquired by RadarSAT-2 from a descending orbit, between 2010 and 2017. In the same figure, an example for a deformation time-series of one of the PS points is shown. These time-series enable historical analyses over the ob-

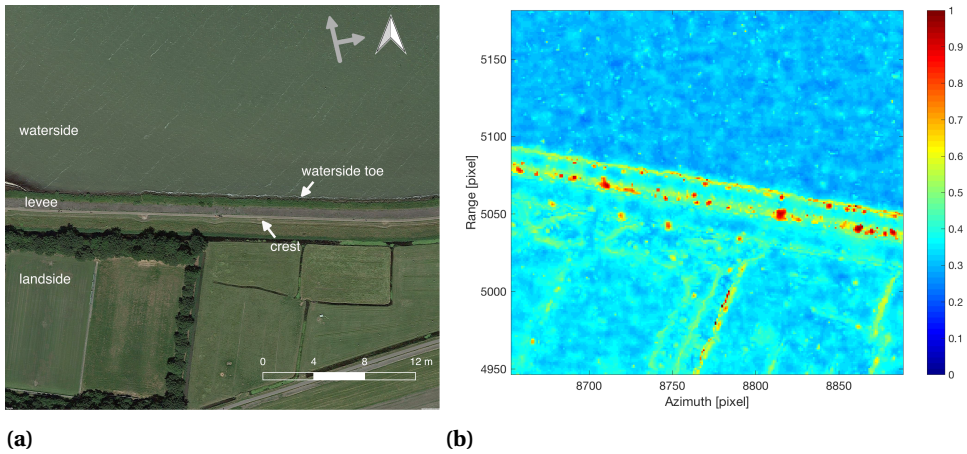


Figure 3.7: (a) Levee segment at the island of Marken, the Netherlands, (b) Coherence estimates of the pixels. Red colour represents high coherence, whereas blue color shows the areas with low coherence. More information on coherence estimation and its bias is discussed by [38].

served period to have a better understanding of levee behaviour in time. Besides, they also have an importance for detecting anomalies, which could be further evaluated by the levee authorities. Indeed, locations marked in red in the figure represent deformations greater than 5 mm per year, which may be indicative of an anomalous levee behaviour. For these locations, additional field observations and analyses could be relevant to evaluate the causes of the behaviour and the effects on safety, for example, on the likelihood of overtopping resulting from subsidence.

Figure 3.9 shows the results from levee deformation monitoring in Flevoland, the Netherlands, which is an area reclaimed from the sea in the late 60s. Linear deformation rates for each coherent scatterer along the monitored levees have been estimated using Envisat from a descending orbit, during 2003–2010. What can be observed from the figure is a clear difference in the deformation rate of the different levee sections which, being close to each other, would be expected to have the same loading conditions and, thus, a similar behaviour. In this case, the largest deformation rates of the levee are found near the nature reserve Oostvaardersplassen where different water level management practices are applied than in the surrounding areas. Hence, this example illustrates how the InSAR data, combined with other available information, such as loading conditions, soil characteristics, management, and maintenance, can support the levee assessments by identifying potential irregularities along the levees.

3.4. PERFORMANCE ASSESSMENT

The previous section addressed the value of InSAR from a data-driven perspective, where the characteristics, applicability, and precision of the measurements were discussed. In the current section, we take a problem-driven perspective, focusing on the question

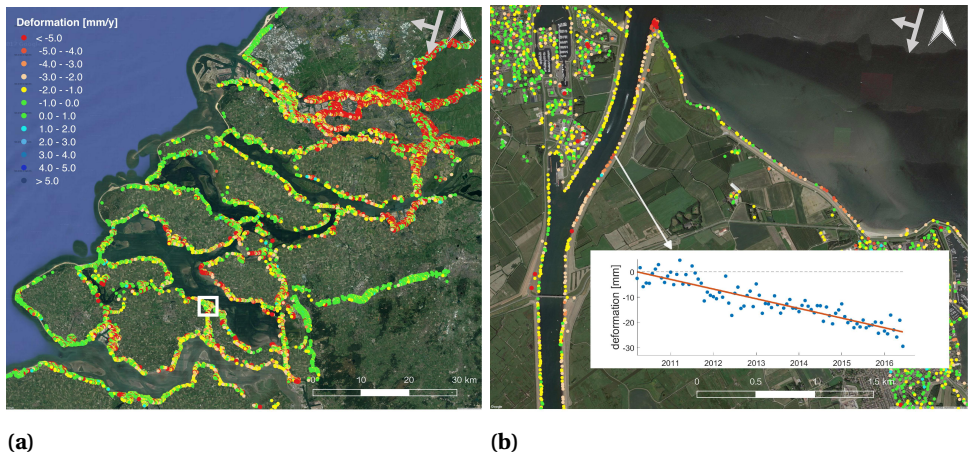


Figure 3.8: (a) Linear deformation rates (mm/year) of the levees in Zeeland, the Netherlands, based on data acquired by RadarSAT-2, descending (2010–2017). (b) An example of deformation time-series with a linear velocity of 4.1 mm/year.

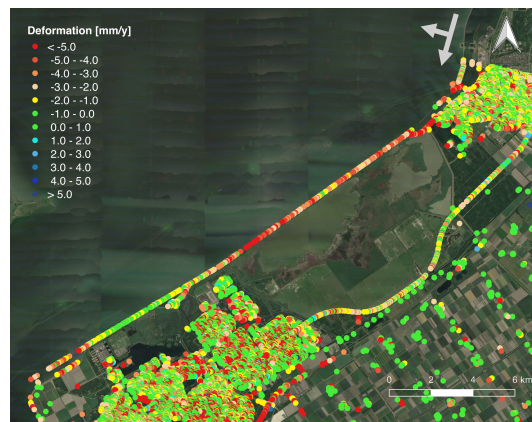


Figure 3.9: Linear deformation rates of a levee segment in Flevoland for the period of 2003–2010 using Envisat.

whether it is possible to detect and monitor a specific type of levee deformation, such as a purely horizontal deformation, or a deformation parallel to the slope of a levee. As such, this is specific for a particular levee, and requires specific metrics, for instance, the particular detectability. This problem-driven approach is relevant for levee asset managers to determine whether it is feasible to detect a particular type of problem.

3.4.1. SENSITIVITY OF DEFORMATION VECTORS

Deformations of levees occur in a three dimensional world, and can be expressed in a global or local reference system (Figure 3.6). Thus, the LOS observation from a radar satellite is a projection of the 3D deformation vector onto the LOS direction. Consequently, the observables in the LOS are sensitive to deformations in almost all directions, albeit with a varying degree of sensitivity. The degree of sensitivity, s , for different directions of the deformation vector varies between 0 (“no sensitivity”), and 1 (“maximum sensitivity”), and is defined as the projection length of a unit vector on the LOS direction [135]. For line-infrastructure, such as a levee, we adopt a local reference system with a vertical axis, a longitudinal axis, and a horizontal complementing axis (Figure 3.6), where the direction of the longitudinal axis, in this case called the levee orientation, is determined relative to the North, with azimuth, β_a . Assuming that the deformation vector does not have a component in the longitudinal direction of the levee, we can express any deformation vector with a (β_a, ζ) coordinate pair, where ζ is the orthogonal elevation angle, in this case called the orientation of the deformation vector (Figure 3.10a). Here, $\zeta = 0^\circ$ corresponds to the horizontal direction to the land side, whereas $\zeta = 180^\circ$ is the horizontal direction at the water side. In Figure 3.10b, all possible deformation vectors are shown in the (β_a, ζ) plane, expressing the sensitivity values of a combined ascending and descending mission.

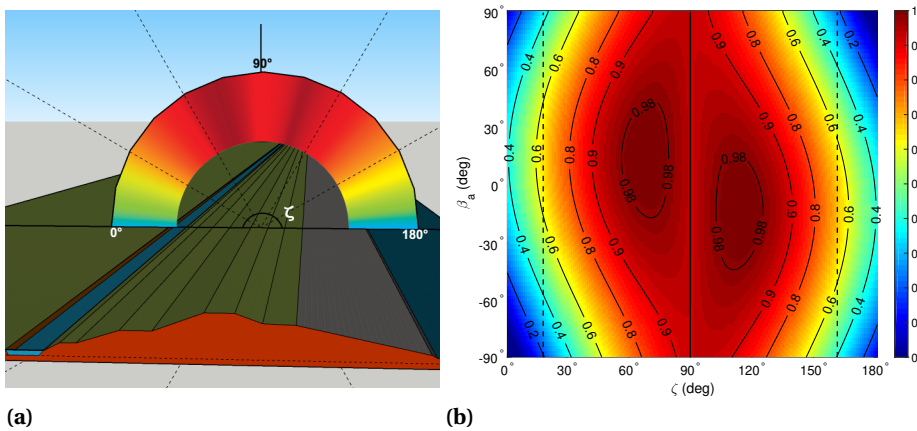


Figure 3.10: (a) Three-dimensional perspective orientation of a conceptual levee. Assuming no deformation along the longitudinal direction, any possible deformation direction is defined by (i) the orientation of the levee, β_a (here $\beta_a = 30^\circ$), and (ii) the orientation of the deformation vector, ζ , which runs from 0° to 180° . (b) Sensitivity direction plot, based on β_a and ζ , for a combined ascending/descending satellite viewing direction, expressing the sensitivity, s , of the measurements as a number between 0 and 1. The dashed lines indicate typical levee slope of 1:2.5, and the solid line indicates vertical deformations.

Figure 3.10b can be used to determine the particular observability of a specific deformation, based only on levee orientation and slope, even before satellite data is acquired.

A sensitivity value higher than 0.3 typically implies that a deformation is observable. Typical 1:2.5 levee slopes are indicated with the dashed lines. From this figure, it can be shown that generally all relevant levee deformations are observable within the levee profile. Dividing the measurement precision (Table 3.1) by the product of the sensitivity, s , (Figure 3.10b), and the coherence, c , yields a number that is proportional to the obtainable deformation precision [38]. Subsequently, it is possible to devise metrics to determine the minimal detectable deformation [135], that is, how likely can a deformation of a given value be observed with a certain level of confidence, allowing levee asset managers to determine whether a particular deformation can be detected.

3.4.2. DECOMPOSITION OF DEFORMATION VECTORS

In the case when (a) radar images are available from two viewing directions, that is, ascending and descending orbits, (b) yielding measurements at the same geographic locations, (c) acquired in the same period of time, and (d) under the assumption that there is no longitudinal deformation ($d_L=0$), the actual direction of the deformation can be retrieved by combining two measurements in a vector decomposition [136] into normal (d_N) and transversal (d_T) directions or into vertical (d_V) and horizontal (d_H) directions [137].

Here, we analyzed the sensitivity of horizontal deformation estimations for the primary flood defenses in the Netherlands based on their orientations (Figure 3.11a). A purely horizontal deformation would be earlier detectable for the green segments that lay on the North–South direction with an orientation between -60° and $+60^\circ$, whereas the orange and red segments, oriented in -90° to -75° and $+75^\circ$ to $+90^\circ$ range, would require a greater deformation to be detectable. Hence, the horizontal deformation of approximately 70% of the primary flood defenses in the Netherlands can be retrieved with good accuracy (Figure 3.11b).

Although deformations in LOS direction can already give significant insight in levee deformations by providing binary spatial information on the stability of a levee (i.e., stable/unstable), two-dimensional (2D) deformation vectors can be particularly relevant for specific failure mechanisms. For instance, deformation in horizontal direction can be an early warning for an instability failure, for example, a peat levee failure near Wilnis, the Netherlands failed in the year 2005 due to a horizontal sliding [138]. Likewise, subsidence of the levee, which is mostly observed in vertical direction, would lead to hydraulic failures, that is, overtopping and overflow. In order to examine whether deformation vectors can be estimated from the SAR data, here we analyze a vector decomposition algorithm [137] that we adapted for levee conditions by using 142 ERS imagery acquired between 1992 and 2001. The method is demonstrated on a 75 km long levee along the Markermeer, the Netherlands, for which the deformation velocity maps from both ascending and descending orbits are given in Figure 3.12.

The deformation velocity (mm/year) with a relative standard deviation, σ , for each measurement point has been estimated from the deformation values by least-squares estimation over the time period considered. In the spatial domain, an interpolation is required since the observation locations for which ascending and descending images are available, are usually different. For the Markermeer levees, most of the reflections are from the waterside slope of the levee, which usually has some hard revetment. A

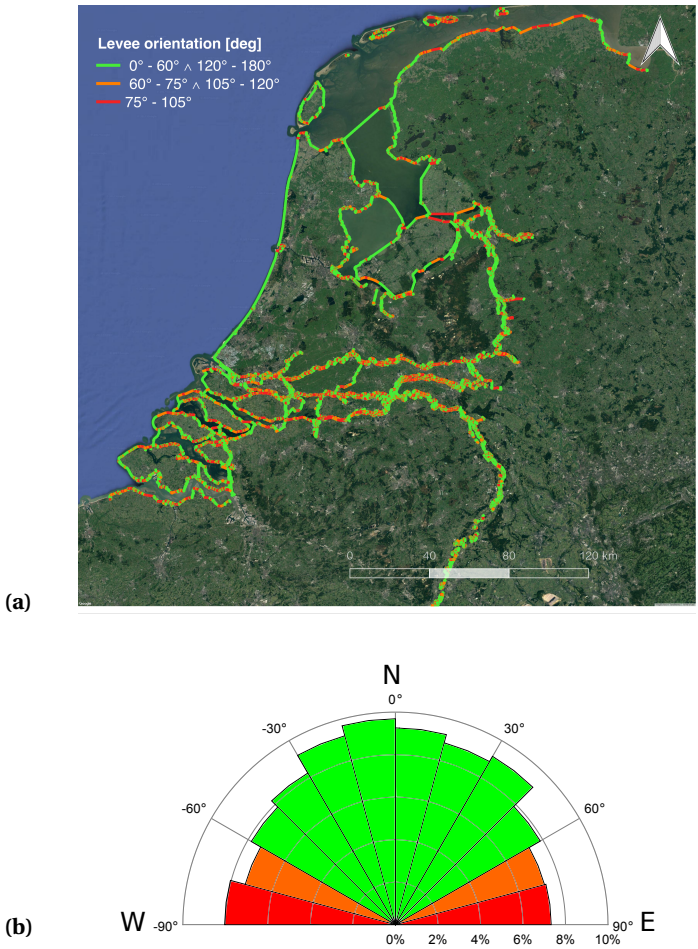


Figure 3.11: (a) Orientation of the primary flood defenses in the Netherlands. (b) Polar histogram indicating the length (in percentage) of primary flood defenses as a function of their orientation, with colors indicating the sensitivity to horizontal deformation.

distance-based interpolation method (inverse-squared distance weighting) [139] is used to interpolate an ascending deformation value on the location of the descending PS from close-by ascending PS's, assuming homogeneous characteristics. Considering the radar characteristics and the orientation and an average slope (1:2.5) of the levees, deformation velocity maps are decomposed into the four different directions (Figure 3.13). Related to the previous section on the sensitivity, values for the levee orientations outside the range of $[-60^\circ, +60^\circ]$ have been removed based on their low SNR level.

To obtain a general idea regarding the estimation sensitivity of deformation velocities in (mm/year), the LOS standard deviations, σ , are propagated for each point. An analysis of the sensitivity of the linear deformation velocities shows that when the levee

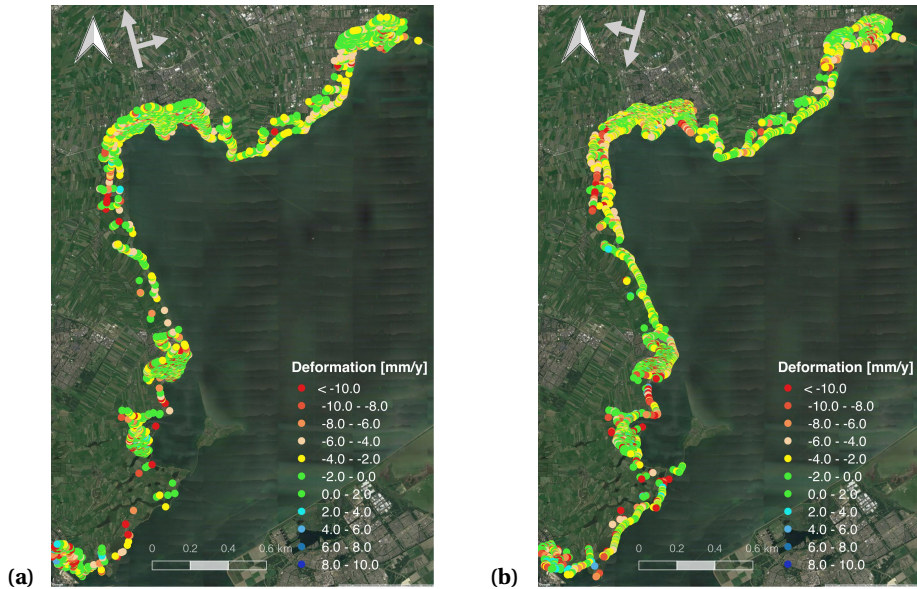


Figure 3.12: Linear deformation velocities (mm/year) in the line-of-sight (LOS) direction of the satellite for the Markermeer levee using the ERS satellite for the period of 1992–2001. (a) Ascending, (b) Descending.

orientation is close to the E–W direction, the σ of the horizontal or transversal deformations increases. In Figure 3.14, standard deviations of the linear deformation velocities in transversal and normal directions are lower than 0.8 and 0.4 mm/year in the $[-60^\circ, +60^\circ]$ range, respectively. Compared to transversal and normal directions, the sensitivity in the vertical direction is higher, with values of the σ of the linear deformation velocities lower than 0.2 mm/year, while the precision in the horizontal direction is lower than 1 mm/year, for the reasons discussed in the previous sections. This also reflects the larger variability for the horizontal estimates in Figure 3.13. In summary, it shows that levee orientation has an important effect on the observability of certain deformation components.

3.5. DISCUSSION ON THE POTENTIAL OF USING SATELLITES FOR LEVEE MONITORING

Being able to monitor the failure processes could contribute to the reduction of model uncertainties and to improvements in levee assessments. For many failure mechanisms as given in Figure 3.15, deformation is an important early indicator for imminent failures [23, 32, 33]. Early detection of these indications would facilitate on-time levee assessment and maintenance before a failure occurs [34].

The temporal sampling of contemporary satellites allows us to monitor changes on a daily scale (e.g., Sentinel-1a, 6 days repeat cycle, average of 1–2 days revisit time in

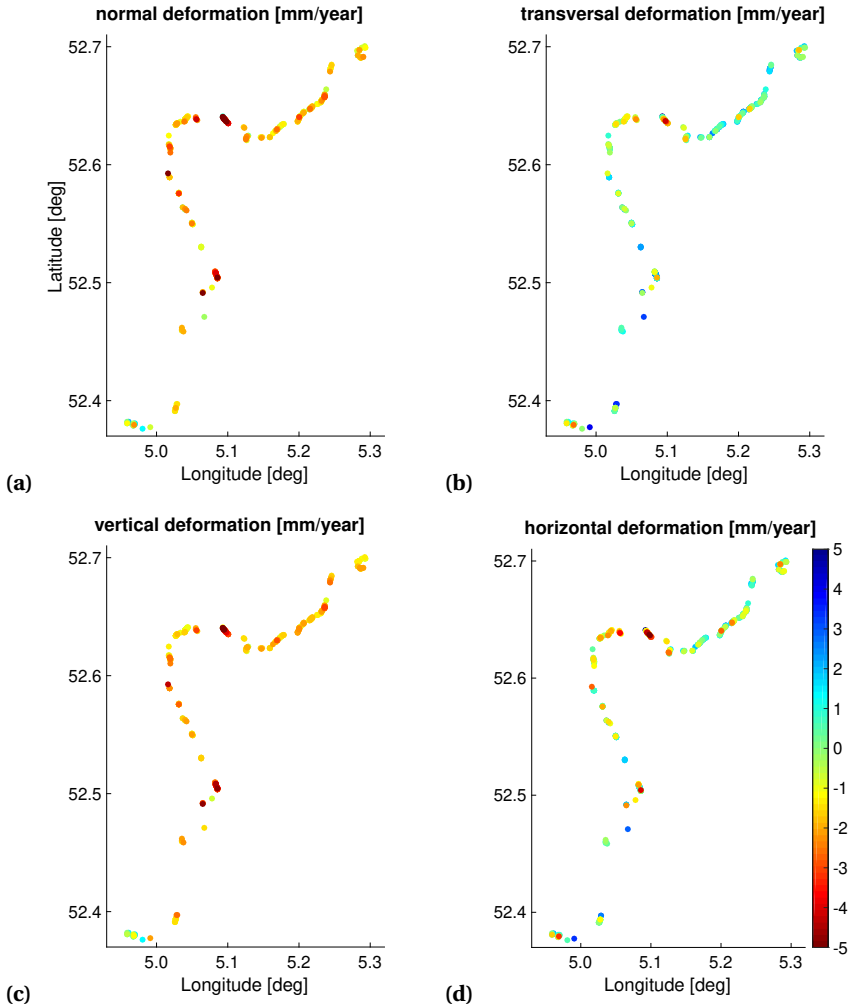


Figure 3.13: Deformation velocity maps (mm/year) decomposed in different directions: (a) normal d_N (b) transversal d_T (c) vertical d_V , and (d) horizontal deformations d_H for Markermeer levee monitored by the ERS satellite for the period of 1992–2001.

the Netherlands). Given this temporal sampling, geotechnical failures occurring in a range of hours to days may not be detectable (Figure 3.16). However, before any sign of a geotechnical failure becomes visible, the levee may have shown subtle degrees of deformations which could indicate a failure being imminent. The ability of detecting these anomalous behaviors, which may happen within a longer time span (from days to months) and can be interpreted as indicators of potential weak spots, is thus an important contribution to levee safety assessment (Figure 3.16). For example, before a piping

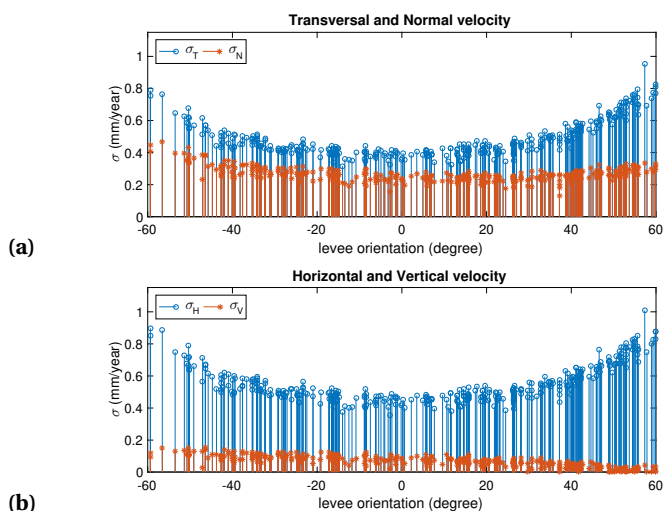


Figure 3.14: Standard deviations (mm/year) for the estimation of the decomposition vectors with respect to the levee orientations. (a) Transversal and Normal velocity. (b) Horizontal and Vertical velocity.

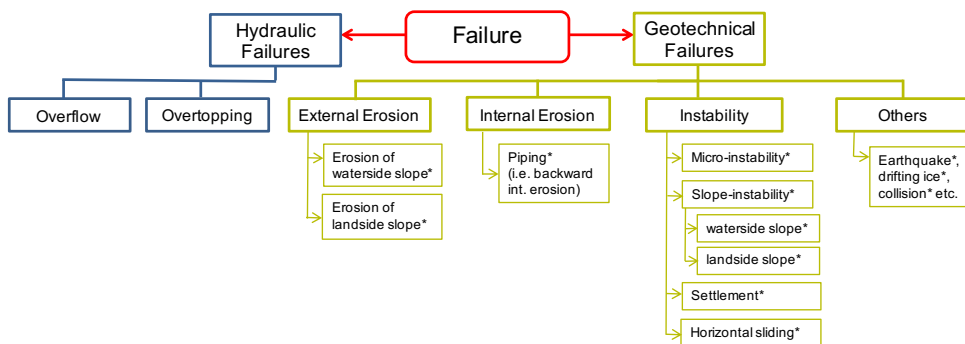


Figure 3.15: Overview of the most common flood defence failure mechanisms (see Figure 1.1). Failures that have deformation as an (early) indicator are marked with an asterisk (*).

failure occurs, the levee may have shown a certain degree of deformation (e.g., uplift) having a time span long enough to be detected. Likewise, anomaly indications of slope instability may be observed during rising water levels prior to the actual failure event as vertical deformations on the crest and larger horizontal deformations at the toe. Furthermore, seasonal changes in meteorological conditions, for example, long drought periods and the consequent shrinkage of the levee, can cause horizontal sliding, which may give anomaly indications (weeks to months) before the actual geotechnical failure occurs (hours to days).

In this context, it is most beneficial to detect (a) which location may be most prone

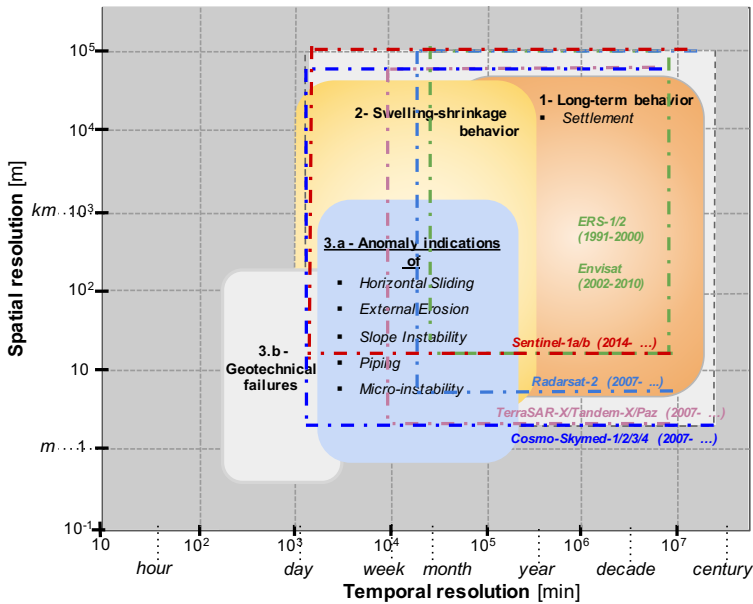


Figure 3.16: Log–log sensitivity diagram for the relation between levee behaviour and the satellite technology. Blue boxes represent the anomaly indications of the given geotechnical failure mechanisms. The numbers in the title of the boxes refer to the three main phenomena indicated in Figure 1.2.

to sudden failures and (b) which levee segments can be considered to be stable. Current satellite missions, having given spatial and temporal resolutions (indicated by means of the dashed lines in Figure 3.16), are capable of detecting these anomaly indications under certain conditions. A possible future application of SAR is the detection of deformation anomalies in the framework of an early warning system. This can be done by analyzing the response of a levee under normal loading conditions in order to identify those locations at risk of failing during extreme loading conditions. Substantial deformations in normal conditions could be precursors of a failure during more extreme circumstances. Even though two subsequent radar images are sufficient to create an interferogram, a longer time period (days to weeks, based on the precision of the observations and the satellite characteristics) may be required to be able to reliably detect an anomaly. Time-series analysis methods, for example, hypothesis testing [41] or machine learning techniques [140] could be used to automate the assessment. Moreover, as temporal and spatial resolution of satellite observations is expected to increase further, it may become possible in the future to observe geotechnical failures directly.

The potential of using SAR data can be explained by considering both the problem-driven and data-driven approaches. Operational management practice is generally considered as problem-driven in case of geodetic measurements. It is first decided what should be measured by levee managers, followed by hiring a contractor that can perform this task efficiently. Consequently, managers usually acquire what type of information

they request with a uniform quality. However, InSAR provides data-driven information, which is not common in management practices. Observations highly depend on the satellite characteristics and local conditions. Hence, satellite observations may not be optimally matched to every specific case, in contrast to conventional in-situ techniques.

The relevant question in this respect is whether it is beneficial to use the information that is already available, even if there is no one explicitly requesting the data. Thus, InSAR data must therefore be seen as complementary to the conventional techniques, as “another tool in the toolbox”. Especially countries having a strong expertise base and a full national InSAR coverage, such as the Netherlands, could improve their monitoring capabilities by making use of the frequent, abundant, and precise measurement data at a relatively low cost. Combining satellite data with other data sources (e.g., remote sensing and geological maps) and management information would provide a richer insight into understanding of levee behavior. In the case of the 22,500 km of flood defenses in the Netherlands, deformation data can be derived quantitatively on a daily basis which can complement levee management efficiently. Local in-situ measurements can be deployed effectively at those locations where it is needed. Also, additional geotechnical site analyses and safety assessments with models can be performed to get more information on the locations for which abnormal behaviors have been observed.

3.6. KEY CONCLUSIONS

Satellite radar imaging can be used to monitor the behavior of levees, which allows to detect deformations on a daily scale with mm-level precision in all weather conditions at low cost. It provides historical deformation data (from 1992 to today), which can be used to investigate trends in deformation and to get more insight into levee behaviour mechanisms. Moreover, technological advances and new generation satellites led to significant improvements in SAR data with reduced revisit time (near-daily) and increased spatial resolution (e.g., 3×3 m), providing frequent observations with large areal coverage (km's).

Frequently recurring technical questions on levee monitoring using SAR technology, related to applicability and precision were addressed. Various time-series processing techniques may be applied to estimate the deformations from the data. The most suitable approach depends on the surface cover, the number of available radar images, the orientation of the structures and the expected deformation signal.

The original *precision* of phase measurement of available satellites varies between 0.2 and 1.4 mm. However, the precision of the estimated observations is affected by the characteristics of the earth's surface (e.g., vegetation, soil types), which determines the *coherence*, and by the orientation of the levee in combination with the deformation vector of interest, which determines the *sensitivity*. Hence, the actual precision of observation varies based on the area of interest. Although most of the coherent scatterers are generally obtained from non-vegetated areas (e.g., roads, revetments, etc.), they may provide an indication of the deformation behaviour of the rest of the levee. Thus, developing processing techniques to extract coherent signals from vegetated levees is an important research priority, with recent studies showing promising results. This would also extend the applicability to fully vegetated levees.

Through a number of examples in the Netherlands, we examined how satellite tech-

nology can be used to complement existing levee stability assessments. These cases also show that we can estimate any deformation vectors in almost all directions with varying degree of sensitivity depending on the orientation and the slope of the levee. A sensitivity plot is presented to conveniently assess the detectability of any kind of deformation. As an example, we showed that horizontal deformation for 70% of the primary flood defenses in the Netherlands can be retrieved with high precision. Even though examples are shown only for the Netherlands, the applicability of this technology could be extended to other parts of the world, supporting levee management especially in countries with extensive flood defense infrastructures.

Although real-time monitoring of potential geotechnical failures is not possible given the temporal sampling of current satellites, sampling intervals (days) are two orders of magnitude higher than conventional monitoring (years). Given the increased temporal resolution, future research will focus on gaining a better understanding of levee behaviour, also in relation to loading conditions, and on detecting anomalies at an early stage, which can give indications of a levee failure being imminent. In summary, the deformation time-series can be used as (a) binary spatial information (i.e., stable/unstable), but also (b) for investigating the temporal behaviour of levee structures, and (c) to provide early warnings for anomalous behaviour preceding potential failures. We conclude that InSAR is moving from being a mere scientific tool towards an operational levee deformation monitoring system, with increased efficiency and quality. Consequently, the continuous analysis of InSAR levee deformation monitoring will assist the responsible levee authorities to take appropriate actions, hence avoiding catastrophic events and contributing to the flood risk reduction activities.

4

SUB-SEASONAL LEVEE DEFORMATION TO ENHANCE FLOOD PROTECTION

In the previous chapter, we explored the applicability of satellite radar imaging for levee management, and focused on long-term deformations to monitor subsidence of the levees. However, as most geotechnical failure mechanisms are related to dynamic levee responses to changes in loading conditions happening on a time scale of days to weeks [51], a better understanding of the short-term behavior of levees is required. Understanding the levee responses in normal conditions can then help to detect or predict the levee response to more extreme conditions, which would increase our capability of detecting anomalies that could identify unsafe situations.

The main aim of this chapter is to understand (1) how sub-seasonal patterns due to swelling and shrinkage can be identified from continuous levee deformation observations obtained with PS-InSAR, and (2) how these patterns are related to meteorological variations and levee safety. Our findings allow to understand the sub-seasonal behavior of the levee in greater detail and to predict swelling and shrinkage due to the variation of the loading conditions. By determining whether the observed deformation is in line with the response predicted from loading conditions experienced by levees and relating it to geohydrological properties of levees, it would become possible to identify problematic locations and apply the appropriate countermeasures.

The chapter is organized as follows. Section 4.1 describes the expected soil behavior under wetting and drying conditions, whereas Section 5.2 introduces the methodology on the developed deformation model (i.e., vPT-model) and hypothesis testing. Section 4.3 shows the modeling results applied on earthen canal levees in Delft, located in the Netherlands. Finally, Section 4.4 concludes the chapter with a discussion to what extend monitoring of sub-seasonal deformation behavior enhance flood protection.

Parts of this chapter have been published within [52].

4.1. SOIL BEHAVIOR UNDER WETTING AND DRYING CONDITIONS

The change in soil volume due to variations in soil moisture content is denoted as the swelling and shrinking behaviour of the soil [141], which has been studied for different soil types, such as clay [142, 143], peat [144–146] and others [147–149]. Swelling and shrinkage result from changes in the pore water pressures inside the levee, which are due to variations in hydrological loading conditions. When the soil saturates, the pore water pressure in the soil increases, reducing effective stresses in the soil matrix and results in swelling. In turn, a reduction in pore pressures due to drying leads to shrinkage of the soil [150].

4

The swelling and shrinkage behaviour of the soil is especially relevant for the safety of the canal levees. Water levels in these canals are fairly constant and typically exceed surface levels of adjacent polders, posing a continuous flooding threat to the hinterland, even under normal conditions. A large part of the flood defense system in the Netherlands (approx. 14,000 km) consists of regional canal levees which were often built centuries ago and strengthened several times using local peat and clay, amply available materials in the region [151]. Especially, due to its hydraulic properties, clay is often used in levees to enhance water resistance and erosion protection, and to reduce through-seepage. However, changes in precipitation and temperature can lead to significant swelling and shrinkage behaviour of these types of soil. In addition, cracks can form when the levee dries and the soil shrinks. Through these cracks water can enter the levee, reducing the soil strength. Another concern is that other materials or debris may enter the crack, preventing it from closing properly when the soil returns to a wet condition again [19]. Hence, the resulting changes in the geohydrology of the levee, which is loaded by a fairly constant water level, can directly lead to instability and failure. Many failures of the canal levees in the Netherlands have been recorded due to the heavy rainfall, e.g., a failure close to Wilnis in 1874 [152] or extreme warm and dry weather, such as failures in Zoetermeer in 1947, Oostzaan near Amsterdam in 1990, Bleiswijk in 1990 [153] and near Wilnis in 2003. Hence, extreme conditions, i.e., too dry (high temperature and low precipitation) or highly saturated soil (mainly heavy precipitation with low temperatures) cause a reduction in the soil strength of the levee, which can lead to a failure.

4.2. METHODOLOGY

In this section, we first describe the study area, meteorological and soil data that we analyzed, and the characteristics of the deformation data obtained from PS-InSAR processing. Later, we introduce the methodology of the developed deformation model (i.e., vPT-model) which aims to describe the swelling-shrinkage behavior of the levees. Lastly, we provide the methodology of Overall Model Test (OMT) in order to analyze how significantly the vPT-model describes the deformation behavior compared to the current application of steady-state linear model.

4.2.1. STUDY AREA: DELFT, THE NETHERLANDS

To evaluate whether levee deformations are predictable and related to meteorological patterns, we focus on earthen canal levees covering a 10×10 km area in south of Delft, located in the Netherlands, where almost 12 million people live in flood prone areas, and reliable flood defenses are essential to prevent catastrophic flood events [101]. The levees used in this study are regional flood defenses, as they are situated along regional rivers and canals. The canals are used to drain excess water from the lower-lying polders to the main rivers and the sea.

4.2.2. SOIL DATA

Soil profiles were obtained from borings performed in 2011 by Water Board Delfland at 17 different locations along the levee. Taking into account the non-uniformity of the soil compositions and the changes in soil moisture content of unsaturated zone, the dominant soil type from 0 to 2 meters below the surface level is being considered.

4.2.3. METEOROLOGICAL DATA

Precipitation [mm/day] and temperature [$^{\circ}\text{C}$] data are obtained from meteorological station 344 from the Royal Dutch Meteorological Institute near Rotterdam. Both precipitation and temperature are measured hourly with electronic sensors with a precision of 0.1 mm and 0.1 $^{\circ}\text{C}$, respectively. The distance from the meteorological station to the study area is approximately 4 km. Hence, the measured data are expected to differ slightly from the meteorological conditions at the study area. However, since cumulative and average meteorological values are used in the model, the effect is assumed to be negligible.

4.2.4. DEFORMATION DATA FROM PS-INSAR PROCESSING

The study area has been monitored using data from TerraSAR-X to estimate the deformation time-series of each PS point between 8 April 2009 and 8 January 2015. This satellite provides X-band high resolution data with a wavelength of 31 mm, 3×3 m pixel size and a repeat cycle of 11 days.

The main principle of satellite radar imaging can be described as follows. Radar sensors transmit pulses of high-frequency electromagnetic waves from space to Earth and record the strength and the fractional phase of the back-scattered signals that are reflected from the surface to construct SAR images. By interfering at least two radar images acquired at different times over the same location, the combined effect of surface deformation, topography and atmospheric signal delay is obtained. In order to estimate and isolate the surface deformation from the other phase contributions, a large stack of SAR images acquired by the same satellite is analyzed by interferometric time-series methods. All deformations are projections of the real deformation [mm] onto the Line-of-Sight (LOS) direction. This direction from satellite to object is determined by the heading angle of the satellite, α_h , and the incidence angle of the radar, θ_{inc} .

Various time-series processing techniques can be applied to estimate the deformations from the satellite data. The most suitable approach depends on a number of factors, such as the number of available radar images, satellite characteristics, the area of interest (e.g., surface cover), and the expected deformation signal. Regardless of the spe-

cific approach used, PS-InSAR analysis typically includes three main steps; 1) stack processing: creating the multiple interferograms from complex data, 2) PSI analysis: detecting Persistent Scatterers (PS) and separating deformation phase from other contributions (such as topography, atmospheric delay [38]) and 3) quality assessment: evaluating the quality of the results [126]. In this study, the interferometric stack processing of the radar data has been performed using the Delft Object-oriented Radar Interferometric Software (DORIS) [125]. The Delft implementation of Persistent Scatterer InSAR (DePSI) [126] has been applied on 168 TerraSAR-X strip-map images in order to estimate the Line-of-Sight (LOS) deformation time-series. The main principles of PS-InSAR and a general overview of the past studies can be found in a review [123], whereas Chapter 3 of this thesis discusses the applicability of the technique to continuous levee monitoring.

4

4.2.5. DEFORMATION MODELING: vPT-MODEL

In order to describe this deformation behavior of earth-filled levees, we consider its relation with respect to those meteorological data, i.e., precipitation and temperature, which are expected to give an indication of soil moisture changes. For this reason, the steady-state model, which considers the inter-annual trend, due to the long-term irreversible behavior of the levee (e.g., subsidence), is extended with the introduction of precipitation, P , and temperature, T , time-series. In this way, it is also possible to evaluate the sub-seasonal and reversible behavior of the levee, i.e. its swelling and shrinkage. Hence, the proposed model, hereafter called vPT-model, is defined as

$$d(t) = d_V(t) + d_{PT}(t), \quad (4.1)$$

where the first term corresponds to the steady-state model,

$$d_V(t) = v \cdot t + b, \quad (4.2)$$

with v the slope in [mm/day] and b the intercept in [mm] of the long-term linear trend. This intercept accounts for the atmospheric signal delay and scattering noise in the master acquisition, which is common in all single-master interferograms [126]. The second term describes the swelling-shrinkage behavior of the levee as a linear combination of precipitation and temperature time-series. We expect the soil to react to variations in precipitation and temperature only after a certain period of time. This requires a regression model which includes a time delay τ between the meteorological data and the observed levee deformation. The second term of Eq. (4.1) is then defined as

$$d_{PT}(t) = c_P (P(t - \tau_P) - \delta_P) + c_T (T(t - \tau_T) - \delta_T), \quad (4.3)$$

where the time-series at time t are indicated as $d(t)$ in [mm] for deformation, $P(t)$ for the cumulative precipitation, in [mm], over a time interval Δt_P , starting at $t - \Delta t_P$ and ending at t , and $T(t)$ for the average temperature, in [°C], over a time interval Δt_T , starting at $t - \Delta t_T$ and ending at t . The offsets for precipitation and temperature time-series are represented by δ_P in [mm] and δ_T in [°C], respectively, while the time delay parameters for $P(t)$ and $T(t)$ with respect to $d(t)$ are denoted as τ_P and τ_T , with their units in [day]. Lastly, c_P in [mm/mm] and c_T in [mm/°C] are the scaling coefficients of the linear combination, between $d(t)$ and $P(t)$ and between $d(t)$ and $T(t)$, respectively.

4.2.6. MODEL PARAMETER ESTIMATION

Soil deformation is expected to result from cumulative and smooth variations in precipitation and temperature. For this reason, the mean temperature and the cumulative precipitation data over time periods $\Delta t_T = 10$ days and $\Delta t_P = 30$ days are considered, respectively. The time period for the cumulative precipitation was chosen to be longer than the time resolution of the deformation data to take into account for the long-term effect of precipitation.

The vPT-model in Eq. (4.1) can be simplified as

$$d(t) = v \cdot t + c_P(P(t - \tau_P)) + c_T(T(t - \tau_T)) - \delta \quad (4.4)$$

where $d(t)$, $P(t)$ and $T(t)$ are the deformation and meteorological data preprocessed as described above, and the global offset coefficient is defined as $\delta = (c_P \delta_P + c_T \delta_T - b)$. This model is non-linear due to the products $c_P \tau_P$ and $c_T \tau_T$. For this reason, we use the cross-correlation method [154] to estimate the τ_P and τ_T parameters. This approach is used to shift $P(t)$ and $T(t)$ with respect to $d(t)$ (after removing the steady-state trend $v \cdot t$) and to compare the two records at each possible time delay, where $\hat{\tau}_P$ and $\hat{\tau}_T$ are selected as the values providing the maximum absolute value in the cross-correlation function. Hence, the precipitation and temperature time-series are aligned to the deformation data (i.e., shifted by $\hat{\tau}_T$ and $\hat{\tau}_P$, respectively).

After the time alignment, the vPT-model is simplified as

$$d(t) = v \cdot t + c_P \tilde{P}(t) + c_T \tilde{T}(t) + \delta, \quad (4.5)$$

where the aligned time-series are defined by

$$\tilde{P}(t) = P(t - \hat{\tau}_P), \quad \tilde{T}(t) = T(t - \hat{\tau}_T). \quad (4.6)$$

The optimal values for the linear parameters of the vPT-model are estimated by minimizing the mean square error between the deformation data and the model estimate

$$\min_{\mathbf{x}} \|\mathbf{d} - \mathbf{A}\mathbf{x}\|_2^2, \quad (4.7)$$

$$\mathbf{x} = [v, c_P, c_T, \delta]^T, \quad \mathbf{A} = [\mathbf{t}, \tilde{\mathbf{P}}, \tilde{\mathbf{T}}, \mathbf{1}]^T \quad (4.8)$$

where \mathbf{d} is the $m \times 1$ vector containing the LOS deformation observations, \mathbf{A} is the $m \times n$ design matrix whose columns are the time vector \mathbf{t} , the vectors $\tilde{\mathbf{P}}$ and $\tilde{\mathbf{T}}$ containing respectively the aligned precipitation \tilde{P} and temperature data \tilde{T} , $\mathbf{1}$ is a vector containing only ones, and \mathbf{x} is the $n \times 1$ vector of the model parameters (the symbol $'$ indicates the transpose). The estimated optimal values of \mathbf{x} are then given by the least squares solution [155] as

$$\hat{\mathbf{x}} = (\mathbf{A}'\mathbf{Q}_d^{-1}\mathbf{A})^{-1}\mathbf{A}'\mathbf{Q}_d^{-1}\mathbf{d}, \quad (4.9)$$

where the covariance matrix \mathbf{Q}_d specifies the dispersion of the measured deformation data. The observations in the time-series are assumed to be uncorrelated, each having a fixed variance of unit weight σ_d^2 . Thus, the variance matrix can be factorized as $\mathbf{Q}_d = \sigma_d^2 \mathbf{I}_m$, with \mathbf{I}_m an $m \times m$ identity matrix.

Once the model parameters are obtained as explained above, they are used in the vPT-model of Eq. (4.4) to obtain the estimated (adjusted) deformation time-series $\hat{\mathbf{d}} = \mathbf{A}\hat{\mathbf{x}}$.

The error between the measured deformation time-series and the estimated one is given by the residual $\hat{\mathbf{e}} = \mathbf{d} - \hat{\mathbf{d}}$ and the quality of the estimation is then evaluated by the mean square error (MSE).

4.2.7. HYPOTHESIS TESTING: OVERALL MODEL TEST (OMT)

The Overall Model Test (OMT) [156] is used to check the validity of the models. Testing is usually performed by comparing a *null hypothesis*, H_0 , versus an *alternative hypothesis*, H_a , where H_0 represents the model under investigation and H_a corresponds to the case where no restrictions are imposed on the observations, as in

$$\begin{aligned} H_0 : E\{\mathbf{d}\} &= \mathbf{Ax}, & D\{\mathbf{d}\} &= \mathbf{Q}_d \\ H_a : E\{\mathbf{d}\} &\in \mathbb{R}^m, & D\{\mathbf{d}\} &= \mathbf{Q}_d, \end{aligned} \quad (4.10)$$

where $E\{\cdot\}$ and $D\{\cdot\}$ denote expectation and dispersion, respectively. To reject or sustain H_0 depends on the test statistic,

$$T_q = \hat{\mathbf{e}}_0' \mathbf{Q}_d^{-1} \hat{\mathbf{e}}_0, \quad (4.11)$$

which follows a central χ^2 -distribution with $q = m - n$ degrees of freedom, and corresponds to a weighted sum-of-squares of the least squares residual vector $\hat{\mathbf{e}}_0$ under H_0 . Given a chosen level of significance α , the critical value k_α follows from the χ^2 -distribution to test the null hypothesis,

$$\text{reject } H_0 \text{ if } T_q > k_\alpha. \quad (4.12)$$

Rejection of H_0 indicates that the deformation behavior is not significantly well described by the chosen model, given the assumed level of significance. For InSAR time-series, α is typically defined in the range of $0.2\% < \alpha < 2\%$, as we prefer to stick to a relatively simple null hypothesis if possible [157]. In this study, we assumed an α value of 1%, but in practice this is a decision to be taken by the local authorities. The variance of unit weight for TerraSAR-X with a 31 mm wavelength is conservatively assumed to be $\sigma_d^2 = 3^2 \text{ mm}^2$ [126, 157].

4.3. MODELING THE SWELLING AND SHRINKAGE BEHAVIOR OF LEVEES

In order to analyze the deformation behavior of the canal levees, we used 168 images recorded from the TerraSAR-X satellite, covering the study area explained in the previous section. We first estimate the deformation time-series of each measurement point (hereafter called PS point) on the canal levees of Delft using the PS-InSAR technique [39, 158] with an approach based on geodetic estimation theory [126]. Deformation time-series are created spanning a period of 6 years (2009-2015) (Figure 4.1a). Although the results are visualized by linear deformation velocity [mm/year], every PS point has a complete time-series of deformation estimates in the Line-of-Sight (LOS) direction.

To examine the swelling and shrinkage behavior of the levees, we developed a predictive deformation model, called vPT-model, considering the meteorological loading conditions (i.e., precipitation and temperature) as indirect indicators of the water content inside the levee. The model is used to analyze the swelling and shrinkage behavior,

and to assess whether these sub-seasonal patterns can be identified in the deformation time-series. Figure 4.1b shows a part of the levee segment in the monitored area, and an associated time-series. A comparison between the time-series of observed deformation from satellite, $d(t)$ and the deformation $\hat{d}(t)$ estimated using the vPT-model, is given in Figure 4.1c for a random PS point and compared with the steady-state model. It can be seen how the steady-state model only describes the inter-annual subsidence trend, whereas the vPT-model, which uses the meteorological data shown in Figure 4.1d, also follows the sub-seasonal swelling-shrinkage variations of the deformation time-series.

Nevertheless, deviations from the vPT-model occur, e.g., in December 2010 and in summer 2011, see Figure 4.1c. For example, the summer period of 2011, indicated by a dashed rectangle in Figure 4.1c, was very dry. During this period, surface of the levees was sprayed with water in order to avoid excessive drying of the soil due to the extreme drought conditions. This situation may explain the unexpected deformation of the levee which showed a swelling behavior not predicted by the model.

4.3.1. APPLICATION OF THE vPT DEFORMATION MODEL

The developed vPT-model has been applied on each PS point along the canal levees in Delft, comprising of 1184 PS points. To assess how well the vPT-model describes the deformation compared to the steady-state model, we apply hypothesis testing to both models independently. Firstly, the significance of the vPT-model is tested using an Overall Model Test (OMT) and compared with the steady-state model for different values of the assumed variance of the observations, σ_d^2 . A lower value for σ_d^2 increases the value of the test statistic and thus the probability that the null hypothesis, H_0 , is rejected. The results are given in Figure 4.2, showing the percentage of PS points for which H_0 is sustained. It can be seen that, already for $\sigma_d^2 = 9 \text{ mm}^2$, the vPT-model is providing a higher number of PS time-series that can be well modeled compared to the steady-state model. By decreasing the value of σ_d^2 , the difference in significance between the two models gets even larger. This higher significance is the result of the improved modeling capability of the vPT-model, which results in better estimates of the observed deformation time-series.

In order to quantify this improved modeling capability, we then evaluate the quality of the estimations by calculating the mean square error (MSE) for each PS time-series. In Figure 4.3, the MSE value per PS point for the entire area is given for both steady-state and vPT-model. The reduction in the MSE for the vPT-model compared to the steady-state model can be clearly observed on the two maps, with green points representing the PS time-series showing a low MSE, and red points representing PS time-series giving high MSE. The MSE values are also given in the histograms, which illustrates the error distribution for the PS points considered. The comparison between the two distributions highlights a clear shift of the MSE towards lower values.

The reduction in the MSE also allows to assume a lower variance σ_d^2 for the observations. For instance, assuming an a-priori variance of 7 mm^2 , the vPT-model gives 79% of the PS points with $\text{MSE} < \sigma_d^2$, while the steady-state model gives only 39%. Hence, for a large number of points, the deformation data can be modeled using the vPT-model with higher quality of the estimations. Thus, for those points that have low MSE, the vPT-model can also provide better indications of the swelling and shrinkage patterns.

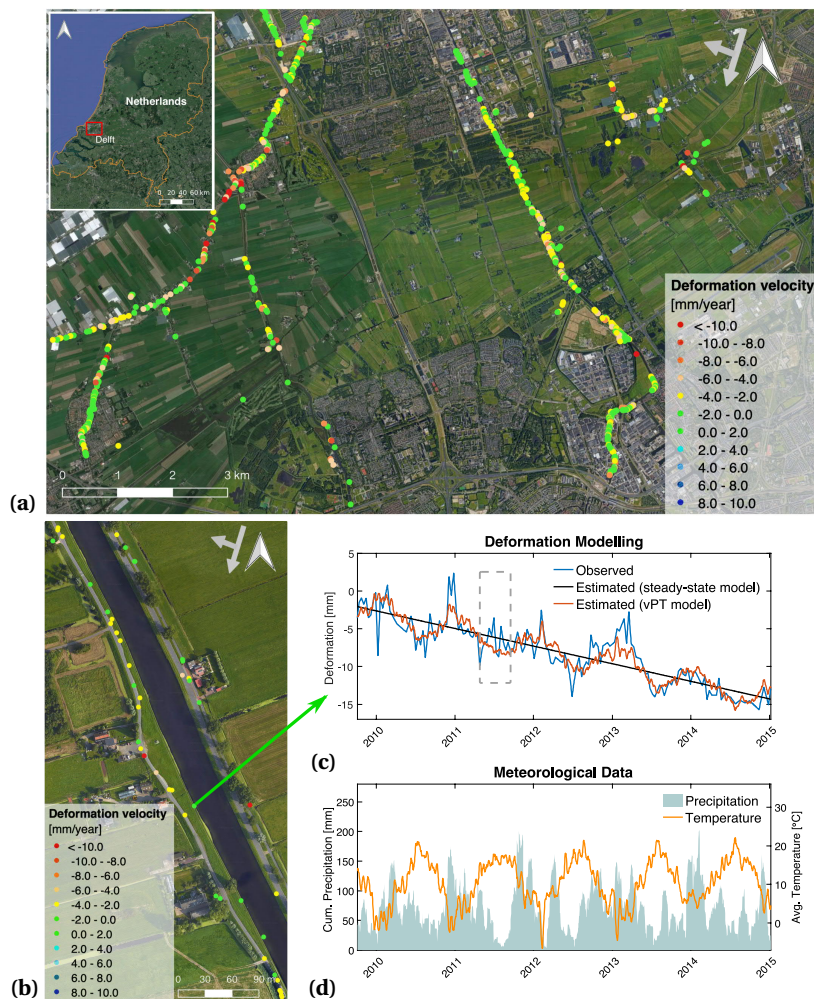


Figure 4.1: Analysis of deformation behavior of the levees in Delft, the Netherlands. **(a)** Deformation behavior of the canal levees has been analyzed based on data acquired by TerraSAR-X, descending orbit (2009-2015) and visualized in the deformation velocity [mm/year] map. **(b)** A part of the levee segment in the monitored area. **(c)** A comparison is given between time-series of observed deformation $d(t)$ and estimated deformation, $\hat{d}(t)$ using the steady-state model with an MSE of 4 mm^2 and the vPT-model with an MSE of 2.1 mm^2 for this specific PS point. The period of summer 2011 is shown in a dashed rectangle. **(d)** Cumulative precipitation [mm] and average temperature [$^{\circ}\text{C}$] data used in the vPT-model. The figure was generated using the QGIS software, (version 2.18.27, <https://qgis.org>). The background image from Map data ©2015 Google is added using the QGIS QuickMapServices (version 0.19.10.1, https://plugins.qgis.org/plugins/quick_map_services/).

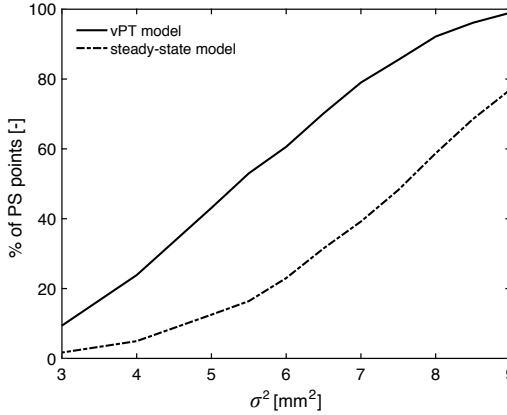


Figure 4.2: Overall Model Test (OMT) results. Percentage of PS points for which vPT-model and steady-state model are sustained for different values of variance of unit weight, σ^2 .

However, deformation estimations with low precision (e.g., MSE above 7 mm²) are still included in the results. In general, a high MSE could be related to several factors, such as radar signal decorrelation [38, 126] (e.g., vegetation, maintenance), or unmodeled deformation behavior due for instance to problematic locations or soil compositions responding differently to meteorological changes [51].

4.3.2. RELATION WITH SOIL TYPES OF THE LEVEE

The deformation behavior of a levee depends on its soil characteristics. In order to assess whether any deformation pattern related to the type of soil can be observed from the model parameters, we focus on a levee segment (Figure 4.4a) for which the soil profiles are provided by the local water authority, Water Board Delfland. Given these soil profiles, we defined three specific levee locations given in Figure 4.4a, whose main soil type for the first 2 meters of depth are considered. Location A is predominantly made of clay, location B shows different mixtures of clay and sand, and location C has sand as its primary soil type. These three locations have been investigated further based on the vPT-model results for those PS points giving an MSE lower than 7 mm². First, we compared the reaction time of the soil, i.e., time delay parameters τ_P and τ_T . Then, we analyzed the scaling coefficients c_P and c_T , which are expected to provide an indication about the reaction magnitude of the different soil types.

Considering the swelling-shrinkage behavior of the types of soil, sandy soil is expected to react faster than clayey soil for the same amount of precipitation received due to larger porosity and higher hydraulic conductivity. On the other hand, clayey soil would react with bigger magnitude compared to the sandy soil due to the organic components in its composition. Large pore volumes in between sand particles would allow the water to drain quicker, which would result in smaller volume changes compared to clayey soil.

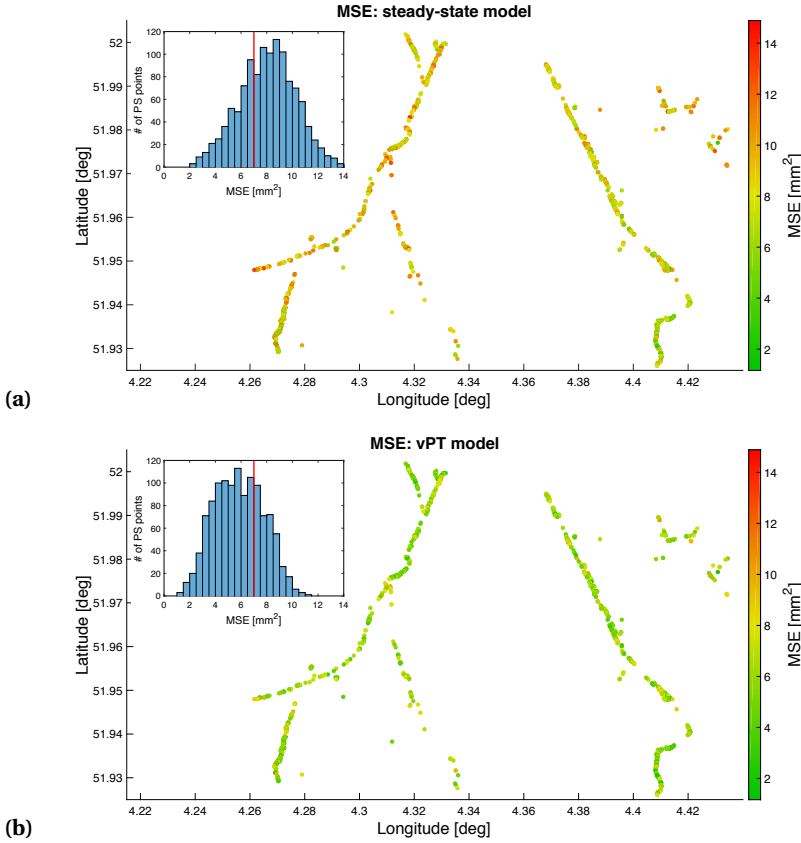


Figure 4.3: Modeling results for the deformation behavior of the canal levees in Delft, the Netherlands, cf. Figure 4.1. MSE values per PS point and distribution of MSE are shown for (a) steady-state model, (b) vPT-model. The comparison between the two maps shows how the vPT-model generally provides a lower MSE over the entire levee structure.

In order to verify if these expected behaviors are observed in the parameters of the estimated vPT-model, Figure 4.4a shows the different PS points within the selected locations (indicated by the rectangles), where the estimated values of the vPT-model parameters are given on a colour scale in Figures 4.4b-4.4e. Figure 4.4b shows the values for the time delay τ_P related to the precipitation data. Location A shows longer τ_P compared to locations B and C. This is in accordance with the expected faster reaction of sandy soil compared to clayey soil. On the other hand, the values of the τ_T parameter (Figure 4.4c) are almost always zero. This is an indication that the levee reacts almost instantaneously with respect to temperature (averaged over 10 days) regardless of the soil type. The few PS points showing higher values for τ_T are considered to be outliers, for which the parameters might have been poorly estimated due to some of the issues discussed before.

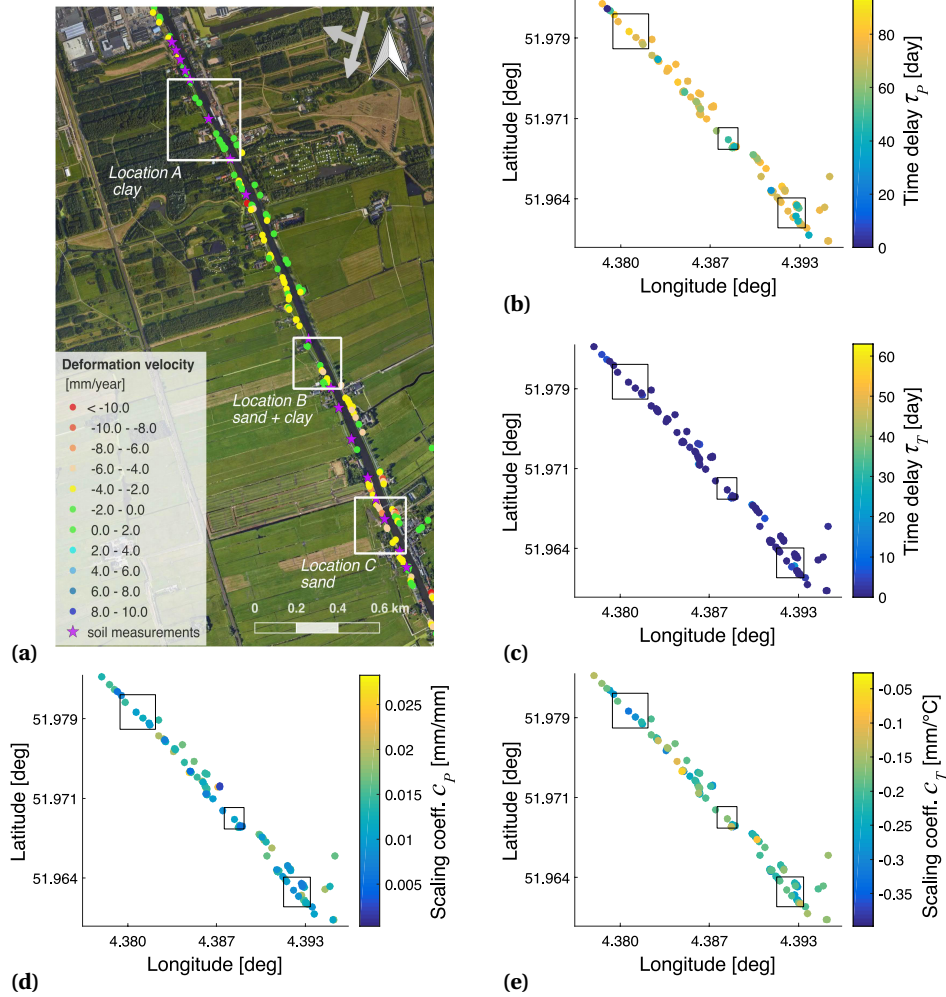


Figure 4.4: The relation between the soil types and the vPT-model parameters. The analysis of the estimated vPT-model parameters for those PS point with MSE lower than 7 mm^2 within (a) the selected locations A, B and C (indicated by the rectangles) on the east levee in the study area with their predominant soil types. (b) time delay for $P(t)$, τ_P [day], (c) time delay for $T(t)$, τ_T [day], (d) scaling coefficient for $P(t)$, c_P [mm/mm], (e) scaling coefficient for $T(t)$, c_T [mm/ $^{\circ}\text{C}$]. The figure in (a) was generated using the QGIS software, (version 2.18.27, <https://qgis.org>). The background image from Map data ©2015 Google is added using the QGIS QuickMapServices (version 0.19.10.1, https://plugins.qgis.org/plugins/quick_map_services/).

The values of the scaling coefficient related to the precipitation data c_P provide no clear indication about the reaction magnitude of the different soil types (Figure 4.4d). A better idea is however provided by the scaling coefficient for the temperature c_T in Figure 4.4e. In this case, it is more evident that the influence of the temperature on the clayey soil (location A) is stronger than on sandy soil (location C).

In general, these results are in accordance with the expected behavior of different soil types to precipitation and temperature changes, regardless of the fact that only a small number of PS points with low MSE is available in each location considered. The variability of the parameter values within the same locations is most likely due to differences in levee characteristics (e.g., different slopes), and heterogeneity of the soil profiles in between two boring measurement locations and other factors. More quantitative results and a better validation of the vPT-model for different soil types would thus require a larger amount of data available and of better quality, and more detailed information about the soil type at specific locations.

4

4.4. ENHANCING FLOOD PROTECTION

The strength of the proposed vPT-model lies in the ability of describing not only the inter-annual subsidence phenomenon, but also the sub-seasonal deformation behavior using meteorological data, i.e., precipitation and temperature, as indirect indicators of the water content inside the levee. This also allows analysing the influence of the meteorological conditions on the swelling and shrinkage behavior on a weekly basis, thus enabling predictions of the expected behavior of the levee due to variations in the loading conditions. Being able to model and predict the sub-seasonal behavior of a levee based on recorded extreme meteorological events would thus increase our ability of identifying critical situations.

In addition, the observed deformation can also be related to changes in geohydrological properties of a levee, such as the moisture content, weight and phreatic line (i.e., groundwater table in an unconfined aquifer). An instability or sliding of the landside slope can in fact occur when the levee loses weight due to drying and/or due to changes in effective stress in the soil. In order to illustrate the potential of satellite monitoring to detect stability problems and thus, to enhance flood protection, we consider the canal levee failure that occurred near Wilnis, the Netherlands, in 2003 as an example.

4.4.1. DEFORMATION ESTIMATION FOR THE LEVEE FAILURE AT WILNIS, THE NETHERLANDS

Extreme drying out of this peat levee during the hot summer led to its loss of weight, triggering levee instability which consequently lead to flooding of the neighborhood behind it. Using the documented information by Van Baars [138] on the weight changes from saturated to unsaturated conditions of the levee and assuming isotropic deformation, we roughly estimate shrinkage on the crest before the actual failure as follows.

In the assessment of the failed levee at Wilnis [138], two scenarios for changes of the phreatic line in the peat levee are considered: (a) fully saturated (phreatic line is at the crest), and (b) unsaturated (phreatic line drops 1 m below the crest level). Relevant information and the cross section of the levee can be found in the original study [138].

Here we estimate the expected deformation of the crest in case the phreatic line drops from scenario (a) to scenario (b), using the data documented by Van Baars [138]. In scenario (a), the volume of saturated soil, $V_{\text{soil-sat}} = 1 \text{ m}^3$. The gravimetric water content, Θ , is described as the ratio between the mass of the water, M_w , and the mass of solids, M_{solids} . For the saturated peat soil at the Wilnis levee, Θ was varying between 600% to 800%, and the unit weight of the saturated peat soil, $\gamma_{\text{sat}} = 11 \text{ kN/m}^3$, and the unit weight of unsaturated peat soil, $\gamma_{\text{unsat}} = 5 \text{ kN/m}^3$ [138, 159, 160]. The ratio between mass and volume of the solids is assumed to be constant.

In the case of fully saturated soil (scenario (a)), the mass of soil, $M_{\text{soil-sat}}$, is equal to sum of mass of water, $M_{w\text{-sat}}$ and mass of solids, $M_{\text{solid-sat}}$. Thus, for the given Θ of the saturated soil, $M_{\text{soil-sat}} = \gamma_{\text{sat}} \cdot V_{\text{soil-sat}} = 11 \text{ kN}$. Using an average Θ of 700%, $M_{w\text{-sat}} = 9.63 \text{ kN}$ and $M_{\text{solid-sat}} = 1.38 \text{ kN}$. Considering the unit weight of water, $\gamma_w = 9.81 \text{ kN/m}^3$, the volume of water in the saturated soil is calculated as $V_{w\text{-sat}} = M_{w\text{-sat}} / \gamma_w = 0.98 \text{ m}^3$ and the volume of solids in the saturated soil is then $V_{\text{solid-sat}} = V_{\text{soil-sat}} - V_{w\text{-sat}} = 0.02 \text{ m}^3$. After a dry period of approximately 100 days, soil samples taken from the crest of the levee show that Θ of the unsaturated soil (scenario (b)) was around 200% [138, 159]. In this case, the mass of water, $M_{w\text{-unsat}}$ reduces to 2.75 kN and the corresponding volume of water in the unsaturated soil is $V_{w\text{-unsat}} = 0.28 \text{ m}^3$. The mass of solids in the unsaturated soil remains unchanged, $M_{\text{solid-unsat}} = 1.38 \text{ kN}$.

Hence, the volume change of the soil, ΔV , between the two scenarios is estimated as 0.175 m^3 in the case of a 1 m drop in the phreatic line with the reduction of Θ from 700% to 200%. This correspond to a deformation of 6% of the total height (i.e., 6 cm) assuming an isotropic shrinkage of the soil. For an initial Θ of 800% and 600%, about 2% to 10% of shrinkage can be observed, respectively. In case of an anisotropic deformation, mostly on the vertical direction, this range can increase up to approximately 20% in a drought period of 100 days. Thus, expected deformations in the first phases of the drying process occurred in the levee are estimated to be already in the range of few centimeters. While no SAR satellite data were available in the period of failure, this range of deformation is well within the observability capabilities of current SAR sensors and PS-InSAR algorithms. The monitoring and modeling of this kind of deformation behavior, which normally takes place over a period of several weeks to months and eventually leads to a failure, could help to flag the extreme shrinkage of the levee. This would allow levee managers to apply timely countermeasures, such as watering or installing stability berms, to prevent instability.

4.5. KEY CONCLUSIONS

A related possible future application of the proposed vPT-model is the detection of deformation anomalies in the framework of an early warning system. For example, when the soil has dried, the shrinkage and the volume change may result in cracks in the soil. In this case, the deformation behavior of the levee will deviate from the expected deformation. This particular event would then be regarded as an anomaly with respect to the normal behavior of the levee, which should be an indication for a potential weakness and a call for more in-depth analysis of the situation. It is also noted that levee deformation and its effect on safety will be highly dependent on local soil and geohydrological conditions of the levee. Further research on these aspects would need to address the

relationship between deformation and geohydrological levee properties and the effects on levee stability for a number of representative situations.

In conclusion, this study shows that a) sub-seasonal deformations obtained from monitoring a levee with the PS-InSAR technique can be observed on the time scale of weeks, that b) these deformations are strongly correlated with the changes in meteorological conditions, that c) deformation changes in time can be estimated using a relatively simple regression model, and that d) deformations can be directly related to geohydrological properties and the safety of the levee. Even though the examples are given for the Netherlands, this technology is applicable to other parts of the world, thus supporting levee management especially in countries with extensive flood defense systems. Findings of this study will assist the future development of reliable early warning methods using continuous deformation monitoring, thus enhancing flood protection.

5

ANOMALY DETECTION ALONG LEVEES

Using satellite radar interferometry for levee safety assessment could be most beneficial when it is used for timely detection of potential problematic locations. An early warning system for levee deformations requires two main aspects to be taken into consideration, namely (a) understanding the deformation response of a levee under normal loading conditions, i.e. explainable deformation, covered in Chapter 3 and 4 of this thesis, and (b) finding the deviations from this normal behavior, i.e. anomalies, which may be early indicators of a potential hazard, addressed in this chapter.

The aim of the current chapter is to introduce a prototype early warning methodology using satellite-based deformation monitoring in order to detect anomalies on levees. More specifically, we explore the use of deformation time-series obtained by PS-InSAR in order to enable continuous levee monitoring, such as detecting, tracking and analyzing changes that can be indicative of potential problematic locations. These locations may be very localized, only detected by a single PS, or cover a longer levee segment, showing a range of anomalously behaving PS. Although the detection of anomalies may not yield conclusive statements on finding potential failure locations, in the later stage, the inclusion of available prior information by the end-users (i.e., levee authorities) can help them to detect weak spots more precisely. This will allow the end-users to critically evaluate the InSAR time-series results, which can be optimally tuned based on their needs and conditions.

The chapter is organized as follows. In Section 5.1, we introduce a set of temporal models to describe the levee deformation behavior, covering the expected normal behavior, as well as the deviations from this normal behavior, i.e. anomalies. Furthermore, we provide a methodology to detect these anomalies (or abnormal behavior) along the levees using a statistical testing procedure applied on each InSAR measurement point. The proposed approach intends to advance the applicability of the technique on analyzing the structural behavior of levees. This is demonstrated in Section 5.2 via two different case studies in which anomalies are detected along the levees (a) in Delft, the

Netherlands, throughout a certain period of time and (b) in Grave, the Netherlands, on a specific date following an accident.

5.1. DETECTING ANOMALIES IN LEVEE BEHAVIOR

In this section, we adapt a probabilistic method for InSAR time-series proposed by [157] in order to analyse temporal deformation patterns along the levees. First, the vPT-model described in Chapter 4 is used to define the normal behavior of levees, whereas additional models are introduced to specify possible abnormal behaviors. Second, the vPT-model is used as the null hypothesis in the multiple hypothesis testing (MHT) framework, whereas the alternative hypotheses are defined as deviations from the vPT-model and used to describe different types of anomaly in the deformation time-series. Third, each PS point time-series is evaluated individually and recursively to determine whether there is an anomaly and, if there is, to assess the type of anomaly.

5.1.1. MODELING THE NORMAL BEHAVIOR AND ANOMALIES

In order to describe the levee behavior, we define four temporal deformation models. The vPT-model is chosen to describe the “normal behavior”, given its higher quality of the estimations compared to the steady-state deformation model, as described in Chapter 4. It is defined as a steady-state levee deformation, see Eq. (4.2), combined with the variations of precipitation and temperature, see Eq. (4.3). We refer to this default model, defined in Eq. (4.5), as Model 0, M_0 ,

- Model 0. M_0 : vPT-model

$$M_0(\mathbf{x}_0) = v \cdot t + c_P \cdot \tilde{P}(t) + c_T \cdot \tilde{T}(t) + \delta \quad (5.1)$$

where $\mathbf{x}_0 = [v, c_P, c_T, \delta]'$ is the vector of unknown parameters defined as in Section 5.2, and \tilde{P} and \tilde{T} are the precipitation and temperature time-series, respectively, where the symbol $\{\tilde{\cdot}\}$ indicates temporal alignment using the cross-correlation method [154].

The levee deformation may deviate from its normal behavior which can manifest itself as, e.g., a sudden change in the deformation time-series, potentially indicating a reduction in the strength of the levee. For this reason, we introduced three additional models. The first model describes a significant change in the deformation trend defined by means of a step function as

- Model 1. M_1 : Step function (SF-) model

$$M_1(s_i) = s_i \cdot u(t - \tau_i) \quad (5.2)$$

where $u(t - \tau_i)$ is the Heaviside Step function [161], centered at τ_i . The offset s_i occurs between two epochs τ_{i-1} and τ_i .

The second model, which describes a change in the deformation velocity, is defined as a piecewise-linear model with a breakpoint at epoch τ_i as

- Model 2. M_2 : Breakpoint (BP-) model

$$M_2(v_i) = \begin{cases} v_i \cdot (t - \tau_i), & \text{for } t \geq \tau_i \\ 0, & \text{for } t < \tau_i \end{cases} \quad (5.3)$$

where v_i is the change in the slope of the linear regression line after τ_i , i.e. the second segment has a slope of $v + v_i$.

Lastly, the third model, describing a transitory reversible deformation, is defined as a scaled impulse function at the epoch τ_i as

- Model 3. M_3 : Impulse function (IF-) model

$$M_3(k_i) = \begin{cases} k_i, & t = \tau_i \\ 0, & t \neq \tau_i \end{cases} \quad (5.4)$$

where k_i can be regarded as the scaling factor of a discrete-time unit impulse function shifted in time.

These canonical models can be used to build different alternative hypotheses ($H_{a_j}, \forall j$) with the aim of defining possible abnormal behaviors of levees. The mathematical expressions of the null hypothesis (H_0) and all possible alternative hypotheses (H_{a_j}) are given by,

$$\begin{aligned} H_0 : E\{\mathbf{d}\} &= \mathbf{A}_0 \mathbf{x}_0 \\ D\{\mathbf{d}\} &= \mathbf{Q}_d = \sigma_d^2 \mathbf{I}_m \\ H_{a_j} : E\{\mathbf{d}\} &= \mathbf{A}_0 \mathbf{x}_0 + \mathbf{A}_j \mathbf{x}_j, \quad \mathbf{x}_j \neq \mathbf{0} \\ D\{\mathbf{d}\} &= \mathbf{Q}_d = \sigma_d^2 \mathbf{I}_m \end{aligned} \quad (5.5)$$

where \mathbf{d} is the $m \times 1$ vector containing the LOS deformation observations with dispersion specified by the covariance matrix \mathbf{Q}_d . As it is not possible to know their stochastic structure in advance, the dispersion of the observations in the time-series is assumed to be constant and uncorrelated. Hence, the covariance matrix is factorized as $\mathbf{Q}_d = \sigma_d^2 \mathbf{I}_m$ where σ_d^2 is the fixed variance of unit weight and \mathbf{I}_m is an $m \times m$ identity matrix. \mathbf{A}_0 and \mathbf{x}_0 are the $m \times n$ design matrix and the $n \times 1$ vector of unknown parameters, respectively, for the null hypothesis. \mathbf{A}_j and \mathbf{x}_j are the $m \times q$ design matrix and the $q \times 1$ vector of unknown extra parameters, respectively, for the j^{th} alternative hypothesis having q degrees of freedom.

In our case, the null hypothesis H_0 is the vPT-model where \mathbf{A}_0 and \mathbf{x}_0 are defined as in Eq. (4.8) and Eq. (5.1). The occurrence of an anomaly results in a change in the deformation time-series which may be detected by an overall model test (OMT) with a given significance level, as described in Chapter 4. When the null hypothesis is rejected, i.e., an anomaly is detected, different alternative hypotheses are needed in order to assess which one is more suitable to describe the anomalous behavior. For this purpose, seven different types of alternative hypothesis, $H_{a_j,i}$ ($j \in [1, 7]$) with their degree of freedom q_j are defined as,

$$\begin{aligned}
H_0 &: M_0(x_0) \\
H_{a_1}^i &: M_0(x_0) + M_1(s_i), & q_1 = 1 \\
H_{a_2}^i &: M_0(x_0) + M_2(v_i), & q_2 = 1 \\
H_{a_3}^i &: M_0(x_0) + M_3(k_i), & q_3 = 1 \\
H_{a_4}^i &: M_0(x_0) + M_1(s_i) + M_2(v_i), & q_4 = 2 \\
H_{a_5}^i &: M_0(x_0) + M_1(s_i) + M_3(k_i), & q_5 = 2 \\
H_{a_6}^i &: M_0(x_0) + M_2(v_i) + M_3(k_i), & q_6 = 2 \\
H_{a_7}^i &: M_0(x_0) + M_1(s_i) + M_2(v_i) + M_3(k_i), & q_7 = 3
\end{aligned} \tag{5.6}$$

A schematization of the defined null hypothesis and alternative hypotheses is given in Figure 5.1 using simulated deformation data. For the alternative hypotheses, it is assumed that the levee behavior follows the same velocity and the same variations of precipitation and temperature (i.e. the vPT-model) before and after the anomaly occurs, with one or more of the additional models describing the change in deformation. Note that for each possible value of the parameter τ_i (corresponding to different SAR acquisition dates, $i = 2, \dots, m-1$) in the SF-, BP- and IF-models, a new alternative hypothesis is generated for each of the seven types defined above. This results in a total of $7(m-2)$ alternative hypotheses. Also, considering the computational efficiency, for each alternative hypothesis with more than two models (i.e. $H_{a_4}^i, H_{a_5}^i, H_{a_6}^i, H_{a_7}^i$), a step, a breakpoint and/or an impulse are assumed to occur at the same acquisition date τ_i .

5.1.2. MULTIPLE HYPOTHESIS TESTING (MHT)

In order to check the validity of H_0 , we first compute the test statistic T_0 , which follows a chi-squared distribution $\chi^2(q, 0)$ with $q = m - n$ degrees of freedom, for a given significance level α_0 , as previously described in Section 5.2. Different than the previous analysis, in case of the rejection of H_0 , we need to compare multiple alternative hypotheses in order to identify the most probable one among them. For each alternative hypothesis $H_{a_j}^i$, we calculate the test statistic $T_{a_j}^i$ which follows a non-central chi-squared distribution $\chi^2(q_j, \lambda_j)$, where λ_j denotes the level of non-centrality [41]. The distributions of every test statistic for H_0 and $H_{a_j}^i$ are given as

$$\begin{aligned}
H_0 &: T_0 \sim \chi^2(q, 0) \\
H_{a_j}^i &: T_{a_j}^i \sim \chi^2(q_j, \lambda_j),
\end{aligned} \tag{5.7}$$

where each $T_{a_j}^i$ is computed as

$$\begin{aligned}
T_{a_j}^i &= \hat{\boldsymbol{e}}_0' \mathbf{Q}_d^{-1} \hat{\boldsymbol{e}}_0 - \hat{\boldsymbol{e}}_a' \mathbf{Q}_d^{-1} \hat{\boldsymbol{e}}_a \\
&= \hat{\boldsymbol{e}}_0' \mathbf{Q}_d^{-1} \mathbf{A}_j (\mathbf{A}_j' \mathbf{Q}_d^{-1} \mathbf{Q}_{\hat{\boldsymbol{e}}_0} \mathbf{Q}_d^{-1} \mathbf{A}_j)^{-1} \mathbf{A}_j' \mathbf{Q}_d^{-1} \hat{\boldsymbol{e}}_0,
\end{aligned} \tag{5.8}$$

where $\mathbf{Q}_{\hat{\boldsymbol{e}}_0}$ is the covariance matrix of the residual vector $\hat{\boldsymbol{e}}_0$ between the measured deformation time-series and the time-series estimated under the null hypothesis, and $\hat{\boldsymbol{e}}_a$ is

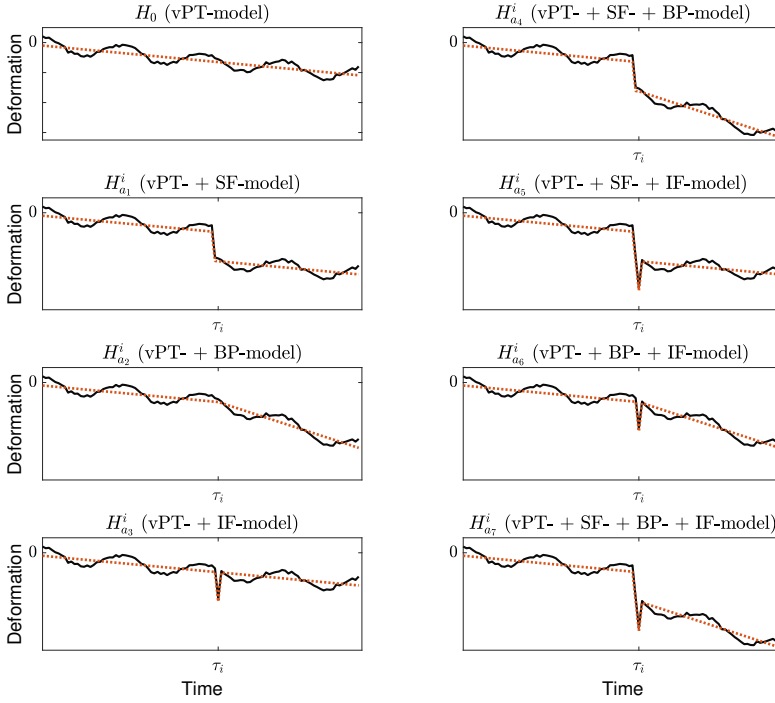


Figure 5.1: A schematization of the null hypothesis, H_0 (i.e. no anomaly) and alternative hypotheses, $H_{a_1}^i$, $H_{a_2}^i$, $H_{a_3}^i$, $H_{a_4}^i$, $H_{a_5}^i$, $H_{a_6}^i$ and $H_{a_7}^i$, representing possible anomalies occurring at epoch τ_i aimed to be detected along the levees. The black line depicts a deformation time-series estimated under the different hypotheses (using simulated data). The dotted red line is a schematic representation of the levee deformation behavior, without the effect of meteorological conditions to better show the modeled anomaly.

the residual vector between the measured deformation time-series and the time-series estimated under the alternative hypothesis $H_{a_j}^i$.

However, alternative hypotheses have different dimensions, which results in their test statistics having different χ^2 distributions. Therefore, the most probable alternative hypothesis cannot be determined directly by using Eq. (5.8). This issue is solved provisionally by normalization, i.e. dividing the test statistics by its critical value $\chi_{a_j}^2(q_j)$ obtained for a predefined level of significance, α_j [162]. The test ratio, $T_{a_j}^i$ can be expressed as [162],

$$T_{a_j}^i = T_{a_j}^i / \chi_{a_j}^2(q_j). \quad (5.9)$$

To be able to compare multiple hypotheses having different dimensions using the normalization above, all the alternative hypotheses should have the same probability

(power) of detection. This is achieved by using the B-method of testing [163] to select the test parameters for a given level of significance α . The identical probability of accepting a particular alternative hypothesis is referred to as the detectability power of the test γ . In this method, we fix the reference power of the test γ_0 and calculate the reference non-centrality parameter λ_0 given the level of significance, α_j , and a given dimension, q_j , as

$$\lambda_0 = \lambda(\gamma_0, \alpha_j, q_j), \forall j. \quad (5.10)$$

The use of fixed values for λ_0 and γ_0 in the computation of the critical values $\chi_{\alpha_j}^2(q_j)$ assures that any particular alternative hypothesis $H_{a_j}^i$ can be sustained with the same probability regardless of its dimension q_j [41, 163].

The B-method of testing requires input values for the level of significance, α_0 , and the detectability power of the test, γ_0 . To be able to select from different models with the same discriminatory power, particularly when these models have different degrees of freedom, α needs to be tuned. An initial value for the significance level α_0 for $q_j = 1$ is used to compute the reference non-centrality parameter λ_0 . The value of α , and thus of the critical value $\chi_{\alpha_j}^2(q_j)$, for the alternative hypotheses with higher dimensions is then tuned so as to keep the power of the test fixed.

5.1.3. PROCEDURE FOR DETECTING ANOMALIES USING MHT

The MHT approach is performed on the InSAR time-series based on the predefined test parameters. Figure 5.2 shows the flow chart of the testing procedure that is applied on each PS time-series.

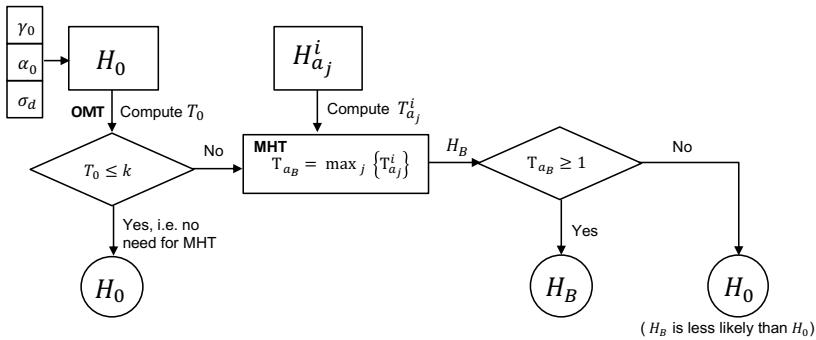


Figure 5.2: A flow chart for the Multiple Hypothesis Testing (MHT) procedure.

Firstly, the significance of the vPT-model is tested using an Overall Model Test (OMT) to decide whether to sustain or reject H_0 . For the given α_0 , the critical value, k , of the χ^2 distribution is calculated. If $T_0 \leq k$, H_0 is sustained and there is no need to perform the MHT.

In case of a rejection of H_0 , i.e., $T_0 > k$, the second step consists of applying the MHT for a given γ_0 in order to identify the optimal alternative hypothesis. The test ratio $T_{a_j}^i$

of each H_{a_j} is calculated and the hypothesis with the largest ratio T_{aB} is sustained as the most probable alternative hypothesis (H_B). If $T_{aB} \geq 1$, the test statistics exceeds its critical value; thereby, the H_B is sustained. When the most probable alternative hypothesis does not pass the test, it is assumed that the deformation data do not represent a "normal behavior" containing an anomaly of the kind defined, but rather a behavior with different characteristics. In this case, the correlation between the data and the time-series estimated under H_B will be still low, and H_0 is sustained since the optimal alternative hypothesis is not more likely than H_0 . It follows that these PS-points, which are assigned to H_0 after the MHT, are points whose deformation time-series cannot be described well by neither the vPT-model nor any additional model considered. In those cases, in-situ observations are recommended.

The assessment of the outcome of the anomaly detection methodology with respect to the actual condition of the levee may result in four different cases (A, B, C, D) explained by the diagram given in Figure 5.3. The rows of the diagram represent the "reality", i.e., whether there is an actual anomaly or not, and the columns the possible outcomes of the anomaly detection methodology, i.e., whether or not an anomaly is detected. Case D represents an actual anomaly being correctly detected (true positive). On the other side, case A corresponds to the situation in which no anomaly is detected because there is no anomaly in reality (true negative). The other two cases correspond to the two possible types of error which can lead to a wrong assessment; in case B, a false alarm is raised by the detection of an anomaly that does not exist in reality (false positive), whereas case C reflects the situation in which the detection methodology misses an actual anomaly (false negative). An optimal use of anomaly detection methodology for levees would be to maximize the likelihoods of detection measurements A and D, while minimizing false detection B and C.

		Anomaly detection methodology	
		No Anomaly detected	Anomaly detected
Reality	No Anomaly	A Correct rejection True negative $(1-\alpha_0)$	B False alarm False positive α_0 (type I error)
	Anomaly	C Missed detection False negative $(1-\gamma_0)$ (type II error)	D Correct detection True positive γ_0

Figure 5.3: A diagram showing four different cases (A, B, C, D) as outcomes of the anomaly detection methodology with respect to the actual condition of the levee.

From a perspective of levee authorities, one needs to assess when a change in the deformation time-series should be detected as an anomaly based on the conditions of the specific location considered. For this purpose, the test parameters, α_0 and γ_0 , should be

predefined by the local or regional authorities. The value of α_0 should be determined by an assessment of the cost of a false warning, whereas the value of γ_0 should be chosen based on the estimated impact of a missed detection, e.g., in terms of loss of lives. For instance, choosing a small α_0 implies that there is a low likelihood of a false warning (type I error), i.e., the probability of an anomaly to be erroneously detected is low. This means that a change in the deformation time-series needs to be larger for being accepted as a significant anomaly, thus avoiding small changes to be flagged. Likewise, a larger γ_0 indicates that there is a higher likelihood that an actual anomaly is correctly detected or, in other words, a lower likelihood that an actual anomaly is not flagged (type II error). As a consequence, an anomaly of small magnitude would be detected with a smaller likelihood. Alternatively, it could also be possible to define minimum detectable values for the deformation parameters in terms of how large a step, an impulse or change in deformation velocity should be in order to be recognized as an anomaly. This can be done by tuning both λ and α for each alternative hypothesis for predefined desired minimum detectable values of the model parameters (s_i, v_i, k_i), while keeping γ_0 constant. For more information on the a-priori performance assessment, see [41, 135].

5.2. APPLICATION ON CASE STUDIES

The proposed approach is demonstrated via two different case study areas. We first focus on the canal levees in polders near Delft, the Netherlands as its swelling-shrinkage behavior was analyzed in the Chapter 4. Secondly, we examine the levees around Grave, the Netherlands, where a ship collision onto a lock on December 29, 2016 has caused a sudden drop in the water level of the Meuse River.

5.2.1. STUDY AREA: DELFT, THE NETHERLANDS

The developed methodology is applied on the deformation time-series of each PS point along the canal levees near Delft, covering the same study area analyzed in Chapter 4 (see Figure 4.1) and using the same meteorological and deformation data. Following the processing procedure given in Section 5.1, the OMT is applied with initial level of significance $\alpha_0 = 0.2\%$, selected within the typical range of InSAR time-series, and detectability power of the test $\gamma_0 = 50\%$, chosen so as to have 50% likelihood that the null hypothesis is correctly rejected [163]. In practice, the selection of the test parameters should be made by the levee authorities based on prior information regarding their specific cases. Considering the analysis in Chapter 4, the a-priori variance of unit weight is assumed to be $\sigma_d^2 = 7 \text{ mm}^2$.

Results show that 84% of PS points sustain the null hypothesis H_0 (i.e. follow the vPT-model), indicating that most parts of the levees are either stable or linearly deforming, and follow the meteorological changes. Then, the rest of the MHT procedure is applied on the remaining PS points in order to find the most probable hypothesis among the different alternatives. In other words, the procedure finds the alternative hypothesis $H_{a_j}^i$ that can better model the anomalous behaviour of the levee at those PS points that did not sustain the null hypothesis. Among the anomalies, 10% of PS points sustain $H_{a_4}^i$ and 4% sustain $H_{a_1}^i$ whereas the remaining 2% are distributed among the other hypotheses ($H_{a_2}^i, H_{a_5}^i, H_{a_6}^i, H_{a_7}^i$). Moreover, for two PS points, all alternative hypotheses are rejected

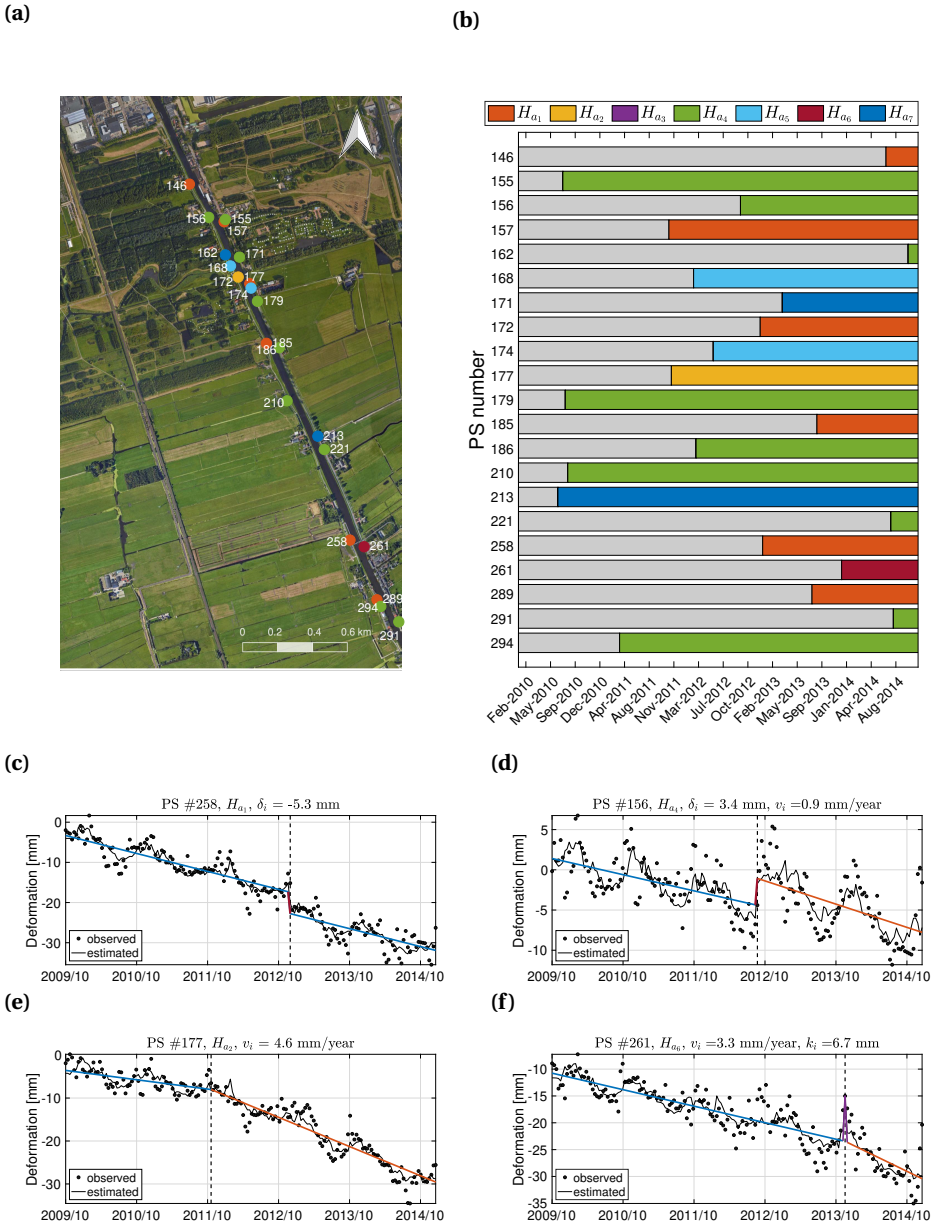


Figure 5.4: Detected anomalies along a section of the levees of the Deltse Schie canal. (a) Spatial distribution of the PS points with related color-coded alternative hypotheses; (b) Temporal distribution of the detected anomalies, with the color-coded bar starting at the corresponding epoch τ_i ; (c-f) examples of time-series for anomalies detected by (c) H_{a1} , (d) H_{a4} , (e) H_{a2} , and (f) H_{a6} . The title of each plot reports the value(s) of the estimated extra model parameter(s).

as none is more likely than the null hypothesis H_0 .

In order to analyze the anomalies in more detail, we focus on the same section of a levee investigated in the previous chapter (see Figure 4.4). Figure 5.4a shows the spatial distribution of these anomalies in the levee section along the east canal, with different colors indicating which alternative hypothesis is sustained for the PS points. Anomalies are detected at different time epochs τ_i , as shown in the temporal distribution of anomalies in the area considered (Figure 5.4b), where the colored bar for each PS-point starts at the corresponding epoch τ . Figures 5.4c to 5.4f show some examples of the detected anomalies, where both the observed and estimated deformation time-series are given together with the schematic representation of the corresponding alternative hypothesis as depicted in Figure 5.1.

This analysis shows that the proposed methodology is capable of detecting different types of changes in the levee deformation behavior at different time epochs. In other words, it allows to record anomalies in the historical evolution of the sub-seasonal patterns of levee. Moreover, analyzing the temporal and spatial distribution of the detected anomalies in an area of interest can provide relevant information on the levee conditions. For instance, multiple anomalies localized on a given section of the levee occurred within a certain period of time could give indications of a potential hazard for levee stability, requiring additional investigations. Since the detection of these anomalies (16% of the PS points) along the levees does not necessarily correspond to problematic locations, further assessments by including a-priori information on the levee conditions are required with the involvement of levee authorities. These assessments should be performed by means of a collaborative approach, where geotechnical and risk analyses contribute to improve the detectability of possible weak spots.

5.2.2. STUDY AREA: GRAVE, THE NETHERLANDS

In the second case study, we analyzed the Grave area in order to illustrate the use of the proposed methodology to diagnose the possible effects of a sudden drop in the water level on a levee. On December 29, 2016, a ship hit a weir in the Maas river, near Grave. As a consequence of the accident, the upstream water level dropped about 3 meters within a day between Grave and Sambeek, given in Figure 5.6 (from +7.90 m NAP to approx. +5.24 m NAP). Water level and discharge measurements at the close-by gauging stations, and the timeline of the events that took place after the collision are given in Figure 5.5.

In order to analyze if any damage occurred in the area due to the sudden drop in water level, the case study area is monitored using data from RadarSAT-2, ascending orbit between April 2015 and October 2017, composed of 57 stripmap images. This satellite provides C-band data with a wavelength of 55 mm, 10×9 m pixel size and a repeat cycle of min. 24 days [51]. We obtain the deformation time-series of each PS point on the levees around the Grave area using the PS-InSAR technique with the same approach based on geodetic estimation theory [126] used in the previous chapters. The deformation velocity [mm/year] map of the monitored area is given in Figure 5.6. For more details on the PS-InSAR processing used, see Chapters 3 and 4 of this thesis. The last SAR image before the failure was on December 21 and the first image after the failure was recorded on January 14.

For the vPT-model, we use precipitation [mm/day] and temperature [°C] data ob-

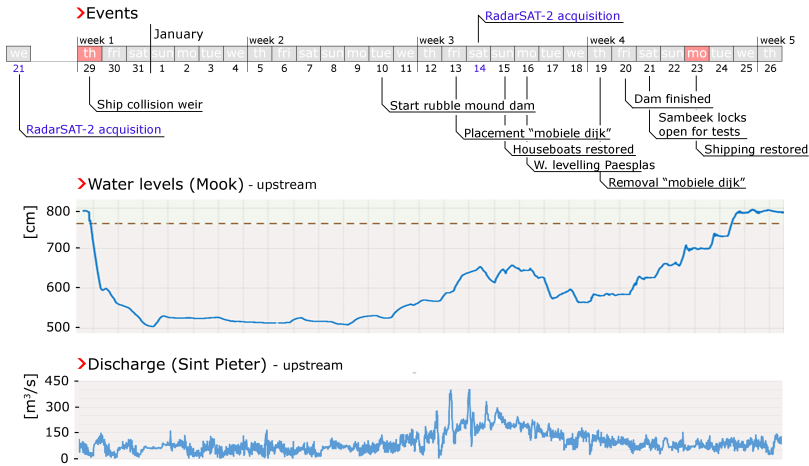


Figure 5.5: Timeline of the events after the collision and the time-series of water levels (cm) and discharge (m³/s).

tained from the closest meteorological station 375 from the Royal Dutch Meteorological Institute near Volkel, with samples of the average temperature and the cumulative precipitation time-series taken every 24 days ($\Delta t_T = \Delta t_P = 24$ days), accounting for the repeat cycle of RadarSAT-2.

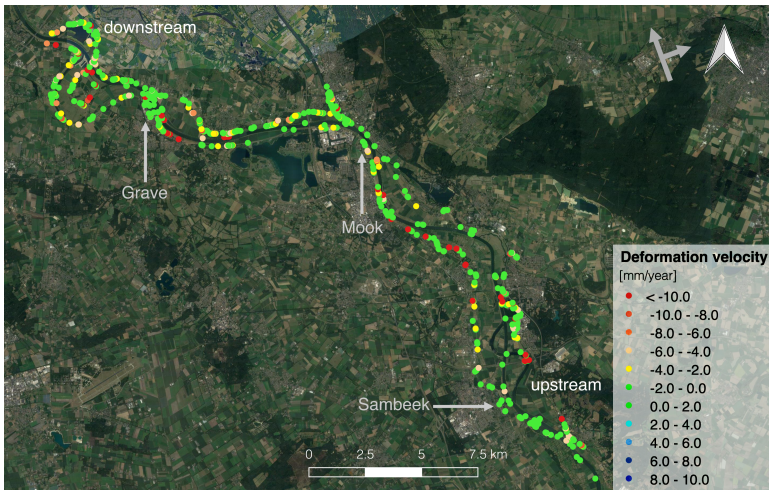


Figure 5.6: Deformation velocity [mm/year] map generated from data acquired by RadarSAT-2, ascending orbit (2015-2017), of the Maas river levees around Grave. The distance between Grave and Sambeek is approximately 30 km.

Differently than the previous analysis in Section 5.2.1, in this case study we focus only on the first SAR image after the failure (January 14, 2017) to check whether the sudden drop in water level due to the ship collision caused any anomaly on the levee behavior. In other words, we attempt to detect any anomaly that may have occurred after the collision by fixing the epoch τ_i at this specific date. Assuming that an anomaly may have occurred after the failure, we calculated a specific a-priori variance of unit weight, σ_a^2 , per PS point only considering the available data until that date (January 14, 2017). Using an individual a-priori variance per PS-point increases the sensitivity for anomaly detection and thus our chances of correctly detecting anomalies.

Moreover, in this analysis, we focused on river levees (i.e. primary flood defenses) which aim to provide a protection for low-lying areas against flooding from major rivers, lakes or coasts in the Netherlands [164]. Considering their high safety standards and design criteria, these levees are expected to be more robust and stable compared to the canal levees (i.e. secondary flood defenses) which is analyzed in Section 5.2.1. Consequently, it is questioned whether the changes in meteorological conditions could potentially have less influence on the deformation behavior of the river levees. In order to assess this, we applied OMT both to the vPT-model and to the steady-state model independently for the deformation time-series of the PS points (up to the collision date), as done in Chapter 4 for the Delft area. The comparison given in Figure 5.7 shows that the difference in the MSE values for vPT-model and steady-state model is not very high, especially compared to the results of OMT on the same models for the Delft area (Figure 4.2). Hence, the effect of meteorological conditions on river levees is indeed identified as less than on canal levees. However, given the general improvement in the modeling accuracy provided by the vPT-model over the steady-state model also for primary levees, we performed the detection of anomalies for Grave area also using the vPT-model as the null hypothesis.

The developed testing framework is applied on each PS point along the river levees in the Grave area, comprised of 565 PS points. The choice of the test parameters for this case study area is defined as in the previous case, with significance level $\alpha_0 = 0.2\%$ and detectability power $\gamma = 50\%$. The results show that 92% of the PS points sustained the null hypothesis, whereas the rest of the PS points follow the alternative hypotheses. Among the anomalies, 3% of PS points sustain $H_{a_2}^i$, 2% sustain $H_{a_4}^i$, and 1.5% sustain $H_{a_7}^i$, whereas the remaining 1.5% of PS points are distributed among the other hypotheses ($H_{a_1}^i, H_{a_3}^i, H_{a_5}^i, H_{a_6}^i$).

The spatial distribution of the anomalies is given in Figure 5.8a, which shows that the majority of these anomalies is concentrated in the vicinity of the weir, which may be an indication of this area (Figure 5.8b) being affected the most by the sudden drop in the water level. Some examples of the observed and estimated deformation time-series from detected anomalies are given in Figure 5.8c-5.8f. The deformation response of a levee to sudden changes in the hydraulic conditions highly depends on the heterogeneity of the soil, and thus it is location specific. For instance, a possible behavior is a rapid shrinkage of the soil, which can be observed as a significant step in the deformation time-series, as shown in Figure 5.8c and Figure 5.8f. In case of an increase in the water level, this rapid shrinkage behavior can also be followed by a swelling behavior of the soil. Some detected anomalies have also been registered in which a swelling behavior (i.e. a posi-

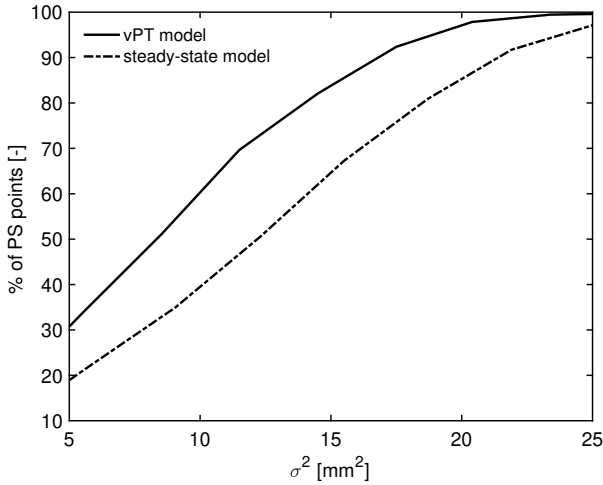


Figure 5.7: Overall Model Test (OMT) results, performed to assess which model represents better the deformation behavior of river levees. Percentage of PS points for which vPT-model and steady-state model are sustained for different values of unit weight, σ_d^2 .

tive step) precedes a change in the long-term deformation trend of the soil, as given in Figure 5.8e. The detected swelling behavior may be the result of the water level being already partially increased with the emergency measures by the first acquisition date after the failure (January 14, 2017) as shown in Figure 5.5. Another impact could be noticed as an unexpected change in the soil deformation behavior, such as a sudden increase in the subsidence rate of a PS point that seemed stable before the failure (Figure 5.8d).

This case study presents a possible application of the proposed anomaly detection methodology as a diagnostic tool for assessing the impact of sudden changes in loading conditions after a failure event. For instance, by analyzing the spatial distribution of the detected anomalies and their estimated deformation time-series, levee experts could be able to direct their attention and efforts towards the locations that may have been affected the most. However, the identification of potentially problematic locations still requires a consideration of all available information about the conditions of the levees and possibly performing additional assessments, as mentioned for the previous case study in Section 5.2.1.

5.3. DISCUSSION AND KEY CONCLUSIONS

In this study, we describe a prototype early warning method for levees which uses multiple hypothesis testing (MHT) to detect anomalies in the levee deformation time-series. The vPT-model is used as the null hypothesis in the MHT framework, whereas the alternative hypotheses are defined as deviations from the vPT-model by including additional functions, such as a step, a breakpoint, and/or an impulse, which are meant to describe anomalous behaviors in the deformation time-series. The method is applied to two case

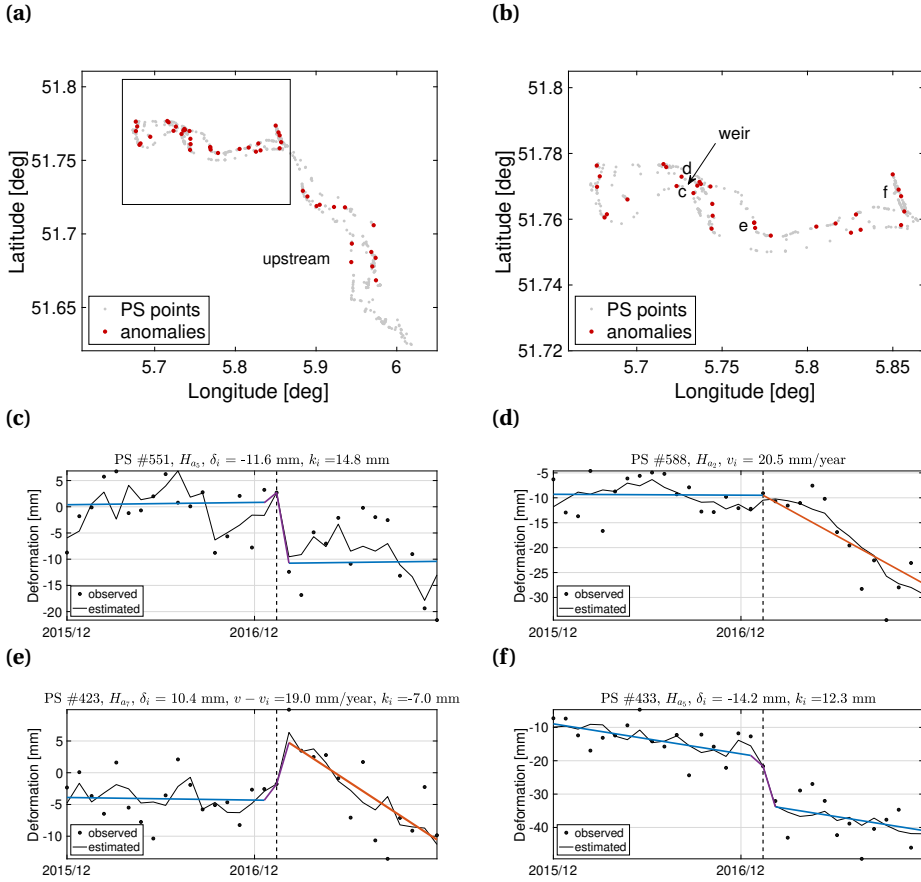


Figure 5.8: Detected anomalies in the Grave case study area. (a) Spatial distribution of the different alternative hypotheses; (b) focused area in the surroundings of the weir showing the location of the detected anomalies, including those presented as examples in (c-f) with their observed and estimated deformation time-series. Notice that the PS points (c) and (d) are located just downstream of the weir.

study areas, with the intent of exemplifying its possible use for continuous levee monitoring and its potential as a diagnostic tool for levee safety assessment after a specific failure event. Preliminary results showed that the proposed approach is applicable to select the optimal models for each PS points and thus, to detect anomalies along the analyzed levees. More specifically, the use of the additional functions in the alternative hypotheses allows not only to detect the occurrence of anomalies but also to classify the deformation behavior, such as a sudden jump in the deformation or a change in the subsidence rate of the levee. Although detection of anomalies may not yield conclusive statements on finding the weak spots and/or potential failure locations, the inclusion of all available prior information about the levees by the levee authorities can improve the

detectability of weak spots more precisely in the later stage.

Conceptually, the overall assessment of levee safety can be carried out in three interdependent levels, given in Figure 5.9. The first level corresponds to the geodetic assessments used to provide data on the structural behavior by continuous surveying. When an anomaly is detected in the levee by these surveys, a geotechnical assessment could be then necessary to evaluate whether this anomaly implies a problematic behavior. This can be done by defining case-specific geotechnical thresholds considering the local conditions, for example the soil heterogeneity of the levee. Although the evaluation of specific cases does not fall within the main scope of geodetic assessments, a close cooperation between experts of these two levels is needed to discuss and analyze the results of the geotechnical investigations. In the last level, the potential risk of a levee failure in the specific area needs to be evaluated in order to make an optimal estimation of the “tolerable” deformation in the levee (e.g., by performing a cost-benefit analysis) and to specify possible countermeasures. Each of these defined levels is considered to be necessary but not sufficient alone to draw conclusions on the overall levee safety. Although each level requires special expertise in the field of interest, the overall assessment should be performed with an intended collaborative approach which involves a robust interaction between the experts. For instance, the decision of the test parameters, e.g., α_0 and γ_0 , can be taken with the involvement of experts from all levels.

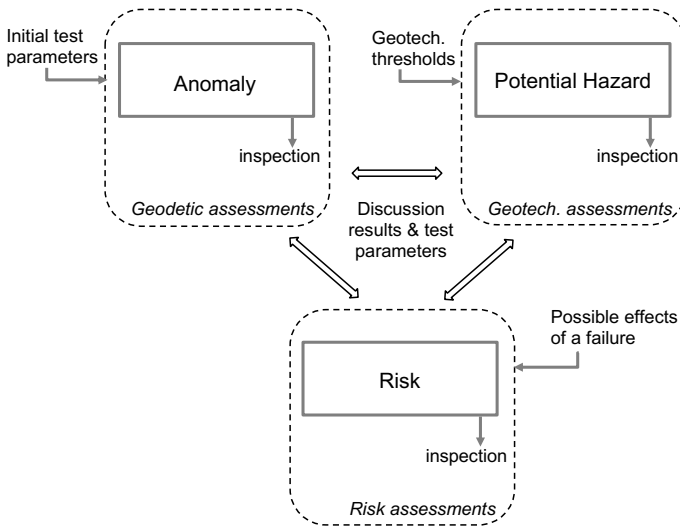


Figure 5.9: A conceptual scheme depicting the three interdependent levels for the assessment of levee safety.

Anomaly detection by using satellite monitoring falls within the category of geodetic assessments which aim to provide the deformation data correctly and to assess whether there is a significant change in the levee behavior (i.e. an anomaly) based on the measurements. In this sense, the proposed prototype early warning method can be a useful tool to assess the levee behavior over extensive areas and to localize levee sections that

require special attention. The presence of these anomalous behaviors in the deformation time-series can be an indication of potential problematic locations which have to be further investigated by the authorities. It is also acknowledged that given the nature of satellite measurements, the applicability and quality of InSAR technique for this specific type of infrastructure is non-uniform and depends on the site-specific characteristics. Considering this, complementary techniques, e.g., in-situ measurements, and post analyses of the results by the local levee authorities may be required in order to validate whether the detected anomalies correspond to actual problematic situations.

The proposed approach also allows the end-users to select the test parameters based on their case-specific choices in order to achieve optimal results. By setting the values for the significance level α_0 and for the detectability power γ_0 (or minimum detectable values for the deformation variations), it is possible to tune the outcome of the anomaly detection as explained in Section 5.1.3. It is worth noting that, in addition to α_0 and γ_0 , the results also depend on the pre-selected value of the variance of unit weight, σ_d^2 given in Eq. (5.5), which represents the assumed dispersion of the observations. In addition, the parametric nature of the anomaly models enables the use of post-processing techniques on the outcome of the MHT, thus making the search for anomalies automatic and tailored to detailed requirements of the user. For instance, apart from being limited in time and space, the analysis can be focused on anomalies showing significant values of the model parameters, such as large values for the step parameter δ or the impulse parameter k , strong changes in the rate of subsidence ν_i , or different combinations of the three. In other words, the model parameters can become useful additional inputs (together with the test parameters of the MHT) for an early warning system, allowing the water authorities to tune their assessments based on their specific needs.

Moreover, such an automated system would allow to monitor very extensive areas, raising alerts only when significant, localized and concurrent anomalies are detected. Also, combining different satellite missions and orbits, spatio-temporal coverage and resolution can be increased, thus enhancing detectability. Further research would need to focus on the inclusion of prior information about the levees to obtain reliable and precise detection in different cases. Aiming towards an automatic detection algorithm for problematic locations, an expert-supported approach can be developed taking into account the collaborative approach discussed above (Figure 5.9). In conclusion, it is acknowledged that a systematic application of the proposed method can contribute to operational monitoring and become a useful tool for timely anomaly detection of levees.

6

CONCLUSIONS AND RECOMMENDATIONS

6.1. CONCLUSIONS

The main objective of the presented study is to improve the understanding of levee deformation behavior as well as levee failure patterns by investigating both historical failures and satellite observations. In particular, we demonstrate the importance of collecting and analyzing historical failure events to gain new insights. Besides, we show how satellite radar interferometry can both provide useful information on the behavior of flood defenses and be applicable in early warning systems.

The conclusions are discussed by answering the research questions which were given in the Introduction (Section 1.3). The scientific and technical contributions of the research findings are explained in Section 6.2. Several recommendations are made based on this research in Section 6.3.

Research question – 1: How can we improve understanding of levee failure mechanisms by analyzing historical failures in order to support flood risk management?

It is evident that understanding levee failures can be significantly improved by investigating historical failures, experiments and performance observations. By analyzing historical data on levee failures and breaches, we identify (a) typical vulnerabilities and common failure mechanisms, (b) breach characteristics, and (c) the density of breach occurrence at the event-level. Considering that flood events and defense systems have specific characteristics and conditions, these insights can be used to complement (local) flood risk assessments.

In order to collect and share valuable data, we develop an International Levee Performance Database (ILPD) as a global, well-structured, open access data-sharing platform¹. The current version of the database contains information on levee characteristics, failure mechanisms, geotechnical investigations and breach processes for more

¹URL: leveefailures.tudelft.nl

than 1500 cases, ready to facilitate research on levee failures in various aspects, as discussed in Chapter 2. Compared to the existing databases, the structure of the ILPD allows for a wide range of data types, inclusion of detailed information and easy dissemination. We thoroughly discuss operational obstacles that must be overcome in order for the ILPD to become broadly applicable and representative, such as data sharing and language issues (Chapter 2). Although the first available version presented in this research provides good coverage of some regions (e.g., the Netherlands for the 20th century), the database mostly consists of general information acquired from specific countries, with limited data on detailed cases. This in fact highlights the importance of transparency in data sharing and collaborations within the parties involved in levee safety. In the near future, the ILPD aims to become an international platform and scientific tool for various purposes. It could give new insights into the field of flood risk and stimulate the development and validation of more accurate techniques and modeling tools.

Based on the current version of the database, we perform a macro-scale analysis of the historical failures and levee breaches to demonstrate the potential of the database in providing insights on levee behavior and supporting flood risk assessments based on historical records. We outline the common failure mechanisms of which external erosion is identified as the most frequent for levees and internal erosion for earthen dams. As an illustrative use of an ILPD sub-set, we examine breach characteristics of over a hundred failures during the flood events occurred in Germany (2002, 2013). Our analysis shows that initial failure mechanisms have an influence on breach characteristics and that failures due to instability and internal erosion are less frequent but lead to larger breaches. Moreover, considering the limited focus on the multiple failures and breaches at the event-level in current flood risk assessments, we perform a breach density analysis. Flood events with higher return periods tend to have higher breach densities, a higher number of failures and higher degrees of damage on the levees. External erosion is more likely to occur for high return periods. The insights provided by the analysis of the historical flood events contained in the ILPD, in combination with hydraulic/geotechnical models, could eventually be used to complement flood risk assessments and to design more robust and resilient flood defenses, with a smaller likelihood of catastrophic breaching.

Research question – 2: To what extent can satellite radar interferometry provide a continuous monitoring for levees and give indications of potential failures?

Satellite radar imaging, in particular InSAR technology, is ready to be used for continuous monitoring of levee behavior which allows to observe deformations on a daily scale with mm-level precision in all weather conditions. It also provides historical deformation data (from 1992 to today), which can be used to investigate trends in levee deformation and to get more insight into levee behavior mechanisms. Our study suggests that InSAR has surpassed the stage of being a mere scientific tool and has moved towards becoming an operational levee deformation monitoring system, with increased efficiency and quality.

In Chapter 3, we address frequently recurring technical questions related to the practical applicability of levee monitoring using InSAR technology. InSAR products are opportunistic by nature, i.e., data is not acquired specifically for levees. Therefore, their

information value should not be assessed by predefined user needs (i.e., its efficacy), but by its post hoc diagnostic value. Since satellite observations may not be optimally matched to every specific case, no generic statements can be given on its applicability in contrast to conventional in-situ techniques. Although the original precision of phase measurement of available satellites is known, the precision of the estimated observations is affected by the characteristics of the earth's surface (e.g., vegetation, soil types), and by the orientation of the levee in combination with the deformation vector of interest. Hence, the actual precision of observations is case-specific. Despite the fact that most of the coherent scatterers are generally obtained from non-vegetated areas, they can still provide indications of the deformation behavior of the rest of the levee. Our study demonstrates that any deformation vector can be estimated in almost all directions with varying degree of sensitivity depending on the orientation and the slope of the levee. For example, the horizontal deformation for 70% of the primary flood defenses in the Netherlands can potentially be retrieved with good accuracy (sensitivity larger than 0.5, in the range between 0 and 1). Various time-series processing techniques may be applied to estimate the deformations from the data. The most suitable approach depends on the conditions, such as the surface cover, the number of available radar images, the orientation of the structures and the expected deformation signal.

The relevant question in this respect is whether it is beneficial to use the information from InSAR that is already available, even if there is no one explicitly requesting the data. Even though the InSAR products are opportunistic by nature, they hold an enormous information value: the deformation data can be derived quantitatively on a daily basis, which can complement levee management efficiently. Especially countries having a strong expertise base, a full national InSAR coverage and extensive flood defenses, such as the Netherlands, could improve the monitoring capabilities by making use of the frequent, abundant, and precise measurement data at a relatively low cost. Combining these satellite data with other data sources (e.g., remote sensing and geological maps) and management information would provide insight into levee behavior. Local in-situ measurements can be deployed effectively at those locations where they are needed.

Considering the complexity of the interpretation of the results, the InSAR technique should not be used as a stand-alone black-box. Wider application of the technique requires a combination of skills, i.e., strong collaboration between satellite experts, geotechnical engineers and policy makers. The overall assessment of levee safety needs to be performed with an intended collaborative approach which involves a robust interaction between the experts.

Research question – 3: How can the observed deformations of levees be interpreted in order to characterize levee patterns and detect anomalous behaviors under dynamic loading conditions?

We conclude that InSAR technology is not only a monitoring tool, but also a diagnostic tool that provides insight into the dynamic structural behavior of levees and enables the identification of critical situations. More specifically, our research demonstrates that the sub-seasonal behaviour of levees can be observed in great detail, thus allowing to predict swelling and shrinkage due to variations of the loading conditions and to increase the ability of detecting anomalies. In this context, we reveal that InSAR deforma-

tion signals contain meaningful diagnostic information, previously interpreted as noise, which is related to the influence of the meteorological conditions on the sub-seasonal levee deformation behavior. We develop a predictive deformation model, called vPT-model (Chapter 4), to identify and analyze this behavior from continuous levee deformation observations obtained using PS-InSAR with an unprecedented level of detail over extensive areas. Being able to model the influence of the meteorological conditions (i.e., precipitation and temperature) on the levee behaviour on a weekly basis enables predictions of the expected behavior of the levee.

By determining whether the observed deformation is in line with this expected behavior, it becomes possible to identify anomalies in the levee deformation time-series. For this purpose, we propose a prototype early warning methodology using a probabilistic approach for post-processing of PS-InSAR results (Chapter 5) in order to detect and analyze these anomalies on levees that can be indicative of potential problematic locations. The systematic application of the proposed methodology can be a useful tool to assess the levee behavior over extensive areas, raising alerts only when significant, localized and concurrent anomalies are detected. By taking into account the collaborative approach introduced in Chapter 5, levee authorities need to critically evaluate the results, which can be optimally tuned based on their case-specific conditions, in order to determine whether further investigation is required. Although the detection of anomalies may not yield conclusive statements on finding these problematic locations, the inclusion of all available prior information about the levees can improve detectability. Giving the nature of InSAR measurements, complementary techniques, e.g., in-situ measurements, and post analyses of the results by the local levee authorities may be required in order to validate whether the detected anomalies correspond to actual problematic situations.

Although the direct monitoring of levee failures using InSAR is not covered in this research, being able to analyze levee behavior processes and to detect anomalies could also contribute to identify potential levee failures. For example, deformation measurements of a levee failure test [165] at Eemdijk, in the Netherlands (also described in Appendix A) demonstrate that the levees may show an observable degree of deformation 4-5 days before the actual failure becomes visible. The temporal sampling of contemporary satellites allows us to monitor changes on a daily scale (e.g., Sentinel-1a, 6 days repeat cycle, average of 1-2 days revisit time in the Netherlands) and to detect these subtle degrees of deformations which could indicate a failure being imminent. Furthermore, the monitoring and modeling of extreme swelling or shrinkage due to severe meteorological conditions, which normally takes place over a period of several weeks to months before leading to a failure (e.g., the Wilnis case analyzed in Chapter 4), can help to flag the anomalous behavior of the levee. This would allow levee managers to apply timely countermeasures, and thus, provides an important contribution to the assessments of levee safety.

As climate projections commonly agree that the future will bring more extreme conditions, such as storms, high river discharge, or drought, innovative and cost-effective complementary techniques for monitoring the dynamic behavior of levees become essential. These techniques will be most beneficial if they contribute to detecting which locations are most prone to sudden failures and estimating far in advance whether a levee

would fail. Consequently, the continuous analysis of InSAR levee deformation monitoring will assist the responsible levee authorities to take appropriate actions, hence avoiding catastrophic events and contributing to the flood risk reduction activities.

6.2. MAIN CONTRIBUTIONS

The main contributions of this research are outlined as follows.

- We develop a global, well-structured, open access data-sharing platform, called International Levee Performance Database (ILPD), to support research in the field of levee safety and flood risk. We establish a uniform terminology for the parameters of the database related to levees and their failures (Chapter 2).
- By analyzing historical data on levee failures and breaches, we identify typical vulnerabilities and common failure mechanisms, breach characteristics, and the density of breach occurrence at the event-level (Chapter 2).
- We outline the most common levee failure mechanisms of which external erosion triggered by overtopping/overflow is identified as the most frequent for levees (Chapter 2).
- We show that initial levee failure mechanisms play an important role in defining the breach characteristics, and that failures due to instability and internal erosion are less frequent but lead to larger breaches (Chapter 2).
- We introduce two new breach density parameters intended to be used in risk assessments of levees. We also identify that flood events with higher return periods tend to have higher breach densities, higher number of failures and higher degrees of damage on the levees (Chapter 2).
- We provide a comprehensive assessment of the state of the art in using time-series InSAR for systematic levee deformation monitoring, and discuss related technical aspects and its practical applicability on levee management (Chapter 3).
- We show how expected levee deformations can give indications related to various levee failure mechanisms. In order to illustrate the potential of satellite monitoring to detect stability problems, we examine the shrinkage behavior of the levee that failed near Wilnis, the Netherlands, in 2003 (Chapter 4).
- We demonstrate that InSAR technology is a valuable diagnostic tool able to provide detailed information about the dynamic behavior of levees over extensive areas (Chapter 4).
- We show that sub-seasonal levee deformations obtained with InSAR can be observed on the time scale of weeks and that these deformations are strongly correlated with the changes in meteorological conditions (Chapter 3 and 4).
- We develop a predictive deformation model to estimate short-term swelling and shrinkage associated with meteorological conditions, thus enabling predictions of

the expected behavior of levee due to variations in the loading conditions (Chapter 4 and 5).

- We propose a prototype early warning method for levees to detect anomalies in the levee deformation time-series (Chapter 5).

6.3. FUTURE RESEARCH

Relevant aspects addressed in this research which are suggested for further investigation are the following:

Extension of the International Levee Performance Database The aim of the database for the future should be to provide more extensive and high-quality datasets to support the development and validation of accurate methods and models for failure mechanisms and breaching of flood defenses. Improving the ILPD towards a global, uniform database requires very systematic and intense data collection, also with the involvement and commitment of the international scientific community, governments, local stakeholders and levee managers. Further research on the levee failures is currently restricted by the limited amount of data shared in the database, which is why a joint effort is required to make the ILPD more complete and representative. For this reason, future work should focus on effective ways of encouraging data sharing and transparency. Even though the main focus of the analyses in this research is at an event-level, ILPD sub-datasets can be used for more detailed analyses of individual failure processes, for instance, to investigate how occurrence of failure mechanisms is related to levee and loading characteristics or to analyze breach properties in more detail.

Breach density analysis Although in this study a general overview on the breach density parameters has been given, further research on this topic is recommended. The observed breach densities and their identified relation with the return periods can be improved and validated on cases from different events that will become available in the database in the future. Such information could be used, for instance in combination with fragility curves, in order to improve risk assessments of levees. A probabilistic analysis could be included by updating the failure probabilities at the failure locations based on the local information affecting the strength of the levee, such as vegetation type, old breaches, changes in soil profile.

Applicability of InSAR for levees Even though the case studies in this research are given for the Netherlands, this technology can be applied to other parts of the world, thus supporting levee management especially in countries with extensive flood defense systems. Findings of this study will assist the future development of reliable early warning methods using continuous deformation monitoring, thus enhancing flood protection. Developing processing techniques to extract coherent signals from vegetated levees is an important research priority, with recent studies showing promising results. This would also extend the applicability to fully vegetated levees. It is also noted that levee deformation and its effect on safety will be highly dependent on local soil and geohydrological conditions of the levee. Further research on these aspects would need to address the

relationship between deformation and geohydrological levee properties and the effects on levee stability (e.g., inclusion of the Factor of Safety) for a number of representative situations.

Early warning systems Aiming towards an automatic detection algorithm for problematic locations, thus an operational early warning system, it is suggested to develop a collaborative, expert-supported approach for future applications. Considering different anomalous behavior of levees, different canonical models can be introduced to be used in the MHT framework. Besides, alternative multiple hypotheses testing approaches can be considered. Also, combining different satellite missions and orbits, spatio-temporal coverage and resolution can be increased, thus enhancing detectability. Further research would need to focus on the inclusion of local monitoring and information (e.g., geotechnical assessments) about the levees to obtain precise detection for different cases. Time-series analysis methods, for example, machine learning techniques could be used to automate the safety assessments. It is acknowledged that a systematic application of the proposed method can contribute to operational monitoring and become a useful tool for timely anomaly detection of levees.

APPENDIX

A

TEST SET-UP: EEMDIJK EXPERIMENT

Within the framework of the SAFElevee project, an external project is carried out in collaboration with *Projectoverstijgende Verkenning (POV) Macrostabieliteit* in order to conduct further research into the applicability of InSAR technology for levee assessments. The goal of this project is to analyze and evaluate the usability of InSAR for levee deformation monitoring based on measurements from a levee failure test performed at Eemdijk, the Netherlands. In order to create a number of good reflection points of the radar signals, corner reflectors are placed on the levee. Despite the fact that the duration of the test is short compared to the measurement frequency of the satellite data, some measurements can still be obtained and be used to assess the potential of the technique for future monitoring.

In the following parts, a general overview on the use of corner reflectors is given; the design of the field experiment is described and the InSAR data processing is explained. Later, the results are discussed and conclusions are given together with some recommendations.

A.1. THE USE OF CORNER REFLECTORS

InSAR requires consistent reflections of the surface over time as explained in Section 3.2. However, it is possible that consistent reflections cannot be obtained at certain locations of interest. The solution to the lack of natural reflection sources is to install corner reflectors at the relevant locations, see Figure A.1. Such a reflector consists of three metal plates that are attached to each other at an angle of 90°. A radar signal is therefore not reflected in all directions, but only in the direction of arrival, so that a strong signal is reflected back and received by the radar satellite. Thus, the corner reflector performs as a Persistent Scatterer (PS) for InSAR processing and, provided that it is properly installed, moves with the surface movement of the levee.

This appendix contains parts of a technical report published within [166].

The design of the corner reflector that is used in the Eemdijk test is shown in Figure A.1. The reflector is placed on a tripod, which makes it easier to adjust the reflector and to optimize the tilt for the angle of the incoming radar signal. The screw under the base plate allows the reflector to be rotated by 360° around the vertical axis and thus to be directed towards the flight direction of the satellite.



Figure A.1: The design of corner reflectors for Eemdijk.

The deformation measurement of PS in each dataset is relative to a reference point. In order to be able to compare the different reflectors obtained from different satellite datasets, a reference corner reflector is installed next to the levee, near by the test location in which the surface is considered to be stable. This reference reflector [167] has two reflectors on the same structure, (see Figure A.5), allowing both images recorded from the ascending and descending satellite orbits to be linked.

A.2. THE DESIGN OF THE EXPERIMENT

This section describes the design of the field experiment at the Eemdijk test location which is constructed to test the reliability of levees. Two independent tests are set up: one for a levee with a sheet pile (blue levee) and one for a levee without a sheet pile (green levee), aiming to analyze their behavioral differences during a failure event and thus to gain more insight into the actual deformation behavior and strength of a sheet pile in a levee. The Eemdijk test area is located South-East of Amsterdam, next to the Eem River (Figure A.2).

A.2.1. INSTALLATION OF THE CORNER REFLECTORS

The first experiment is the failure of the green levee. The original plan was to place three reflectors on the green levee and three reflectors on the blue levee. However, the test



Figure A.2: Google Earth image for the Eemdijk test location, which also shows the location of the levees.

for the green levee was moved to an earlier date, before the blue levee was completed, i.e., no sheet piles were installed in the levee body. Therefore, it is decided to place four corner reflectors only on the crest of the green levee, as given in Figure A.3, taking into account the integrity of the levee and the other measuring techniques (such as drone, tachymetry). The experience gained with this set-up could then be used for the design of the reflectors on the blue levee.

To provide a stable construction, the tripods are used to install the reflectors and are fixed with sandbags and ropes, see Figures A.1 and A.4. The reference reflector is placed on a Stelcon plate next to the levee (Figures A.3 and A.5). Before installing the Stelcon plate, a layer of sand is applied to the ground. Despite this layer, it is noticed that the reference reflector itself can also experience a subsidence due to the weak subsoil. After installation, the corner reflectors are oriented in the direction perpendicular to the Sentinel-1 satellite track and the optimum direction for the different radar signals. Subsequently, the phase center point of the corner reflectors was measured by means of RTK-GPS (Table A.1).

On January 19, 2018 around 4:00 PM, the installation of the corner reflectors was completed as shown in Figure A.4 and A.5. The reflectors were removed after the collapse of the levee, i.e., January 30, 2018.

A.3. DATA PROCESSING

The displacement of the corner reflectors, and therefore the deformation of the levee, can be measured by analyzing a set of SAR images. Various SAR satellite missions are operational, each with their own characteristics, such as spatial and temporal resolutions, wavelength and polarization of the radar signal, as discussed in Chapter 3. For every application and project, a consideration can be made regarding which satellite mission is



Figure A.5: The reference corner reflector [167] installed on a Stelcon plate, on top of an extra layer of sand.

Table A.1: The phase center point of the reflectors in RD and ETRS89 coordinates.

Corner reflector no.	RD coord.		ETRS89 coord.	
	X (m)	Y (m)	Lat (deg)	Lon (deg)
CR.1	150978.446	474511.479	52.25862182	5.32830226
CR.2	150985.749	474503.566	52.25855075	5.32840932
CR.3	150993.379	474494.882	52.25847276	5.32852118
CR.4	151001.114	474485.901	52.25839210	5.32863457
Ref.	151074.014	474519.507	52.25869466	5.32970192

Recordings from four different satellite positions are possible for the Eemdijk location, which is due to the use of both the ascending and descending satellite orbits the 50% overlap of the recorded strips above the Netherlands. This means that the test location is sampled on average every 1 or 2 days, which also applies to the whole of the Netherlands. The four Sentinel-1 SAR datasets used are shown in Table A.2.

The following steps are applied for processing the data:

1. Download of the SAR images.
2. Co-registration of the SAR images, so that the different images are exactly on top of each other and they can be analyzed in the time domain.

Table A.2: Characteristics of the Sentinel-1 datasets used in this analysis.

Track	Orbit	Heading angle (deg)	Incidence angle (deg)	First image date - every 6 days repeated	Time (UTC)
088	Ascending	344.5	33.2	06 Nov 2017	17:25
161	Ascending	344.5	41.8	12 Oct 2017	17:33
037	Decending	195.5	44.6	16 Oct 2017	05:49
110	Decending	195.5	36.7	15 Oct 2017	05:58

3. Identification of the signals from the corner reflectors based on the GNSS measurements and optimization of the position based on the maximum reflection strength.
4. Analysis of the reflection strength (Radar Cross Section (RCS)) and the deformation.

The entire processing is carried out by software developed within the Delft University of Technology. The first results of the analysis are described in the following section.

A.4. INITIAL RESULTS

In this section, the initial results of the data processing are presented for the green levee which collapsed on the morning of 30 January 2018. The length of the slip surface was approximately 25 meters (Figure A.6).

A.4.1. IDENTIFYING THE SIGNALS

During the data processing for the green levee, it was found that the identification of the signals from the corner reflectors was not possible. The reason is that the opening on top of the containers was not taken into account in the design of the measurement set-up. Hence, the containers themselves function as radar reflectors which, due to their larger size, produce strong reflected signals obscuring the signals from the corner reflectors. This is visible in Figure A.7 where the reflection strength (RCS) for an image from track 37 is shown. Instead of four relatively strong reflections for the corner reflectors, six to eight strong reflections are visible (depending on the satellite orbit) which correspond to the containers on top of the levee. Therefore, the reflections from the corner reflectors cannot be identified and their analysis is not possible.

Then, it is decided to analyze the reflections from the containers. Since no direct GNSS measurement for the position of the containers is available, the positions from the radar images are estimated by optimizing the reflection strength. For instance, the estimated location of containers 6 (CNT6, all eight containers are designated CNT1-8, see Figure A.8) is shown in Figure A.7. The reflection strength and deformations are then analyzed for these positions.



Figure A.6: The failure of the green levee.

A.4.2. MEASURED REFLECTION STRENGTH AND DEFORMATION

The analysis of the four different datasets shows that 3 to 5 reflections from the containers can be detected, depending on the dataset. This detection is based on the previously determined positions and the reflection pattern in the specific datasets. The results for tracks 37, 110 and 88 are shown in Figures A.9, A.10 and A.11. For each dataset, both the reflection strength (expressed in Radar Cross Section (RCS)) and the vertical deformation with respect to the reference reflector are shown based on the measured phase. The figures show that the reflection strength of the reference reflector is indeed stable with an RCS of approximately 28 dBm^2 . The detected containers show a similar strength. This is significantly more than the installed corner reflectors on the levee, which are much smaller compared to the reference reflector. The figures also show that the reflection strength changes after the failure of the levee, probably due to the tilting of the containers, and possibly in combination with the influence of water in the containers. The measured values of the phase are translated into deformations in millimeters relative to the reference reflector. The measurement is in the viewing direction of the radar, which

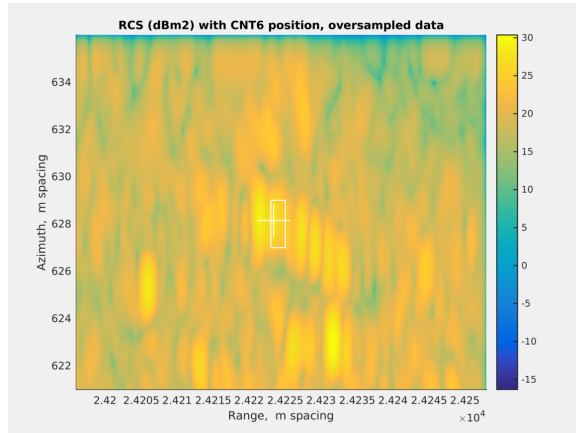


Figure A.7: Reflection strength (RCS) of the radar signal for an image from dataset from track 37.



Figure A.8: Numbers of the containers on the green levee (indicated in the text with CNT1-8). Container 8 is located further on the levee and is not shown in the Figure.

is determined by the heading angle of the satellite and the incidence angle of the signal, see Table A.2. These are different for the four different datasets. The viewing directions from the descending with respect to the ascending orbit differ by about 180° . Thus, it can be assumed that two different angles of the containers have been measured. Direct comparison of the measurements is difficult due to the different viewing directions and measured points. To make some comparison possible, the measurements are transformed into deformations in the vertical direction. Any horizontal movements that have taken place are also translated into a vertical movement.

An initial analysis of the deformations shows that a number of consistent measure-

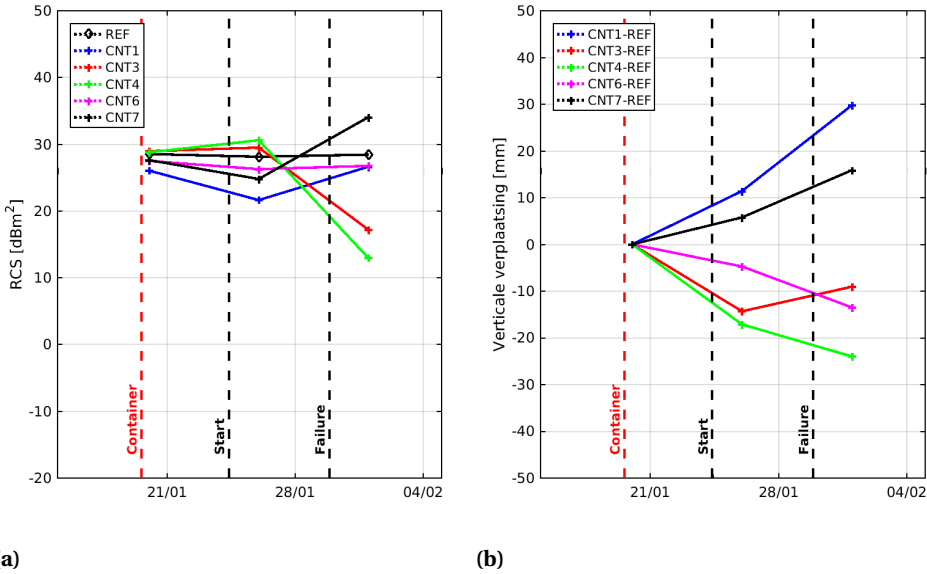


Figure A.9: Radar measurements from Sentinel-1, track 37 (descending) for the reference reflector (REF) and various containers. (a) Radar reflection strength expressed in Radar Cross Section (RCS). (b) Deformation in the vertical direction. The date of placement of the containers, the start of the test, and the failure of the levee are shown in dashed lines.

ments is obtained. For instance, the measurements for descending orbits 37 and 110 show a similar drop of about 8 mm from CNT6. A similar value is measured from ascending orbit 88. For other containers, however, the image is more diffuse which could be explained by the fact that the deformation of the other containers is larger. In particular, phase measurements (measured between $-\pi$ and $+\pi$) have a phase ambiguity. For Sentinel-1, this corresponds to a 31 mm deformation in the vertical direction. Deformations of more than half of these values are therefore represented with a module of 31 mm. For example, a subsidence with -17 mm becomes +14 mm. Accordingly, no distinction can be made between a subsidence of -8 and -39 mm. By combining the available measurements from the descending and ascending orbits, better estimates of the deformation of the container and the phase ambiguity could possibly be obtained. Given the limited scope of this project, this analysis is not performed.

A.5. CONCLUSIONS AND RECOMMENDATIONS

The unexpected strong reflections from the containers made impossible to measure the corner reflectors installed on the green levee. Hence, the reflections from the containers have been detected and analyzed instead. Despite the fact that a number of consistent reflections and deformations are derived, the phase ambiguity of the signals and

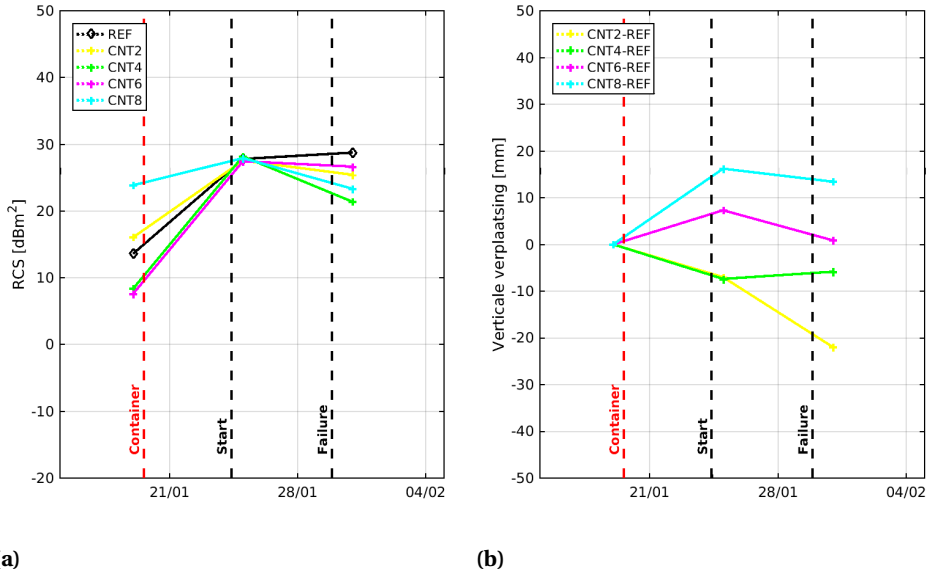


Figure A.10: Radar measurements from Sentinel-1, track 110 (descending) for the reference reflector (REF) and various containers. (a) Radar reflection strength expressed in Radar Cross Section (RCS). (b) Deformation in the vertical direction.

other environmental factors, such as the influence of water in the containers, make further analysis complex. The problem of the strong reflections from the open containers, and thus the invisibility of the installed corner reflectors, soon became clear through the near-real-time analysis of the satellite data during the test of the green levee. This also led to the conclusion that installation of the corner reflectors for the test with the blue levee was not useful.

Although it would be possible to further analyze the reflections of the containers, the complexity of the signals makes the interpretation not unique. Since the use of satellite deformation measurements during the test was primarily aimed at evaluating the applicability of the technique for corner reflectors, and given the limited number of acquisitions during the test, further elaboration of the data does not seem meaningful.

The test has shown that the radar reflections of the satellite signals are dependent on the conditions of the levee. Even though the interpretation of the reflections from the containers during the short duration of this test is complex, in a different situation similar objects could provide valuable observations over a longer period of time. In addition to objects, in many cases also stone revetments and pavements provide good reflections from levees. This thesis has shown that these 'natural' reflections of the levee surface can provide thousands of valuable measuring points for the levees.

The results of this test show that a good analysis of the spatial situation is of great importance for a correct estimate of satellite deformation measurements with InSAR. In

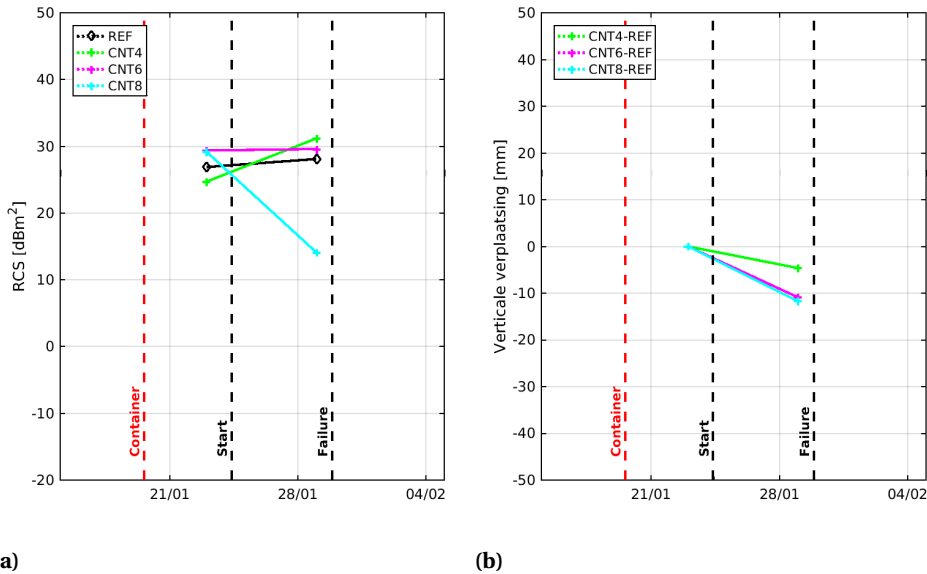


Figure A.11: Radar measurements from Sentinel-1, track 88 (descending) for the reference reflector (REF) and various containers. (a) Radar reflection strength expressed in Radar Cross Section (RCS). (b) Deformation in the vertical direction.

this exceptional situation, for which the levee was specifically built for the test, no investigation was performed in advance. However, this could be generally possible for most of other applications. As indicated in this thesis, the existing levees in the Netherlands already provide hundreds of thousands of natural measurement points, which can be systematically monitored. Given the country-wide availability of satellite data, with a repeat frequency of 1 to 2 days, this seems desirable and the feasibility of such a new flow of information in day-to-day management practice should be investigated. On levees where no usable natural reflections have been detected so far, for example through grass cover, further research should be encouraged to develop and test data processing techniques. Promising results are already being achieved for meadows and fields. These techniques should be further optimized for use on the smaller grass areas on levees.

For locations where natural reflections are nevertheless not detected, artificial reflectors can be installed. Experience from the past shows that corner reflectors, as used in the Eemdijk test, are very sensitive to blockage due to rainwater and dirt, damage and even theft. An undisturbed signal over a longer period of time cannot therefore be guaranteed. Active radar transponders are a valuable alternative. These electronic devices actively transmit the radar signal. The advantage is that these transponders are smaller and less heavy compared to the corner reflectors. The disadvantage is that they need an energy source, in the form of a battery, possibly combined with a solar panel. Sensitivity to theft or vandalism can also be a problem.

Given the disadvantages of the corner reflectors and the active transponders, designing a new type of levee cover that ensures good radar reflection is an alternative option. This levee cover should have a certain degree of roughness to ensure good reflection. In addition to that, it might also be possible to develop objects that ensure good radar reflection.

REFERENCES

- [1] UNISDR (2011). Global assessment report on disaster risk reduction – revealing risk, redefining development. Tech. report, United Nations, Geneva, Switzerland.
- [2] IPCC (2012). Managing the risks of extreme events and disasters to advance climate change adaptation. a special report of working groups I and II of the intergovernmental panel on climate change. Tech. report, Cambridge University Press, Cambridge, UK / New York, NY, USA.
- [3] CRED (2019). Natural Disasters 2018. Tech. report, Centre for Research on the Epidemiology of Disasters, Brussels, Belgium.
- [4] Melillo, J. M., Richmond, T., and Yohe, G. (2014). Climate change impacts in the United States: The third national climate assessment. Tech. report, U.S. Global Change Research Program, Washington, DC.
- [5] Li-An, C., Billa, L., and Azari, M. (2018). Anthropocene climate and landscape change that increases flood disasters. *International Journal of Hydrology*, 2(4):487–491.
- [6] OECD (2016). *Financial Management of Flood Risk*. OECD Publishing, Paris, France.
- [7] UNDRR (2013). 2013 floods a "turning point". UN Office for Disaster Risk Reduction, <https://www.unisdr.org/archive/33693>. Accessed online: 01 Nov 2019.
- [8] CRED (2019). The international disaster database (EM-DAT). <https://www.emdat.be/>. Accessed online: 30 May 2019.
- [9] Jongman, B., Ward, P. J., and Aerts, J. C. (2012). Global exposure to river and coastal flooding: Long term trends and changes. *Global Environmental Change*, 22(4):823–835.
- [10] Tebaldi, C., Strauss, B. H., and Zervas, C. E. (2012). Modelling sea level rise impacts on storm surges along US coasts. *Environmental Research Letters*, 7(014032).
- [11] Buchanan, M. K., Kopp, R. E., Oppenheimer, M., and Tebaldi, C. (2016). Allowances for evolving coastal flood risk under uncertain local sea-level rise. *Climatic Change*, 137:347–362.
- [12] Kulp, S. A. and Strauss, B. H. (2019). New elevation data triple estimates of global vulnerability to sea-level rise and coastal flooding. *Nature Communications*, 10(4844).
- [13] Stocker, T. F., Qin, D., Plattner, G. K., Tignor, M. M. B., Allen, S. K., Boschung, J., Nauels, A., Xia, Y., Bex, V., and Midgley, P. M. (2013). IPCC, 2013: Climate Change 2013: The Physical Science Basis. Contribution of Working Group I to the Fifth Assessment

- Report of the Intergovernmental Panel on Climate Change. Tech. report, Cambridge University Press, Cambridge, United Kingdom and New York, NY, USA.
- [14] Kopp, R. E., Horton, R. M., Little, C. M., Mitrovica, J. X., Oppenheimer, M., Rasmussen, D. J., Strauss, B. H., and Tebaldi, C. (2014). Probabilistic 21st and 22nd century sea-level projections at a global network of tide-gauge sites. *Earth's future*, 2(8):383–406.
- [15] Nauels, A., Meinshausen, M., Mengel, M., Lorbacher, K., and Wigley, T. M. (2017). Synthesizing long-term sea level rise projections-the MAGICC sea level model v.2.0. *Geoscientific Model Development*, 10(6).
- [16] Bakker, A. M. R., Wong, T. E., Ruckert, K. L., and Keller, K. (2017). Sea-level projections representing the deeply uncertain contribution of the West Antarctic ice sheet. *Scientific Reports*, 7(3880).
- [17] Wong, T. E., Bakker, A. M., and Keller, K. (2017). Impacts of Antarctic fast dynamics on sea-level projections and coastal flood defense. *Climatic Change*, 144(2):347–364.
- [18] Jonkman, S. N. and van den Bos, J. P. (2017). *Flood Defences lecture notes CIE5314*. Delft University of Technology, Delft, the Netherlands, second edition.
- [19] Sharp, M., Wallis, M., Deniaud, F., Hersch-Burdick, R., Tourment, R., Matheu, E., Seda-Sanabria, Y., Wersching, S., Veylon, G., Durand, E., et al. (2013). *The International Levee Handbook*. CIRIA, London, England.
- [20] ENW (2017). Grondslagen voor hoogwaterbescherming. Tech. report (in Dutch), Expertisenetwerk Waterveiligheid, Utrecht, the Netherlands.
- [21] Kanning, W. (2012). *The weakest link: spatial variability in the piping failure mechanism of dikes*. PhD thesis, Delft University of Technology, Delft, the Netherlands.
- [22] Jonkman, S. N. (2005). Global perspectives on loss of human life caused by floods. *Natural Hazards*, 34(2):151–175.
- [23] Özer, I. E., van Damme, M., Schweckendiek, T., and Jonkman, S. N. (2016). On the importance of analyzing flood defense failures. In *Proceedings of the 3rd European Conference on Flood Risk Management (FLOODrisk 2016)*, volume 7, page 03013.
- [24] Schweckendiek, T., Vrouwenvelder, A. C. W. M., and Calle, E. O. F. (2014). Updating piping reliability with field performance observations. *Structural Safety*, 47:13–23.
- [25] Horlacher, H. B., Bielagk, U., and Heyer, T. (2005). Analyse der Deichbrüche an der Elbe und Mulde während des Hochwassers 2002 im Bereich Sachsen. Tech. report (in German), TU Dresden. Forschungsbericht 2005/09.
- [26] Simm, J., Flikweert, J., Hollingsworth, C., and Tarrant, O. (2017). Ten years of lessons learned from English levee performance during severe flood events. In *Proceedings of the 5th Annual Meeting of International Commission on Large Dams*, Prague, Czech Republic. ICOLD.

- [27] Heyer, T. (2016). Reliability assessment of levees based on failure investigations. *Vodohospodářské technicko-ekonomické informace*, 58(3):28–33.
- [28] Lopez, J. P. A., Warmink, J. J., Schielen, R. M. J., and Hulscher, S. J. M. H. (2012). *Book of Abstracts 2012*, chapter Safety assessment of multifunctional flood defences, pages 1–2. University of Twente.
- [29] van Baars, S. and van Kempen, I. M. (2009). The causes and mechanisms of historical dike failures in the Netherlands. *e-Water*.
- [30] Danka, J. (2015). *Dike failure mechanisms and breaching parameters*. PhD thesis, Hong Kong University of Science and Technology, Hong Kong.
- [31] DWR (2015). DWR levee breach database. State of California, Department of Water Resources, <http://www.dwr-lep.com>. Accessed online: 10 Nov 2019.
- [32] Dentz, F., Halderen, L., Possel, B., Esfahany, S. S., Slobbe, C., and Wortel, T. (2006). On the potential of satellite radar interferometry for monitoring dikes of the Netherlands. Tech. report, Delft University of Technology.
- [33] Hanssen, R. F. and van Leijen, E. J. (2008). Monitoring water defense structures using radar interferometry. In *Proceedings of the 2008 IEEE Radar Conference*, pages 1–4, Rome, Italy.
- [34] Tarrant, O., Hambidge, C., Hollingsworth, C., Normandale, D., and Burdett, S. (2017). Identifying the signs of weakness, deterioration, and damage to flood defence infrastructure from remotely sensed data and mapped information. *Journal of Flood Risk Management*, 10(4):1–14.
- [35] Rijkswaterstraat (2001). Hydraulische randvoorwaarden 2001 voor het toetsen van primaire waterkeringen. Tech. report (in Dutch), Rijkswaterstraat, Delft, The Netherlands.
- [36] Swart, L. M. T. (2007). Remote sensing voor inspectie van waterkeringen. Tech. report (in Dutch), Swartvast, Nieuw-Vennep, The Netherlands.
- [37] Bakkenist, S. W. and Zomer, W. S. (2010). Inspectie van waterkeringen: een overzicht van meettechnieken. Tech. report (in Dutch) 2010-31, STOWA, Amersfoort, The Netherlands.
- [38] Hanssen, R. F. (2001). *Radar Interferometry: Data Interpretation and Error Analysis*, volume 2. Springer Science+Business Media, Dordrecht, the Netherlands.
- [39] Ferretti, A., Prati, C., and Rocca, F. (2001). Permanent scatterers in SAR interferometry. *IEEE Transactions on Geoscience and Remote Sensing*, 39(1):8–20.
- [40] Gernhardt, S., Adam, N., Eineder, M., and Bamler, R. (2010). Potential of very high resolution SAR for persistent scatterer interferometry in urban areas. *Annals of GIS*, 16(2):103–111.

- [41] Chang, L., Dollevoet, R. P., and Hanssen, R. F. (2017). Nationwide railway monitoring using satellite SAR interferometry. *IEEE Journal of Selected Topics in Applied Earth Observations and Remote Sensing*, 10(2):596–604.
- [42] Perissin, D. and Wang, T. (2011). Time-series InSAR applications over urban areas in China. *IEEE Journal of Selected Topics in Applied Earth Observations and Remote Sensing*, 4(1):92–100.
- [43] Perissin, D., Wang, Z., and Lin, H. (2012). Shanghai subway tunnels and highways monitoring through Cosmo-SkyMed persistent scatterers. *ISPRS Journal of Photogrammetry and Remote Sensing*, 73:58–67.
- [44] Cigna, F., Bianchini, S., and Casagli, N. (2013). How to assess landslide activity and intensity with persistent scatterer interferometry (PSI): the PSI-based matrix approach. *Landslides*, 10(3):267–283.
- [45] Hooper, A., Segall, P., and Zebker, H. (2007). Persistent scatterer interferometric synthetic aperture radar for crustal deformation analysis, with application to Volcán Alcedo, Galápagos. *Journal of Geophysical Research: Solid Earth*, 112(B7).
- [46] Cigna, F., Osmanoğlu, B., Cabral-Cano, E., Dixon, T. H., Ávila-Olivera, J. A., Garduño-Monroy, V. H., DeMets, C., and Wdowinski, S. (2012). Monitoring land subsidence and its induced geological hazard with Synthetic Aperture Radar Interferometry: A case study in Morelia, Mexico. *Remote Sensing of Environment*, 117:146–161.
- [47] Dixon, T. H., Amelung, F., Ferretti, A., Novali, F., Rocca, F., Dokka, R., Sella, G., Kim, S.-W., Wdowinski, S., and Whitman, D. (2006). Space geodesy: subsidence and flooding in New Orleans. *Nature*, 441(7093):587–588.
- [48] Brooks, B. A., Bawden, G., Manjunath, D., Werner, C., Knowles, N., Foster, J., Dudas, J., and Cayan, D. (2012). Contemporaneous subsidence and levee overtopping potential, Sacramento-San Joaquin Delta, California. *San Francisco Estuary and Watershed Science*, 10(1).
- [49] European Commission (2004). Communication from the Commission to the Council, the European Parliament, the European Economic and Social Committee and the Committee of the Regions - Flood Risk Management; Flood Prevention, Protection and Mitigation. Tech. report COM(2004)472, Commission of the European Communities, Brussels, Belgium.
- [50] Özer, I. E., van Damme, M., and Jonkman, S. N. (2020). Towards an International Levee Performance Database (ILPD) and its use for macro-scale analysis of levee breaches and failures. *Water*, 12(119).
- [51] Özer, I. E., van Leijen, F., Jonkman, S. N., and Hanssen, R. F. (2018). Applicability of satellite radar imaging to monitor the conditions of levees. *Journal of Flood Risk Management*, page e12509.

- [52] Özer, I. E., Rikkert, S. J., van Leijen, F. J., Jonkman, S. N., and Hanssen, R. F. (2019). sub-seasonal levee deformation observed using satellite radar interferometry to enhance flood protection. *Scientific Reports*, 9(1):2646.
- [53] Kool, J. J., Kanning, W., Heyer, T., Jommi, C., and Jonkman, S. N. (2019). Forensic analysis of levee failures: the Breitenhagen case. *International Journal of Geoenvironment Case Histories*, 5(2).
- [54] van Damme, M. (2020). An analytical process-based approach to predicting breach width in levees constructed from dilatant soils. *Natural Hazards*.
- [55] NPDP (1999). National performance of dams program. Stanford University, http://npdp.stanford.edu/data_library. Accessed online: 01 Nov 2019.
- [56] Fry, J. J., Le Bourget du Lac, F., Courivaud, J. R., and Blais, J. P. (2004). Dam Accident Data Base DADB -The web-based data collection of ICOLD. In *Proceedings of the 13th Conference on British Dam Society and the ICOLD European Club Meeting*, pages 298–304. 22-26 June, 2004.
- [57] Xu, Y. (2010). *Analysis of dam failures and diagnosis of distresses for dam rehabilitation*. PhD thesis, Hong Kong University of Science and Technology, Hong Kong.
- [58] Froehlich, D. C. (1987). Embankment-dam breach parameters. In *Proceedings of the Hydraulic Engineering 1987 National Conference*, pages 570–575, Williamsburg, USA. ASCE.
- [59] Peng, M. and Zhang, L. M. (2012). Breaching parameters of landslide dams. *Landslides*, 9(1):13–31.
- [60] Foster, M., Fell, R., and Spannagle, M. (2000). The statistics of embankment dam failures and accidents. *Canadian Geotechnical Journal*, 37(5):1000–1024.
- [61] Fry, J. J. (2012). Dam failures by erosion: lessons from ERINOH database. In *Proceedings of the 6th International Conference on Scour and Erosion (ICSE-6)*, pages 273–280. Société Hydrotechnique De France. August 27-31, 2012.
- [62] ASDSO (2019). Lessons learned from dam incidents and failures. <http://damfailures.org/>. Accessed online: 10 Nov 2019.
- [63] McClelland, D. M. and Bowles, D. (2002). Estimating life loss for dam safety risk assessment - A review and new approach. Tech. report, Institute for Dam Safety Risk Management.
- [64] USBR (2014). Reclamation consequence estimating methodology, dam failure and flood event case history compilation. Tech. report, U.S. Department of the Interior Bureau of Reclamation.
- [65] DFO (2019). Dartmouth flood observatory of large floods. University of Colorado, <http://floodobservatory.colorado.edu/Archives/index.html>. Accessed Online: 30 May 2019.

- [66] Scussolini, P., Aerts, J. C., Jongman, B., Bouwer, L. M., Winsemius, H. C., de Moel, H., and Ward, P. J. (2016). FLOPROS: an evolving global database of flood protection standards. *Natural Hazards and Earth System Sciences*, 16(5):1049–1061.
- [67] Barbetta, S., Camici, S., Maccioni, P., and Moramarco, T. (2015). National levee database: monitoring, vulnerability assessment and management in Italy. In *Proceedings of the EGU General Assembly*, volume 17, Vienna, Austria. April 12–17, 2015.
- [68] USACE (2016). National Levee Database. U.S. Army Corps of Engineers, <http://nld.usace.army.mil/>. Accessed online: 30 Apr 2019.
- [69] Seed, R. B., Bea, R. G., Athanasopoulos-Zekkos, A., Boutwell, G. P., Bray, J. D., Cheung, C., Cobos-Roa, D., Harder Jr, L. F., Moss, R. E., Pestana, J. M., and Riemer, M. F. (2008a). New Orleans and Hurricane Katrina III: The 17th street drainage canal. *Journal of Geotechnical and Geoenvironmental Engineering*, 134(5):740–761.
- [70] Seed, R. B., Bea, R. G., Athanasopoulos-Zekkos, A., Boutwell, G. P., Bray, J. D., Cheung, C., Cobos-Roa, D., Ehrensing, L., Harder Jr, L. F., Pestana, J. M., and Riemer, M. F. (2008b). New Orleans and Hurricane Katrina. II: the central region and the lower Ninth Ward. *Journal of Geotechnical and Geoenvironmental Engineering*, 134(5):718–739.
- [71] Horlacher, H. B., Heyer, T., Carstensen, D., Bielagk, U., Bielitz, E., and Müller, U. (2007). Analysis of dyke breaks during the 2002 flood in Saxony/Germany. In *Proceedings of the LARS 2007–Catchment and Lake Research*, Arba Minch, Ethiopia. FWU Water Resources Publications. May 7–11, 2007.
- [72] Visser, P. (1998). *Breach growth in sand-dikes*. PhD thesis, Delft University of Technology, Delft, the Netherlands.
- [73] Sills, G. L., Vroman, N. D., Wahl, R. E., and Schwanz, N. T. (2008). Overview of New Orleans levee failures: lessons learned and their impact on national levee design and assessment. *Journal of Geotechnical and Geoenvironmental Engineering*, 134(5):556–565.
- [74] Vinet, F., Lumbroso, D., Defosse, S., and Boissier, L. (2012). A comparative analysis of the loss of life during two recent floods in France: the sea surge caused by the storm Xynthia and the flash flood in Var. *Natural Hazards*, 61(3):1179–1201.
- [75] Bisschop, F. (2018). *Erosion of sand at high flow velocities*. PhD thesis, Delft University of Technology, Delft, the Netherlands.
- [76] TAW (1999). Water retaining earth structures. Tech. report (in Dutch), Technical Advisory Committee on Water Defences.
- [77] van Damme, M., Ozer, I. E., and Kool, J. J. (2019). Guidance of the International Levee Performance Database (ILPD). Tech. report, Delft University of Technology.

- [78] ICOLD (2013). Bulletin 164 on internal erosion of existing dams, levees and dikes, and their foundations. Tech. report 1, International Commission on Large Dams, Paris, France.
- [79] Nagy, L. (2006). Estimating dike breach length from historical data. *Periodica Polytechnica Civil Engineering*, 59(2):125–138.
- [80] Morris, M. W. (2011). *Breaching of earth embankments and dams*. PhD thesis, The Open University, Milton Keynes, England.
- [81] Thieken, A. H., Müller, M., Kreibich, H., and Merz, B. (2005). Flood damage and influencing factors: New insights from the August 2002 flood in Germany. *Water Resources Research*, 41(12).
- [82] Thieken, A. H., Kienzler, S., Kreibich, H., Kuhlicke, C., Kunz, M., Muhr, B., Müller, M., Otto, A., Petrow, T., Pisi, S., and Schroter, K. (2016). Review of the flood risk management system in Germany after the major flood in 2013. *Ecology and Society*, 21(2)(51).
- [83] Jüpner, R. and Henning, B. (2015). Deichbruch Fischbeck - zwei Jahre danach. *Wasser und Abfall*, 11:16–20. (in German).
- [84] Weichel, T. (2013). Failure of the Breitenhagen levee 2013 - drone film. Landesbetrieb für Hochwasserschutz und Wasserwirtschaft Sachsen-Anhalt.
- [85] BfG (2013). Das Juni-hochwasser des Jahres 2013 in Deutschland. Tech. report (in German), The German Federal Institute of Hydrology, Koblenz, Germany.
- [86] Jüpner, R. (2018). Coping with extremes – experiences from event management during the recent Elbe flood disaster in 2013. *Journal of Flood Risk Management*, 11:15–21.
- [87] Gocht, M. (2004). Deichbrüche und Deichüberströmungen an Elbe und Mulde im August 2002. Tech. report (in German), Ökonomische Beratung für Wasser und Umwelt.
- [88] Wahl, T. L. (2004). Uncertainty of predictions of embankment dam breach parameters. *Journal of Hydraulic Engineering*, 130(5):389–397.
- [89] Froehlich, D. C. (2008). Embankment dam breach parameters and their uncertainties. *Journal of Hydraulic Engineering*, 134(12):1708–1721.
- [90] Kakinuma, T. and Shimizu, Y. (2014). Large-scale experiment and numerical modeling of a riverine levee breach. *Journal of Hydraulic Engineering*, 140(9).
- [91] Temple, D. M., Hanson, G. J., Neilsen, M. L., and Cook, K. R. (2005). Simplified breach analysis model for homogeneous embankments: Part 1, Background and model components. In *Proceedings of the 25th Annual United States Society on Dams (USSD) Conference*, Salt Lake City, USA. June 6–10, 2005.
- [92] Morris, M. W. (2009). Breach initiation and growth: Physical processes (FLOODsite report T06-08-11). Tech. report, HR Wallingford, Wallingford, UK.

- [93] Michelazzo, G. (2014). *Breaching of river levees: Analytical flow modelling and experimental hydro-morphodynamic investigations*. PhD thesis, University of Braunschweig, Braunschweig, Germany.
- [94] Curran, A., De Bruijn, K. M., and Kok, M. (2018). Influence of water level duration on dike breach triggering, focusing on system behaviour hazard analyses in lowland rivers. *Georisk: Assessment and Management of Risk for Engineered Systems and Geohazards*, pages 1–15.
- [95] Jonkman, S. N., Vrijling, J. K., and Kok, M. (2008). Flood risk assessment in the Netherlands: A case study for dike ring South Holland. *Risk Analysis*, 28(5):1357–1373.
- [96] Bernitt, L. and Lynett, P. (2010). Breaching of sea dikes. In *Proceedings of the 32nd International Conference on Coastal Engineering*, volume 1, pages 1–10. June 30 - Jul 5, 2010.
- [97] ICOLD (2016). European levees and flood defences, inventory of characteristics, risks and governance (EURCOLDFLD-WG meeting 2016). Tech. report, EurICOLD.
- [98] LHW (2014). Bericht u^{ber} das Hochwasser im Juni 2013 in Sachsen-Anhalt: Entstehung, ablauf, management und statistische einordnung. Tech. report (in German), Landesbetrieb fu^{ur} Hochwasserschutz und Wasserwirtschaft Sachsen-Anhalt, Magdeburg, Germany.
- [99] Schröter, K., Kunz, M., Elmer, F., Mühr, B., and Merz, B. (2015). What made the June 2013 flood in Germany an exceptional event? a hydro-meteorological evaluation. *Hydrology and Earth System Sciences*, 19:309–327.
- [100] Thieken, A. H., Bessel, T., Kienzler, S., Kreibich, H., Müller, M., Pisi, S., and Schröter, K. (2016). The flood of June 2013 in Germany: How much do we know about its impacts? *Natural Hazards and Earth System Sciences*, 16:1519–1540.
- [101] Jorissen, R., Kraaij, E., and Tromp, E. (2016). Dutch flood protection policy and measures based on risk assessment. In *Proceedings of 3rd European Conference on Flood Risk Management (FLOODrisk 2016)*, volume 7, page 20016, Lyon, France.
- [102] Vergouwe, R. and Sarink, H. (2014). De veiligheid van Nederland in kaart: eindrapportage. Tech. report (in Dutch), Rijkswaterstaat.
- [103] Cundill, S. L., van der Meijde, M., and Hack, H. R. G. (2014). Investigation of remote sensing for potential use in dike inspection. *IEEE Journal of Selected Topics in Applied Earth Observations and Remote Sensing*, 7(2):733–746.
- [104] Mériaux, P. and Royet, P. (2007). *Surveillance, maintenance and diagnosis of flood protection dikes: a practical handbook for owners and operators*. Editions Quae.
- [105] Bakkenist, S. and van Dam, O., van der Nat, A., Thijs, F., and de Vries, W. (2012). Standaard inspectieplan: invulversie voor inspectieplan op maat. Tech. report (in Dutch), STOWA.

- [106] Bakkenist, S. (2012). [DL.2]: inspectiewijzers waterkeringen: technische informatie uitvoering inspecties. Tech. report (in Dutch), STOWA, Amersfoort, The Netherlands.
- [107] Bishop, M., Dunbar, J. B., and Peyman-Dove, L. P. (2003). Integration of remote sensing (LiDAR, electromagnetic conductivity) and geologic data toward the condition assessment of levee systems. In *Proceedings of the International Symposium on Remote Sensing*, pages 400–407. International Society for Optics and Photonics.
- [108] Bertels, L., Houthuys, R., Sterckx, S., Knaeps, E., and Deronde, B. (2011). Large-scale mapping of the riverbanks, mud flats and salt marshes of the Scheldt basin, using airborne imaging spectroscopy and LiDAR. *International Journal of Remote Sensing*, 32(10):2905–2918.
- [109] Moser, G. M. and Zomer, W. S. (2006). Inspectie van waterkeringen: een overzicht van meettechnieken. Tech. report (in Dutch), STOWA, Amersfoort, The Netherlands.
- [110] Stramondo, S., Trasatti, E., Albano, M., Moro, M., Chini, M., Bignami, C., Polcari, M., and Saroli, M. (2016). Uncovering deformation processes from surface displacements. *Journal of Geodynamics*, 102:58–82.
- [111] Schunert, A. and Soergel, U. (2012). Grouping of persistent scatterers in high-resolution SAR data of urban scenes. *ISPRS Journal of Photogrammetry and Remote Sensing*, 73:80–88.
- [112] van Leijen, F. J. and Hanssen, R. F. (2007). Ground water management and its consequences in Delft, the Netherlands as observed by persistent scatterer interferometry. In *Proceedings of FRINGE 2007*, Frascati, Italy.
- [113] Cuenca, M. C. and Hanssen, R. (2008). Subsidence due to peat decomposition in the Netherlands, kinematic observations from radar interferometry. In *Proceedings of FRINGE 2007*, pages 1–6.
- [114] Chang, L. and Hanssen, R. F. (2014). Detection of cavity migration and sinkhole risk using radar interferometric time series. *Remote sensing of environment*, 147:56–64.
- [115] Hanssen, R., van Leijen, F., van Zwieten, G., Dortland, S., Bremmer, C., and Kleuskens, M. (2007). Validation of PSI results of Alkmaar and Amsterdam within the Terrafirma validation project. In *Proceedings of FRINGE 2007*, pages 26–30.
- [116] Ketelaar, G., van Leijen, F., Marinkovic, P., and Hanssen, R. (2006). On the use of point target characteristics in the estimation of low subsidence rates due to gas extraction in Groningen, the Netherlands. In *Proceedings of FRINGE 2005*, volume 610.
- [117] Cuenca, M. C., Hooper, A. J., and Hanssen, R. F. (2013). Surface deformation induced by water influx in the abandoned coal mines in Limburg, the Netherlands observed by satellite radar interferometry. *Journal of Applied Geophysics*, 88:1–11.

- [118] Bamler, R. and Hartl, P. (1998). Synthetic aperture radar interferometry. *Inverse problems*, 14(4):R1–R54.
- [119] Zebker, H. A. and Villasenor, J. (1992). Decorrelation in interferometric radar echoes. *IEEE Transactions on Geoscience and Remote Sensing*, 30(5):950–959.
- [120] Berardino, P., Fornaro, G., Lanari, R., and Sansosti, E. (2002). A new algorithm for surface deformation monitoring based on small baseline differential SAR interferograms. *IEEE Transactions on Geoscience and Remote Sensing*, 40(11):2375–2383.
- [121] Colesanti, C., Ferretti, A., Novali, F., Prati, C., and Rocca, F. (2003). SAR monitoring of progressive and seasonal ground deformation using the permanent scatterers technique. *IEEE Transactions on Geoscience and Remote Sensing*, 41(7):1685–1701.
- [122] Berger, M., Moreno, J., Johannessen, J. A., Levelt, P. F., and Hanssen, R. F. (2012). ESA’s sentinel missions in support of Earth system science. *Remote Sensing of Environment*, 120:84–90.
- [123] Crosetto, M., Monserrat, O., Cuevas-González, M., Devanthery, N., and Crippa, B. (2016). Persistent scatterer interferometry: A review. *ISPRS Journal of Photogrammetry and Remote Sensing*, 115:78–89.
- [124] Osmanoglu, B., Sunar, F., Wdowinski, S., and Cabral-Cano, E. (2016). Time series analysis of InSAR data: Methods and trends. *ISPRS Journal of Photogrammetry and Remote Sensing*, 115:90–102.
- [125] Kampes, B. M., Hanssen, R. F., and Perski, Z. (2003). Radar interferometry with public domain tools. In *Proceedings of FRINGE 2003*, volume 3, Frascati, Italy.
- [126] van Leijen, F. J. (2014). *Persistent scatterer interferometry based on geodetic estimation theory*. PhD thesis, Delft University of Technology, Delft, the Netherlands.
- [127] Samiei-Esfahany, S. (2017). *Exploitation of distributed scatterers in synthetic aperture radar interferometry*. PhD thesis, Delft University of Technology, Delft, the Netherlands.
- [128] Hanssen, R. F. (2004). Stochastic modeling of time series radar interferometry. In *Proceedings of the International Geoscience and Remote Sensing Symposium, IGARSS2004*, volume 4, pages 2607–2610, Anchorage, AK, USA. IEEE.
- [129] Mahapatra, P. S., Samiei-Esfahany, S., van der Marel, H., and Hanssen, R. F. (2014). On the use of transponders as coherent radar targets for SAR interferometry. *IEEE Transactions on Geoscience and Remote Sensing*, 52(3):1869–1878.
- [130] Dheenathayalan, P., Cuenca, M. C., Hoogeboom, P., and Hanssen, R. F. (2017). Small reflectors for ground motion monitoring with InSAR. *IEEE Transactions on Geoscience and Remote Sensing*, 55(12):6703–6712.
- [131] Dheenathayalan, P., Small, D., Schubert, A., and Hanssen, R. F. (2016). High-precision positioning of radar scatterers. *Journal of Geodesy*, 90(5):403–422.

- [132] Morishita, Y. and Hanssen, R. F. (2015a). Deformation parameter estimation in low coherence areas using a multisatellite InSAR approach. *IEEE Transactions on Geoscience and Remote Sensing*, 53(8):4275–4283.
- [133] Morishita, Y. and Hanssen, R. F. (2015b). Temporal decorrelation in L-, C-, and X-band satellite radar interferometry for pasture on drained peat soils. *IEEE Transactions on Geoscience and Remote Sensing*, 53(2):1096–1104.
- [134] Sarabandi, K. and Chiu, T.-C. (1996). Optimum corner reflectors for calibration of imaging radars. *IEEE Transactions on Antennas and Propagation*, 44(10):1348–1361.
- [135] Chang, L., Dollevoet, R. P. J., and Hanssen, R. F. (2018). Performance assessment metrics for line-infrastructure monitoring with multi-sensor SAR data. In *Proceedings of the International Geoscience and Remote Sensing Symposium*, pages 4423–4426.
- [136] Ferretti, A., Savio, G., Barzaghi, R., Borghi, A., Musazzi, S., Novali, F., Prati, C., and Rocca, F. (2007). Submillimeter accuracy of InSAR time series: Experimental validation. *IEEE Transactions on Geoscience and Remote Sensing*, 45(5):1142–1153.
- [137] Chang, L., Dollevoet, R., and Hanssen, R. (2014). Railway infrastructure monitoring using satellite radar data. *International Journal of Railway Technology*, 3(2):1–13.
- [138] Van Baars, S. (2005). The horizontal failure mechanism of the Wilnis peat dyke. *Géotechnique*, 55(4):319–323.
- [139] Fotheringham, A. S., Brunsdon, C., and Charlton, M. (2000). *Quantitative Geography: Perspectives on Spatial Data Analysis*. Sage.
- [140] van de Kerkhof, B., Pankratius, V., Chang, L., van Swol, R., and Hanssen, R. F. (2017). Information extraction from dynamic PS-InSAR time series using machine learning. In *Proceedings of AGU Fall Meeting 2017*, New Orleans, United States.
- [141] Peng, X. and Horn, R. (2013). Identifying six types of soil shrinkage curves from a large set of experimental data. *Soil Science Society of America Journal*, 77(2):372–381.
- [142] Al-Homoud, A., Basma, A., Husein Malkawi, A., and Al Bashabsheh, M. (1995). Cyclic swelling behavior of clays. *International Journal of Geotechnical Engineering*, 121(7):562–565.
- [143] Tripathy, S., Rao, K. S., and Fredlund, D. (2002). Water content-void ratio swell-shrink paths of compacted expansive soils. *Canadian Geotechnical Journal*, 39(4):938–959.
- [144] Price, J. S. and Schlotzhauer, S. M. (1999). Importance of shrinkage and compression in determining water storage changes in peat: the case of a mined peatland. *Hydrological Processes*, 13(16):2591–2601.
- [145] Camporese, M., Ferraris, S., Putti, M., Salandin, P., and Teatini, P. (2006). Hydrological modeling in swelling/shrinking peat soils. *Water Resources Research*, 42(6).

- [146] Gebhardt, S., Fleige, H., and Horn, R. (2010). Shrinkage processes of a drained riparian peatland with subsidence morphology. *Journal of Soils and Sediments*, 10(3):484–493.
- [147] Peng, X. and Horn, R. (2005). Modeling soil shrinkage curve across a wide range of soil types. *Soil Science Society of America Journal*, 69(3):584–592.
- [148] Peng, X. and Horn, R. (2007). Anisotropic shrinkage and swelling of some organic and inorganic soils. *European Journal of Soil Science*, 58(1):98–107.
- [149] Leong, E. and Wijaya, M. (2015). Universal soil shrinkage curve equation. *Geoderma*, 237:78–87.
- [150] Mitchell, J. K., Soga, K., et al. (2005). *Fundamentals of Soil Behavior*, volume 3. John Wiley & Sons, New York, US.
- [151] TeBrake, W. H. (2002). Taming the waterwolf: hydraulic engineering and water management in the Netherlands during the Middle Ages. *Technology and Culture*, 43(3):475–499.
- [152] Grundmann, P. (1996). Een incident tijdens de droog making in 1874. *De Proost-koerier*, 3:4–9. (in Dutch).
- [153] Vonk, B. F. (1994). Some aspects of the engineering practice regarding peat in small polders. In den Haan, E., Termaat, R., and Edil, T., editors, *Advances in understanding and modelling mechanical behaviour of peat*, pages 389–402, Rotterdam, the Netherlands. A.A. Balkema.
- [154] Zabihi Naeini, E., Hoeber, H., Poole, G., and Siahkoohi, H. R. (2009). Simultaneous multivintage time-shift estimation. *Geophysics*, 74(5):V109–V121.
- [155] Teunissen, P. J. G. (2000). *Adjustment Theory; An Introduction*. VSSD, Delft, the Netherlands, first edition.
- [156] Teunissen, P. J. G. (2006). *Testing Theory; An Introduction*. VSSD, Delft, the Netherlands, second edition.
- [157] Chang, L. and Hanssen, R. F. (2015). A probabilistic approach for InSAR time-series postprocessing. *IEEE Transactions on Geoscience and Remote Sensing*, 54(1):421–430.
- [158] Kampes, B. M. (2006). *Radar interferometry*, volume 12. Springer, Dordrecht, the Netherlands.
- [159] Dekker, J., van der Meij, R., Kruse, G., Bezuijen, A., van der Hoek, E., Pruiksma, J., den Haan, E., and Greeuw, G. (2004). Achtergrondrapport sterkteonderzoek oorzaak kadaverschuiving Wilnis. Tech. report (in Dutch) CO-411242-0025, GeoDelft.
- [160] Bezuijen, A., Kruse, G. A. M., and Van, M. A. (2005). Failure of peat dikes in the Netherlands. In *Proceedings of the International Conference on Soil Mechanics and Geotechnical Engineering*, volume 16, page 1857, Osaka, Japan.

- [161] Weisstein, E. W. (2008). *Heaviside Step Function*. MathWorld-A Wolfram Web Resource, Champaign, IL, USA.
- [162] de Heus, H., Joosten, P., Martens, M., and Verhoef, H. (1994). Geodetische deformatie analyse: 1D-deformatie analyse uit waterpasnetwerken. Tech. report, Delft University of Technology, Delft, the Netherlands.
- [163] Baarda, W. (1968). A testing procedure for use in geodetic networks. *Netherlands Geodetic Commission*, 2(5).
- [164] Slomp, R. (2012). *Flood risk and water management in the Netherlands: a 2012 update*. Rijkswaterstaat.
- [165] Lengkeek, H. J., Post, M., Bredeveld, J., and Naves, T. (2019). Eemdijk full-scale field test programme: ground dike and sheet pile dike failure test. In *Proceedings of the XVII European Conference on Soil Mechanics and Geotechnical Engineering*, Reykjavik, Iceland. Sept. 01 - 06, 2019.
- [166] Özer, I. E. and van Leijen, F. J. (2018). Satellietdeformatiemetingen Eemdijk. Tech. report (in Dutch), POV Macrostabieliteit, Delft, the Netherlands.
- [167] Hanssen, R. F. (2017). Device with integrated double SAR corner-reflectors, GNSS, leveling, triangulation and photogrammetric benchmarks. *Netherlands patent application*, 2019103. 21 June 2017.

CURRICULUM VITÆ

Işıl Ece ÖZER

01-03-1988 Born in Istanbul, Turkey.

EDUCATION

2008–2012 B.Sc. in Environmental Engineering
Faculty of Civil Engineering
Istanbul Technical University, Turkey

2012–2014 M.Sc. in Water Resources Engineering
Faculty of Bioscience Engineering
KU Leuven, Belgium

2014–2015 M.Sc. in Safety Engineering
Faculty of Engineering Science
KU Leuven, Belgium

2015–2020 Ph.D. in Civil Engineering
Faculty of Civil Engineering and Geosciences
Delft University of Technology, the Netherlands

MORE INFO



LIST OF PUBLICATIONS

JOURNAL ARTICLES

13. **I.E. Özer**, M. van Damme, S.N. Jonkman, *Towards an International Levee Performance Database (ILPD) and its use for Macro-scale Analysis of Levee Breaches and Failures*. *Water* **12**, 119 (2020).
12. **I.E. Özer**, S.J.H. Rikkert, F.J. van Leijen, S.N. Jonkman, R.F. Hanssen, *Sub-seasonal Levee Deformation Observed Using Satellite Radar Interferometry to Enhance Flood Protection*. *Scientific Reports* **9**, 2646 (2019).
11. **I.E. Özer**, F.J. van Leijen, S.N. Jonkman, R.F. Hanssen, *Applicability of satellite radar imaging to monitor the conditions of levees*. *Journal of Flood Risk Management*, **e12509** (2018).

PROFESSIONAL JOURNALS

10. **I.E. Özer**, S.J.H. Rikkert, F.J. van Leijen, S.N. Jonkman, R.F. Hanssen, *Dijkinspecties vanuit de ruimte: droom of werkelijkheid?*, *Land+Water: vakblad voor civiel- en milieutechniek*, **5**, in Dutch (2019).
9. **I.E. Özer**, F.J. van Leijen, S.N. Jonkman, R.F. Hanssen, *Satellites look down at dike safety*. *DeltaLinks*, **16** (2020).

CONFERENCE PROCEEDINGS

8. **I.E. Özer**, M. van Damme, S.N. Jonkman, *Understanding levee failure patterns to complement flood risk assessments*, In Proceedings of System-Risk Conference, 17-19 Sept 2019, Potsdam, Germany (2019).
7. M. van Damme, **I.E. Özer**, S.J.H. Rikkert, F.J. van Leijen, *Preliminary results of SAFElevee Project*. In Proceedings of ICOLD World Congress, 1-7 July 2018, Vienna, Austria (2018).
6. **I.E. Özer**, M. van Damme, F.J. van Leijen, S.N. Jonkman, R.F. Hanssen, *Detection and Analysis of Weak Spots in Levees Based on Satellite Radar Interferometry*. In Proceedings of Fringe 10th International Workshop on Advances in the Science and Applications of SAR Interferometry and Sentinel-1 InSAR, 5-9 July 2017, Helsinki, Finland (2017).
5. **I.E. Özer**, M. van Damme, T. Schweckendiek, S.N. Jonkman, *On the importance of analysing flood defence failures*. In Proceedings of FLOODrisk2016: 3rd European Conference on Flood Risk Management, 17-21 Oct 2016, Lyon, France, **03013**, (2016).

TECHNICAL REPORTS

4. **I.E. Özer**, J. Kool, M. van Damme, S.N. Jonkman, *SAFELevee: Het verbeteren van de betrouwbaarheid van waterkeringen door een beter begrip van de faalmechanismen*, TU Delft, Tech. report (in Dutch) (2019).
3. **I.E. Özer**, F.J. van Leijen, *Satellietdeformatiemetingen Eemdijk: Technisch Report*, POV Macrostabiliteit, Tech. report (in Dutch) (2018).
2. M. van Damme, **I.E. Özer**, J. Kool, *International Levee Performance Database (ILPD) Guidance*, TU Delft, Tech. report (2018).

MEDIA

1. TU Delft Story of Science, *The breathing of dikes*. Accessed: 2020-02-02.
URL: www.tudelft.nl/en/ceg/research/stories-of-science/the-breathing-of-dikes/.